A STUDY OF MECHANOCHEMICAL ACTIVATION IN SOLID-STATE SYNTHESIS OF ADVANCED CERAMIC COMPOSITES

By

BABAK FOTOOHI

A thesis submitted to
The University of Birmingham
for the degree of
MASTER OF PHILOSOPHY

School of Chemical Engineering
Interdisciplinary Research Centre (IRC) in Materials Processing
The University of Birmingham
July 2010

ABSTRACT

Mechanical methods of the activation of chemical processes are currently widely used for the synthesis of various compounds. Intensive (dry) milling of ultra-fine and nanometer-sized powders is considered to be a way of applying "mechanochemical activation" that involves dispersion of solids, generation and migration of defects in the bulk and plastic deformation of particles. Taking into consideration of the possible benefits (such as increasing particle contacts and modifying the structure), such mechanical activation was employed in this study. Using high purity hydrated silicates (kaolinite, talc) and boehmite as precursors, effect of process parameters mainly milling time, milling method and sintering temperature on densification and microstructure of the sintered bodies were investigated. In first series of tests, mechanically induced phase transformations (e.g. formation and transformation of mullite) were observed and studied carefully in differently milled material sintered at temperatures about 1000 °C, 2 h. SEM-EDX analysis and density/porosity measurements showed the differences in grain growth and densification process conditions applied. Formation of specific intermediate phases such as MAS (or μ-cordierite) and the effect of intense mechanical action on phase compositions after sintering were well recognized. Later, experiments were performed at 1300 °C, using the selected milling method from earlier tests, wherein Yttria-stabilised zirconia (YSZ) and ceria were also added as dopants to study the possible effects on sintering behaviour and the resultant microstructure of the composite material. Mechanochemical milling of cordierite precursors mixed with predetermined amounts of YSZ resulted in substantial destabilisation of tetragonal zirconia and formation of zircon after sintering rest time of 2 h. When the additive ratio ceria/YSZ was 1/4, increasing the milling time resulted in peaks indicative of reduced crystallinity in sintered samples. However, in case the ratio was 4, mechanical activation resulted in an increase in the degree of crystallisation in the sintered material, which otherwise (without or with less milling) had a more glassy structure due to the fluxing effect of cerium oxide. Ceria was found to be effective in stabilisation of zirconia and reduction of the transformation to zircon. When ceria was added alone (4 wt%) to the precursor mixture, mechanochemical milling resulted in an increase in the densification and crystallisation of the sintered cordierite. The results of this research could be further investigated an applied for controlled mechanochemical structural modifications based on the required final (physical/chemical) properties of the material in solid-state synthesis of advanced ceramics.

Acknowledgments

I would like to express my greatest appreciation to my supervisor Prof. Stuart Blackburn who accepted the supervision of my research at the School of Chemical Engineering and provided the necessary advice whenever needed throughout the project. He also kindly helped to use research facilities, services and equipments available at the IRC in Materials Processing at Metallurgy and Materials.

Professor Jan Baeyens is gratefully acknowledged for providing the one-off scholarship of £1500.00 to help with the study costs at the School of Chemical Engineering. I would also like to thank Mrs. Lynn Draper, the postgraduate research students' secretary, for her warm welcome to the department and her always helpful guidance over administration and student affairs.

Special thanks to Dr Richard Greenwood the Programme Manager in Formulation Engineering at Chemical Engineering, who was the first academic in the school to meet and consult with. He provided useful guides and instructions on looking for reference data, facilitated the contact with my current supervisor, and helped in preparing materials.

The current research thesis would not be possible to be accomplished without certainly helpful guides and advice on different technical and practical aspects. Therefore, hereby I very much appreciate the kind consultancy and help from John Wedderburn (ceramics processing lab technician, gas adsorption and mercury porosimetry tests), Katy Lewis (ceramics lab safety advisor and catalyst and particulate technician), Paul Stanley and Theresa Morris (manger and technician respectively at the Centre for Electron Microscopy), Louise Male (X-Ray diffraction facility officer at School of Chemistry), and Jane Harris (laboratory manager at Earth Sciences & Geography).

Helps and advice from other people in both of the schools (Chemical Engineering and Metallurgy and Materials) are also well appreciated including staff: Geoff Dolman (dilatometry), Rachel Bridson (laser diffraction size analysis), Samantha Jones (sintering), Jeff Sutton (XRD), and research students: Angela Murray, Tafadzwa Motsi and Stewart Welsh.

Finally, the last but definitely not the least, my deep gratitude to my parents and family who not only provided the amenities of living and studying throughout my life, but gave the warmest encouragements from the distance.

Contents

List of Figures

List of Tables

1. INTRODUCTION

1-1- Background

Ceramics are a class of materials broadly defined as *inorganic, nonmetallic solids*, which arguably provide the broadest range of functions of all known materials. They are synthesized as glasses, polycrystals, and single crystals, and in many forms dictated by their end use, including fine powders, monoliths, thin films, and composites. They are also frequently integrated with other materials in advanced structures and devices. Study of chemically and electrochemically active types of ceramics are considered as a separate topic in which fundamental research is particularly needed according to a National Science Foundation report [1]. Basic research on defects, electronic and ionic transport, crystallography, microstructure, surfaces, and interfaces all have impact on advanced ceramics used in some areas such as heterogeneous catalysis. With the exception of glass, ceramics manufacturing has historically been based primarily on powder processes. The basic fabrication steps consist of powder synthesis, powder forming, and sintering. An important role of basic research is to address the chemical and physical phenomena involved in each of these steps.

The kinetics of solid state chemical reactions in manufacturing of ceramics material is generally limited by the rate at which the reactants are able to diffuse across the phase boundaries and through intervening product layers; therefore conventional techniques usually require processing temperatures high enough to overcome kinetic constraints. However, such temperatures usually lead to formation of coarse-grained reaction products due to grain growth, which are generally undesirable for advanced engineering ceramics due to poor

sinterability and mechanical properties. The apparent necessity for high processing temperatures in solid state synthesis reactions can be avoided through the use of mechanochemical processing, which simply entails high-energy milling of a reactant powder mixture [2].

Mechanochemistry, first defined by Ostwald in the late 19th century, originated from industrial phenomenology, in other words, from mineral processing and the related practices of comminution and grinding. Tribochemistry, or impact chemistry, came from different origins but deals with similar subjects, and nowadays both expressions are unified as mechanochemistry [3]. Mechanochemistry has had a rich history which has led to the use of ball mills for processing a wide range of materials, ranging from minerals to advanced materials. An important feature of mechanochemical processing (MCP) is the refinement of microstructure [4]. In contrast to coarse grinding and even fine grinding, the objectives pursued by mechanical activation are not simply particle size reduction but changes in the structure, produced by mechanical energy, because they determine reactivity. In fact, deep stages of activation substitute fine grinding when the size of particles approaches the grinding limit. The mechanochemical processing and synthesis has attracted interest since the early 1980s for the production of metal and alloy powders. Whereas less attention has been paid to ceramic systems, the method has been investigated for the preparation of several oxide, carbide, nitride, boride, and silicide powders [5, 6].

Cordierite (a magnesium aluminium silicate) is widely used in glass–ceramic compositions for manufacturing multilayer circuit boards, catalytic converters, filters, kiln furniture, thermal insulation materials, etc. Cordierite has traditionally been used in those applications (many of which it can substitute alumina for advantage) requiring a low thermal expansion

coefficient (as low as 0.7×10^{-6} K^{-1}, 25–1000 ºC), low dielectric constant in the high-frequency region and high electrical resistivity as well as mechanical and chemical stability at elevated temperatures (Figure 1-1). Glass ceramics such as cordierite (dielectric constant: 5-6 at 1 MHz lower than that of Al_2O_3) offer certain advantages for use as packaging materials. Researchers at IBM have shown that addition of mullite ($3Al_2O_3.2SiO_2$) to cordierite allows tailoring of the thermal expansion coefficient of the composite, so that a composite consisting of 65 vol% cordierite and 35 vol% mullite has a thermal expansion coefficient matching that of Si. High thermal shock resistance and relatively high refractoriness of this material is advantageous in operating conditions such as severe exhaust environments at high temperatures [7, 8].

A variety of mixtures has been successfully used to synthesise cordierite, the most commonly employed being mixtures of clay (kaolin), talc and alumina or silica. A wide range of synthesis methods have been proposed in order to decrease the synthesis temperature, and improve the physical properties of cordierite. Production methods such as co-precipitation, sol–gel and solid-state synthesis have been investigated. The temperature required for complete transformation of components to cordierite via solid-state synthesis is generally higher than 1300 °C [8, 9].

It is well established that it is difficult to sinter pure cordierite bodies without any sintering aid. The use of sintering aids not only increases the thermal expansion coefficient but deteriorates the dielectric characteristics of cordierite. Therefore, polycrystalline cordierite ceramics with high strength, high density and low thermal expansion coefficient (TEC or CTE) of stoichiometric composition ($2MgO.2Al_2O_3.5SiO_2$), are difficult to obtain because of the very narrow, impurity-sensitive firing range of this compound [8]. Consequently, taking

into account the advantages of mechanochemical processing in ceramics powder synthesis, many researchers have shown the benefits of mechanical activation (such as simplifying the process, decreasing sintering temperature and time, achieving a homogeneous and high purity structure) in preparation of cordierite ceramics made of different precursor materials [8-15].

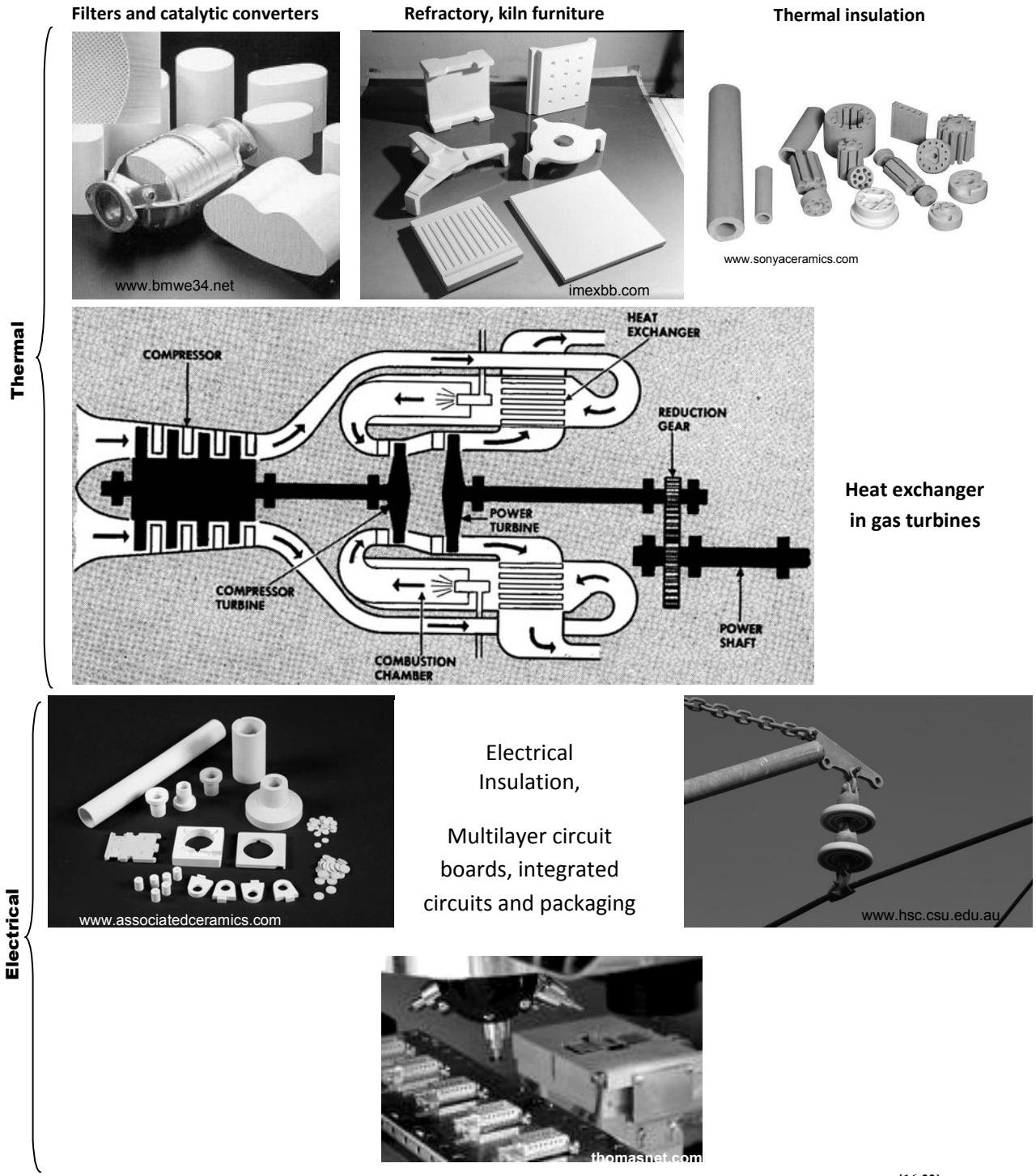

Figure 1-1: Most important advanced applications of cordierite ceramics in industry [16-22]

The improvement of diverse physical properties has already been demonstrated for variety of nanophase and nanocomposite ceramics obtained in the past decade. In fact, fabrication of composites is a common strategy to design a new substance with properties that cannot be achieved for a monolithic non-hybrid material. It is established that an introduction of special (transition metal) oxide additives improves the strength of ceramics. The cordierite system is particularly attractive for enhancement of mechanical properties by zirconia additions, because it has many potential applications, arising from its excellent thermal and dielectric properties. It has been shown that fine zirconia dispersions in ceramic matrices can affect the sinterability, there are investigations carried out to study the effects of ZrO_2 dispersions on the mechanical properties of cordierite [23-25]. On the other hand, rare earth elements manifest themselves as highly active substances and their oxides are excellent flux for sintering of ceramics. Ceria, CeO_2, is a common rare earth oxide with high melting temperature (2400 °C). An appropriate addition in the manufacture of advanced ceramics is used to promote sintering, thus resulting in stability and desirable modification of the microstructure. The activation energy of the glass containing CeO_2 for crystallization is lower than that of the CeO_2-free glass, therefore, crystallization properties could be enhanced [26, 27].

1-2- Objectives

Considering the basic research needs in the processing of the advanced ceramics such as cordierite, including microstructural and process thermodynamic studies, it was the aim of this research to investigate the effects of mechanochemical processing on the solid-state synthesis of cordierite and its derivatives. Several studies have been undertaken on solid-state synthesis of cordierite from hydroxide and natural silicates, moreover there are other researches concerned with the application of mechanochemical milling as a preparation step

prior to sintering. In this project, taking advantage of the advanced methods in microstructure analysis such as SEM-EDX, XRD and porosity measurements, it is intended to combine the studies of the effects due to the mechanochemical activation and addition of oxides of zirconium and cerium on sintering behaviour (microstructure, phase transformation and densification) of a cordierite mixture. For this purpose, investigation of three different dry milling methods as well as different sintering temperatures was considered in order to characterise different phases formed and the properties of the sintered material.

1-3- Organisation of the thesis

The main body of this thesis comprises 7 chapters. The introductory information about the topic of the research and its significance followed by the objectives (presented earlier) are presented in Chapter 1. Chapter 2, introduces the mechnochemical process and background theory, reviewing the relevant grinding methods with an emphasis on the activation process related advantages and applications specifically targeting the solid-state synthesis of ceramics. Chapter 3 reports on research related to the field of mechanochemical activation as well as cordierite sintering experiments wherein the effect of special additive oxides has been studied. The materials and methods are introduced in Chapter 4. Chapter 5 presents and discusses the findings and results of experimental programme. To conclude, Chapter 6 summarise major findings and gives the final discussion. Finally, a future outlook with recommendations for continuing further complementary tasks regarding this research is provided in Chapter 7.

2. MECHANOCHEMICAL PROCESSING

2-1- Mechanochemistry: theory

Severe and intense mechanical actions on solid surfaces are known to lead to physical and chemical changes in the near-surface regions where the solids come into contact under mechanical forces. These mechanically initiated chemical and physicochemical effects in solids are generally termed mechanochemical effects; a subject in which historically, researchers in tribology, wear, and geochemistry have shown great interest [28].

The theoretical considerations concerning the relationship between chemical and mechanical energy date back to the end of 19th century when F.W. Ostwald defined mechanochemistry as "a branch of chemistry dealing with the chemical and physico-chemical changes of substances in all states of aggregation". During the 20th century, an extensive accumulation of knowledge in the field of solid-state mechanochemistry was obtained when studying the influence of high pressure and combined action of pressure and shear on the phase transition in crystals and on the rate of chemical solid-state reactions. A short history about the development of mechanochemistry and early applications can be found in a paper by Boldyrev and Tkacova [29].

Mechanochemical systems behave as open non-equilibrium systems. The structure of all mechanochemical systems is hierarchic, heterogeneous, self-consistent and is controlled by the principle of the minimum entropy production (Prigogine, 1945). Therefore, analysis of the mechanochemical processes requires the use of non-equilibrium thermodynamics methods. The large majority of mechanochemical reactions in which solids take part occur in surface layers at the interface and these reactions are all heterogeneous in nature. It is well known that

the linear dependence of the Gibbs free energy on pressure (P) for solids is satisfactorily conserved in the experiments up to super-high pressures. This is because the expansion of the volume in terms of pressure value, V(P), in the equation of state is primarily defined by the zero order term due to low compressibility of condensed phases. In other words, the linear character of the chemical potential (μ) dependence on pressure results from the following expression [30, 31]:

$$\Delta\mu = \int_{P_1}^{P_2} V(P)dP = \int_{P_1}^{P_2} V_0 \exp(-\chi P)dP \cong V_0\Delta P \qquad (2\text{-}1)$$

where V_0 is the initial volume. Since the compressibility coefficient for solids, χ is ≈ 10^{-6} and $\chi P \ll 1$, the exponents in the above equation can be expanded into series confined to the first two terms; therefore for the substance under excess pressure (ΔP), the chemical potential will be [30]:

$$\mu = \mu_{\Delta P=0} + \Delta P V_m \qquad (2\text{-}2)$$

where V_m is the molar volume of the substance. According to the definition of the thermodynamic activity at ΔP=0,

$$\mu = \mu_{\Delta P=0} + \Delta P V_m = \mu_0 + RT ln a + \Delta P V_m = \mu_0 + RT ln \bar{a} \qquad (2\text{-}3)$$

where μ_0 is the chemical potential in standard state. The quantity ā is called *mechanochemical activity* (Gutman 1967) and is found from the following formula [30]:

$$\bar{a} = a\, exp\frac{\Delta P V_m}{RT} \quad \text{or the corresponding coefficient: } \bar{f} = f\, exp\frac{\Delta P V_m}{RT} \qquad (2\text{-}4)$$

where $\Delta PV_m = \Delta\mu_0$, and taking into account the relationship c=a/f, between thermodynamic activity, a, activity coefficient, f, and amount/concentration of substance, c.

As indicated by equation 2-4, when the thermodynamic activity (a) decreases, i.e. when the concentration of the mechanically activated atoms decreases, mechanochemical activity can increase if the increase ΔP is sufficiently large. Thus, the mechanochemical activity is determined by the level of the chemical potential, and the mechanical factor (ΔP) increases the mechanochemical activity (ā) and not thermodynamic activity (a). As also indicated by equation 2-3, the increase of the chemical potential of the substance as a result of the mechanical effect (at a= const) is caused by an increase of the standard chemical potential (μ_0) by the value ΔPV_m.

There is a significant body of information available almost exclusively in the mineral processing literature that gives detailed description of the machine and operating parameters on the grinding rates of minerals and ores. In case of ball milling, for example, studies have shown that particles caught between the colliding balls experience stresses of several GPa. These particles go from the completely stress-free state to these high-stress conditions within a very short duration (only tens of microseconds). Therefore, the rate of change of stress is enormously high. Further, the effective collision energy (total collision energy minus that dissipated as heat, sound waves, etc.) is exerted over a small area of contact between the grinding media. The so-called highly transient and localized "hot spots" are created in the region of contact points where temperatures are high enough to cause atom mobility in the near-surface regions. When particles become very fine (of the order of 1 μm), even brittle materials such as silica are known to undergo plastic deformation, indicating higher atom mobility in the near-surface regions [28]. A review of several models investigated in the study of mechanochemistry is provided by Balaz [32].

In grinding mills used to grind feed materials for several tens of hours, the number of collisions in the mill can be astronomical. Further such mills are known to run very warm, with the mill contents heating up to over 200 °C in some industrial mills used for batch dry grinding up to 20-30 hours. In such conditions, particles are possible to be heated in the range of Tammann temperatures of the material (a rough temperature limit above which time- and load-dependant plastic flow or rupture is expected [33]), and as a consequence any physicochemical change in the solid state namely decomposition, synthesis, polymer chain degradation, phase transformation, and crystalline-amorphous transformation, are quite feasible [28].

As grinding proceeds into the ultrafine region, conditions that are of little significance during normal operations, gradually become controlling parameters in the process. These conditions are mainly increasing resistance to fracture and increasing tendency to aggregate. In the milling process, the reduction of particle size terminates at a size called "grind limit" which depends on material properties, the type of the milling device used and operating conditions, such as milling time. Factors responsible for more resistance to fracture in the fine grinding condition would include [34]:

- Increase of the relative strength of the particles as they decrease in size (decrease of probability for crack initiation)
- Shielding of smaller particles from impact by larger ones (screening effect)
- Agglomeration of the smaller particles (reduction of specific surface energy of the particulate system

The activation free energy of the comminuted material, gained by the increase of specific surface energy and stored elastic strain energy can be dissipated by different ways of energy transitions. The surface activation can be relaxed as the newly exposed fracture surfaces are

becoming active to the extent that agglomeration or adsorption of environmental gaseous species and moisture takes place. The bulk activation can be relaxed by fracturing of brittle materials, or otherwise by crystallographic lattice rearrangements in the polymorphic transformation, mechanical alloying (of solid-solution), mechanochemical decomposition or synthesis [34].

During preliminary mechanochemical treatment, the main reason for the reactivity changes is fragmentation of a solid and formation of new surfaces. As activation continues (beyond the grind limit or the critical size) generation of various defects in materials during mechanochemical processing is considered as one of the main reasons for changes of the reactivity. The formation of defects is also characterized by non-equilibrium conditions; therefore, solids after mechanical treatment should be regarded as metastable. The plastic deformation of a solid can be regarded as one of the methods of energy storage in solids and therefore can be recommended as one of the methods of producing metastable states. It follows that the treatment of a solid by short but powerful mechanical pulses can be regarded as one of the methods of producing an "active" or "metastable" state of solids. The mechanical metastability is different from other methods of producing metastable states (such as freezing or melting, chemical reaction and irradiation) in that it can result in any of the three basic types of metastability: morphological, structural and compositional [35].

According to the theory of the active state of the matter (developed by Fricke and Hüttig (1943)), an activated solid is formed of a thermodynamically and structurally metastable arrangement of lattice elements. Such a state is defined by thermodynamics in terms of the difference in Gibbs free energy, ΔG, between activated and equilibrium states as:

$$\Delta G_T = G_T^* - G_T = (H_T^* - H_T) - T(S_T^* - S_T) \xrightarrow{at\ room\ temperature} \Delta G_T \cong H_T$$

in which starred letters indicate activated state, H_T, S_T and T are enthalpy, entropy and absolute temperature respectively. The excess enthalpy increment of the particulate solid can be determined either from the difference between molar heat capacities, or from the difference in heats of dissolution of the solid in the activated and equilibrium states [36]. According to the results of application of the common calorimetric method for determination of the heats of dissolution of ground magnesite ($MgCO_3$), Figure 2-1-a, the heat of dissolution increases linearly with the amount of carbonate dissolved, however the slope of the line increases with increasing the amount of activation energy consumed.

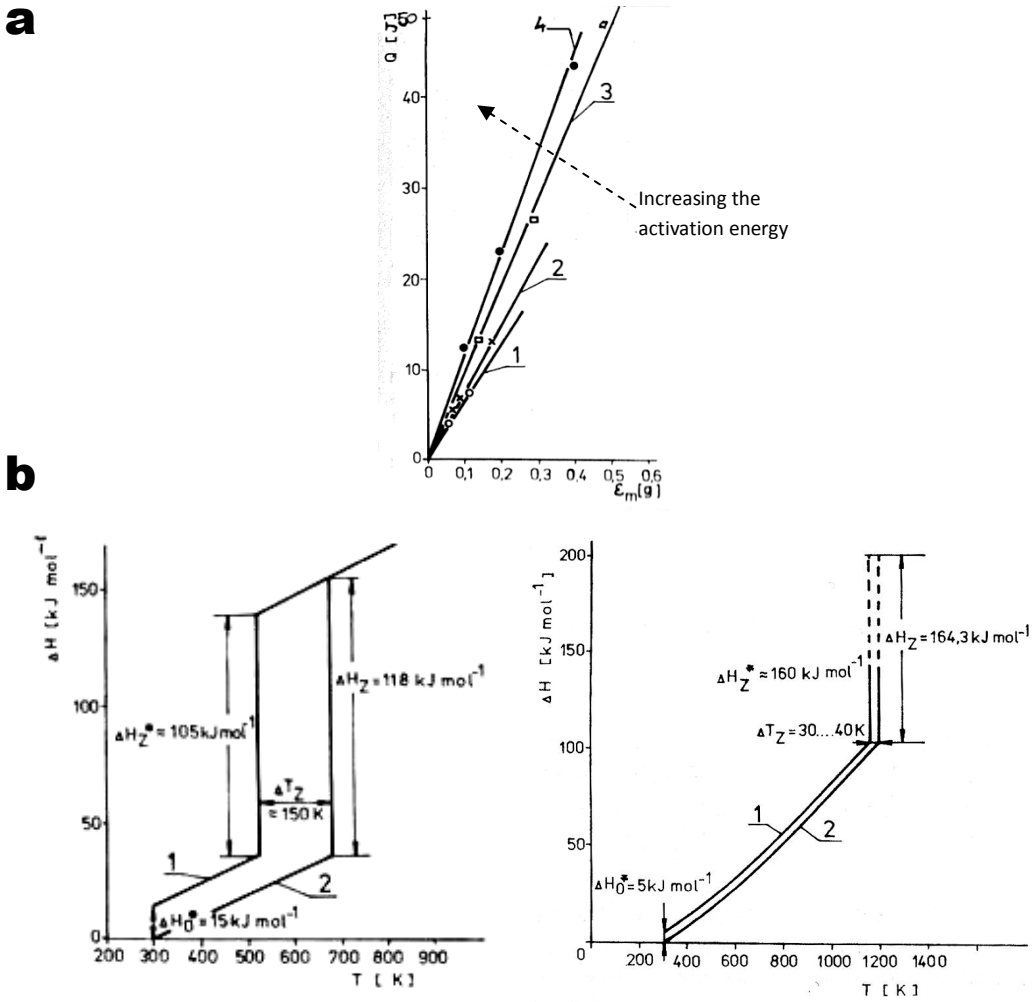

Figure 2-1: a) Heat of dissolution (Q) of various amounts (ε_m) of mechanically activated/ground magnesite; b) Enthalpy changes (ΔH) versus temperature (T) during decomposition of activated, "1", and non-activated, "2", carbonates (left diagram: magnesite; right diagram: calcite) [36]

Moreover, when the enthalpy changes during thermal decomposition of activated and non-activated samples of magnesite and calcite are compared, there is a much greater decrease of the decomposition temperature of magnesite (Figure 2-1b, left) compared to calcite (Figure 2-1b, right); this arises to some extent from the fact that calcite is less affected by activation compared to magnesite.

2-1-1- Grinding methods for mechanochemical processing

There are three main types of milling devices used for the purpose of mechancohemical processing based on the mechanism of grinding action [29]:

1. The mills of shock action: fluid energy or jet mills, turbulent mills, and high peripheral-speed pin mills. In these devices mechanical action is produced as a result of the collision of a particle, accelerated to high speed in gas jet, with a target (jet mills), or, conversely, as a result of the collision of the moving solid blade with the particles (high peripheral-speed pin mills or disintegrators).
2. The devices of shear action such as roller mills. Here, mechanical action is produced by a shift when one solid surface moves across another, the substance under treatment being placed on the latter.
3. Ball mills of various kinds, planetary and vibration devices, mixer mills such as Spex mill. In these devices, mechanical action occurs due to pressure and shear. The relation between pressure and shear can be varied over a wide range, depending on construction features of a mill and its operation regime.

It is not intended here to describe different milling apparatus or mechanisms, and more information on the application of grinding machines used for mechanochemical purposes can be obtained elsewhere [37, 38].

2-1-2- Special considerations about hydrated oxides

Since all of the three main precursor powders used in this study are either natural or synthetic hydrated oxides/silicates, it is worth discussing what special features and possible advantages are provided by such compositions during mechanochemical preparation. Hydroxides (among other compounds such as carbonates, chlorates, nitrates) can be decomposed under mechanical stresses. Enhanced reactivity of solids during structural change and phase transformation is known as the Hedvall effect II which seems to occur in the course of mechanical treatment of solid mixtures. Hydroxides which easily transform under mechanical stress, are therefore often superior to oxides as a starting material for solid-state reactions [3].

While some hydroxides such as bauxite, $Al(OH)_3$, or oxyhydroxides such as boehmite, AlO(OH), and goethite, FeO(OH), are quite easily dehydrated during grinding, crystalline hydroxides are not always very sensitive to mechanical stress. An example is the persistence of crystalline magnesium hydroxide, $Mg(OH)_2$, after prolonged grinding in the absence of silica particles (which would otherwise facilitate ion-exchange reaction under conditions of mechanical stress and presence of hydroxide) [39, 40]. Most of the chemisorbed water molecules or residual hydroxyl groups on the activated surface could easily change into their activated state which is characterised by excess polarization due to unsaturated coordination of the substrate atoms caused by local plastic deformation and structural imperfections created under the influence of shear stress. All these reactions containing water molecules do not require a high energy density; a relatively small shear stress would suffice to promote the polarisation and atomic exchange at the interparticle contact points. The mechanochemical processes involving hydroxides are sometimes referred to as “soft mechanochemical synthesis” which could control the various properties of the products, particularly when a preliminary mechanochemical treatment is coupled with a subsequent or simultaneous heating process.

These rather new routes of fabricating complex compounds could find their application in a large number of fields of advanced materials [40, 41].

Soft mechanochemical processes have many common features with other well-known and widely used methods, such as co-precipitation and hydrothermal synthesis. In fact, co-precipitation allows components to be mixed at an atomic level, and almost the same process is realized by mechanical activation of mixtures of hydroxides and hydrated oxides. Formation of water (as a reaction product) and local heating under mechanical activation as a result of collisions, friction and plastic deformation of solid particles give rise to the conditions for the reactions to occur via a dissolved state (hydrothermal-like synthesis) [37].

Although, no such reaction (to create a new composition) is expected to happen among the three main constituent minerals during mechanical activation in the current experiments, there are many studies undertaken to evaluate the effects of grinding on hydrated silicates such as clay minerals, and more extensively on kaolinite [42-45] and talc [46-49]. These studies conclude that intense mechanochemical effects occur during prolonged grinding, leading to the destruction of the laminar structure of those substances and hence, amorphisation takes place. There is a critical grinding time from which a reaggregation process among particles starts through adhesion forces. Grinding also increases the reactivity of such powders. Therefore, it would be both interesting and important to study those effects in a mixture of different minerals, such as happens in the current study.

2-2- Mechanochemical effects: activation or reaction

The term mechanical activation, introduced by Smécal (1952), is regarded as a process involving an increase in reaction ability of a substance which remains chemically unchanged;

however, it is also considered as a multi-step process that unites the four processes: accumulation of defects, amorphisation, formation of metastable polymorphs and chemical reaction. Structural relaxation plays an important role in mechanical activation, and occurs via different channels such as production of heat, formation of new surface, plastic deformation, aggregation, adsorption, etc.; therefore its rate is quite variable [29, 32].

It has been found to be rather important to clarify the two most applied expressions related to the application of mechanochemical processes. As one might come across "mechanochemical synthesis" quite extensively through the literature to refer to almost every process involving mechanochemistry in materials treatment processes, it is not the same with "mechanical or mechanochemical activation". Mechanochemical synthesis which presumably refers to the occurrence of a reaction during mechanical process (e.g. preparing polymers or composites), is also the term used by some authors for those processes in which the actual reaction between the main components takes place after subsequent treatment (such as heat processing). For the purpose of the mechanochemical preparation of oxide/hydroxide materials in this research, while structural modifications such as plastic deformation, development of the defects and dehydration are likely to occur during the mechanical process, polymorphic transformations and chemical reactions between the individual compositions which constitute the mixture are not expected to happen. Therefore, the author prefers to use the term "activation" to put more emphasis on the microstructural modifications caused by intensive mechanical action.

Mechanochemical processes (MCP) use mechanical energy to activate chemical reactions and structural changes. Referring to the applications of MCP or its effects on the materials, three different types of processing are recognised: mechanical milling (MM), mechanical alloying (MA) and reaction milling (RM) [4, 50]. During the application of the last two types of

mechanochemical actions, solid-state reactions accompanied by formation of one or more product phases are expected. However in the first type (MM), which could be regarded as the target in this research, the refinement of microstructure including particle size, shape, surface and bulk properties and at the most extent, amorphisation and formation of metastable phases are generally the main goals. But the boundary between the mechanical activation and mechanochemical reactions is diffuse, since both of them involve common physicochemical changes of solids under the influence of mechanical energy [3].

In the broadest view, mechanochemical processing could result in any or a combination of the following effects [51, 52]:

- Disintegration, formation of new surface or surface aggregation
- Plastic deformation and formation of lattice disorder and defects
- Polymorphic transformations and alterations in physical properties of the bulk phase
- Mechanical activation and changes in solid surface properties
- Recrystallisation, decrystallisation or amorphisation
- Mechanochemical solid state reactions (decomposition, ionic change, oxidation-reduction, etc.) either at the surface or in the bulk

High-energy milling can provoke chemical reactions that are induced by the transfer of mechanical energy; this has been applied advantageously in the preparation of magnetic oxide-metal nanocomposites via displacement reactions in the so-called mechanical alloying process. The nature of such reactions depends on thermodynamic parameters, the microstructure of the reaction mixture, and the way the microstructure develops during the milling process. The interest in such processes to produce nanocrystalline materials is due to the simplicity of the method and the possibility for scale-up manufacturing [53].

Aluminosilicates of alkaline earths such as cordierite ($Mg_2Al_4Si_5O_{18}$) are widely used as initial raw material in ceramic materials science. They are the components of feldspars in natural resources, and their structure consists of chains composed of four-membered rings of SiO_4 and AlO_4 tetrahedrons elongated along the crystal's C axis. As a rule, they are synthesized by solid-phase methods from ordinary or complex oxides by heating the mixtures at high temperatures (1100 – 1400 °C) for a long time (100–185 h). Therefore, mechanical activation of the mixtures of precursor hydrated oxides, while not leading to the formation of new phases, provides good mixing at the cluster level giving aggregates that form cordierite during the subsequent thermal treatment. This is the method that can open a new way of synthesising complex oxide materials, since initial complex formation via a mechanical route can be done quickly enough under gentle conditions when a starting mixture contains ingredients with hydroxyl groups or water [3, 37].

2-3- Mechanochemical activation: advantages and applications

Mechanical treatment of organic and inorganic solids has become extremely important in many processes in chemical technology, materials science, ore dressing and various other fields including food, paint, ceramic, metallurgical, cement, pharmaceutical and plastics industries. It has been shown that mechanical activation substantially increases the kinetics of solid-state chemical reactions, such as oxidation-reduction reactions. As a consequence, reactions that require high temperatures to occur, due to the separation of the reacting phases by the product phases, will occur at low temperatures in a mill without any need for external heating. It is also known that mechanically stimulated synthesis can be performed at temperatures up to 50% lower than those in conventional synthesis routes. One can encounter situations when traditional synthesis of a compound is impossible whilst mechanically

stimulated synthesis (e.g. by changing the reaction temperature) makes the synthesis possible [4, 50, 51].

The principal attributes of mechanochemical processing include mineral and waste processing, metals refining, combustion reactions, ultrafine powder production, production of a fine dispersion of second-phase particles, extension of solubility limits, refinement of the matrix microstructure/nanoparticle formation, synthesis of novel crystalline phases, formation of amorphous phases, the possibility of alloying difficult-to-alloy elements, and scaleability [4]. Some examples of the most important applications/advantages of mechanochemistry in the fields of minerals and materials processing are summarised below [30, 51]:

- Preparation or regeneration of drilling mud, and production of drill-hole cementation mixtures
- Production of special concretes and other building materials
- Simplifying the production of cement by milling the reactants (lower furnace temperature and reaction time)
- Grinding of clinker (improvement of compressive strength and reduction of the setting time of concrete)
- Production of diphosphate
- Increase of fertilizer reactivity
- Simplifying or improving parameters of further processing of a product; increasing efficiency of separation/reaction by changing the properties of the mixture
    - Activation of flotation feed
    - Activated sintering of powders
    - Activation of ore concentrates, i.e. intensification of dissolution and leaching processes

      (e.g. to separate titanium from Ti-containing magnetite ore followed by heat treatment and dissolution in acid)

    - Activation of raw mixtures for glass making (lowered processing temperature)
    - Activation of foodstuffs, raw meal and flour
- Mechanical alloying
- Processing some secondary materials (which could not be used in classic technological systems) to high quality industrial materials

  (e.g. mechanical regeneration of spent hydration catalysts)
- To process materials from initial sources that cannot be or difficult to process by other methods

  (e.g. transforming apatites of low quality to fertilizers of approximately the same efficiency as superphosphates)
- To carry out certain high temperature reactions with acceptable rates at normal pressure
- To combine two or more technological processes

  (e.g. simultaneous refining, activation and mixing in the production of filled polymers during mechanical activation)
- To produce a product of higher quality or with newer properties by mechanical processing of initial or intermediate products
- To produce materials with unique properties which cannot be obtained by other methods

Through the last two decades of the 20th century, mechanochemistry of dispersed solids has made a significant contribution to the development of novel, high-performance, and low-cost materials and to development of novel technologies. Attempts were made to apply mechanochemistry to pharmacy, synthesis, and preparation of catalysts and manufacture of pigments. Mechanochemical procedures can also be considered environmentally friendly for bringing the following advantages in comparison with the traditional technological procedures [29]:

- Decrease in the number of technological stages. Simplification of the process;

- Ecological safety of the method, resulting from excluding the operations that involve the use of solvents, intermediate fusion, etc.;
- The possibility of obtaining a product in the metastable state, which is difficult (or impossible) to obtain using traditional technological methods.

Mechanochemistry is a promising branch of solid chemistry for achieving "Green Chemistry" goals too. Some practical examples of the mechanochemical processes related to principles of *green* chemistry - chemical research and engineering that encourages using products and processes that minimize the generation of hazardous substances- are as following [50]:

- Mechanochemical degradation of pollutants
- Mechanochemical syntheses of some functional materials (like pigments)
- Nanocomposites formation
- Biomaterials synthesis
- Catalysts synthesis

In the organic materials science, apart from solely organic processes such as esterification, oxidation, acid neutralisation, acylation, modification of polymers, etc., where mechanochemical methods have provided significant advantages [54], production of organic-inorganic hybrids and polymer nanocomposites are considered as the most important processes wherein mechanochemistry can be involved. One significant area of research and application in organic-inorganic hybrid materials is the manufacture of organically modified clays (organoclays) that not only have their own diverse uses in industry (as adsorbents of organic pollutants in soil, water and air; rheological modifier in paints, cosmetics, refractory varnish, drug delivery, etc.) but also they are considered as functional fillers essential to develop polymer nanocomposites, which is also one of the most developed areas in

nanotechnology. Mechanochemical surface modification by polymer grafting (applicable in water and organic media) induces a compatible layer on particles by means of chemical adsorption. Application of such methods to improve mechanical and fluid properties of plastics filled with modified calcium carbonate and also the rheological properties of paints with modified titanium dioxide has proved to be successful [55, 56].

The use of organoclays as precursors to nanocomposite formation has been extended into various polymer systems (thermosets and thermoplastics). The intercalation chemistry of polymers when mixed with appropriately modified layered silicates has long been known. For true nanocomposites, the clay nanolayers must be uniformly dispersed and exfoliated in the polymer matrix. Once nanolayer exfoliation has been achieved, the improvement in properties can be manifested as an increase in tensile properties, as well as enhanced barrier properties, decreased solvent uptake, increased thermal stability and flame retardance [57, 58].

According to the literature [59-61], mechanochemical polymerization has proved very useful as a surface modification method of inorganic powder fillers to be incorporated in polymer matrices where the mechanical process helps to achieve homogeneity in the solids dispersion. Problems such as thermal degradation and instability as well as non-melting properties of some polymers, which exist in some traditional processing methods, also add to the applicability of mechanochemical in-situ polymerisation as a low temperature and solvent free reactive milling operation in the synthesis of composite materials.

2-3-1- Mechanochemical activation in solid-state synthesis of ceramics

In ceramics manufacturing, solid-phase reactions are usually activated by high-temperature treatment; however, the practical efficiency of this process is rather low due to the low diffusion rate through a product layer, no tight contacts between the particles of components,

a non-uniform particle size distribution, etc. Therefore, the search for new methods to enhance solid-phase reactions is frequently carried out. Among the various methods (such as self-propagating high-temperature synthesis or application of shock waves) developed and used for this purpose, mechanical activation of mixtures in a grinding apparatus has become more widely used due to its relative simplicity and availability. Grinding enhances the chemical reactivity of powders. Rupture of bonds during particle fracture and deformation results in surfaces with unsatisfied valences. This, combined with the generated high surface area favours reaction between mixed particles and their surroundings [6, 37].

The best way to show how mechanochemical processing could be of benefit in the ceramics synthesis is through examples from practice. In a research study [62], an alumina–zirconia nanocomposite powder was synthesised by mechanical activation of a dry powder mixture of $AlCl_3$, $ZrCl_4$ and CaO. Mechanical milling of the above raw materials under the adopted conditions resulted in the formation of a mixture consisting of crystalline CaO and amorphous aluminium and zirconium chlorides phases. There was no sign of chemical reaction occurring during milling stage when evaluated by X-ray diffraction (XRD) studies. Subsequent heat treatment of the milled powder at 350ºC resulted in the occurrence of a displacement reaction and the formation of ZrO_2 and Al_2O_3 particles within a water soluble $CaCl_2$ matrix.

In other work, high-energy ball milling has been employed for mechanochemical treatment to enhance the solid-state reaction of TiO_2 and ZrO_2 to form $ZrTiO_4$. This occurred (according to the results obtained from Raman scattering, XRD and HRTEM studies) because the formation of $ZrTiO_4$ seeds had already started during milling, while the rest of the sample was the mixture of amorphous material, comprising nanosized TiO_2 (II) and nanosized m-ZrO_2 [63]. Other examples from study of mechanochemical synthesis in preparation of ceramic

composites include the work by Hwang and Lee [64], where they made nanocomposite powders of Cu–Al_2O_3 by high-energy attrition milling of precursor powders at room temperature, as well as the study by Zyryanov and Kostrovskii, in which ceramic powders of the composition $Zr_{0.88}Sc_{0.1}Ce_{0.01}Y_{0.01}O_{1.955}$ with an improved quality for the use as solid electrolytes in fuel cells were prepared by the mechanochemical synthesis from nanoprecursors [65].

Cordierite ceramics in industry are usually obtained by calcination of the mixtures containing talc, kaolinite and silica at 1300-1450 °C for 20-60 h. The product contains the impurity phases such as spinel, mullite, clinoenstatite, etc., that reduce the performance characteristics of cordierite. Mechanical activation of this mixture does simplify the interaction between the powder components, and hence it could be sufficient to heat the activated mixture for 2 h at a temperature of 1260 °C to obtain practically homogeneous cordierite without the impurity phases [37].

3. REVIEW OF SOME STUDIES REALTED TO CORDIERITE SINTERING AND USE OF DOPANTS

3-1- Synthesis of cordierite - general

Considerable work has been reported on conventional processing of cordierite material. The most common method to synthesize cordierite is the high temperature reaction in the solid state. Sintering of oxide powders through solid state reactions or crystallization of glass powders is by far the most popular method [66]. However, several difficulties have been encountered in solid-state reactions, namely sintering temperature and poor mechanical properties, which have prevented its widespread applications. So it is difficult to sinter pure and dense cordierite without employing sintering aids. One of the non-conventional chemical routes developed to overcome the above difficulties and to produce pure and crystalline cordierite powders is the sol-gel technique. Many authors have described the synthesis of nanocrystalline cordierite by sol-gel methods in the early nineties such as the work by Kikuchi *et al*. [67] or a more recent works by Yamuna *et al.* [68], Zhang *et al.* [69], and Mu-Tsun [70].

Extensive work has also been carried out by many authors in using natural mineral resources as the raw material for the preparation of cordierite [9, 12-14, 71-74]. In this respect, the following mixtures have been tried in the preparation of cordierite [9]:

- Simple compounds like oxides, hydroxides and carbonates
- Double compounds like clays, talc, sepiolite, spinel, mullite, forsterite
- Triple compounds (containing MgO, Al_2O_3 and SiO_2 all together) such as chlorite

Stoyanova *et al.* attempted to prepare mullite-cordierite like catalyst supports by precipitation of boehmite in an aqueous suspension of clay minerals in presence of MgO at 1150 ºC. In their research, the effect of the preparation procedure and higher homogeneity obtained by using co-precipitation on better dispersity of the precursors and lower formation temperature of cordierite as well as improved structural and textural characteristics of the resulting supports were established [71]. Elsewhere, high temperature solid-state reactions of precursors (talc and kaolinite) were applied in synthesis of cordierite liners for casting applications. In this research [75], Trumbulovic *et al.* showed that cordierite possessing suitable mechanical and thermal properties can be sintered easily from inexpensive raw materials.

Using thermodynamic analysis, Logvinkov *et al.* [76] investigated the possibility of purposeful synthesis of corundum-mullite-cordierite refractories by a single-stage method from talc-kaolin- alumina raw compositions. The aim of the research was to calculate the stoichiometric proportion of the raw ingredients and to evaluate the thermodynamic probability of synthesis of just the specified phases with a predetermined cordierite-to-corundum ratio. It has been found that although the probability that cordierite would exist in the entire temperature range is high; it is difficult to obtain "pure" cordierite in the manufacturing process.

Yamuna *et al.* studied the potentiality of kaolin-based cordierite as catalyst supports in air pollution control. They applied both conventional and sol-gel methods as well as property evaluations using different physical, mechanical, thermal and microstructural analyses. Finally the mixture containing fine (<40μ) kaolin and talc, after 24 h of ball milling and compressing sintered at 1350 ºC/ 3 h, gave single-phase cordierite and presented low coefficient of thermal expansion and good compressive strength as well as good extrudability for production of honeycomb structures [68].

3-2- Synthesis of cordierite - mechanochemical processing of precursors

In recent research by Yalamac and Akkurt [9], mechanochemical processing was applied in the synthesis of cordierite made of the required amounts of kaolin, talc and gibbsite. Statistical techniques were used to understand the effects of process variables on the amount of synthesized product. The cordierite mixture was completely amorphised by grinding in their experiments, and ultimately the mechanical amorphisation in combination with magnesium borate addition as mineraliser decreased the sintering temperature down to about 1000 °C. Tamborenea and co-workers [13] studied the effect of amorphisation of talc, clay and gibbsite by grinding on cordierite formation. They found significant differences in thermal behaviour of the activated and non-activated samples during DTA-TG analysis. These differences in the temperature range 1200–1360 °C proved some variations exist in the sequence and direction of the reactions within the two samples. Formation of intermediate phases in the amorphised mixtures was found responsible for different reaction mechanisms. Finally, structural modifications produced by milling resulted in the formation of cordierite as the equilibrium phase at lower temperatures.

The effect of intensive ball milling on rheological behaviour of concentrated aqueous dispersions of kaolin-talc-alumina mixtures was studied in the work by R.Neto and Moreno [12]. In their research, the high speed planetary milling process up to 45 minutes, though not significantly changed the rheological properties of the mixture, served to decrease the amount of pores and result in highly dense structures. Above 1280 ºC, the cordierite phase was practically the only phase detected in the activated samples, whereas in the unmilled powder other phases such as coarse silica existed even up to 1350 ºC.

Elsewhere, the influence of mechanical activation of the component oxide mixture on electrical properties of the sintered cordierite bodies was investigated in the work of Dordevic and Jovanic [11]. They found that higher amounts of indialite (hexagonal cordierite) are formed at sintering temperature 1100 ºC in the mechanochemically activated samples than in the unmilled material. They also indicated that the mentioned amount increases considerably as the sintering temperature increases from 1100 ºC up to 1300 ºC. The obtained results proved the positive influence of activation time on the formation temperature of cordierite ceramics, with no significant changes in electrical properties of the product.

3-3- Effects of zirconia and ceria additives during processing of cordierite ceramics

Dispersion toughening of oxide ceramics by a zirconia second phase is a well-established process and has been successfully employed to improve the mechanical properties and sinterability of alumina, mullite, spinel and cordierite. Toughening mechanisms such as stress-induced transformation toughening, microcracking and crack deflection have been found to be responsible for improvement of the mechanical properties of such composites, as a result of the volume expansion associated with the tetragonal to monoclinic transformation in zirconia structure. Assuming that the zirconia is retained in the metastable tetragonal phase, the ZrO_2 particles are transformed into the stable, monoclinic phase in the stress field near a crack tip; since the crystals can be kept small (Figure 3-1) and still be transformed, the inherent flaws that they introduce are also small, and the strength of the material is thereby increased. The attainable toughening is dependent upon the volume fraction of transformable tetragonal phase, size and distribution of the zirconia particles, the elastic constraining properties of the matrix and the size of the transformed zone around the crack. Two

conventional routes that have been followed in investigation of the effects of systematic zirconia additions on cordierite ceramics are glass ceramic processes and solid-state synthesis using either sintering or hot pressing of powders [8, 77-79].

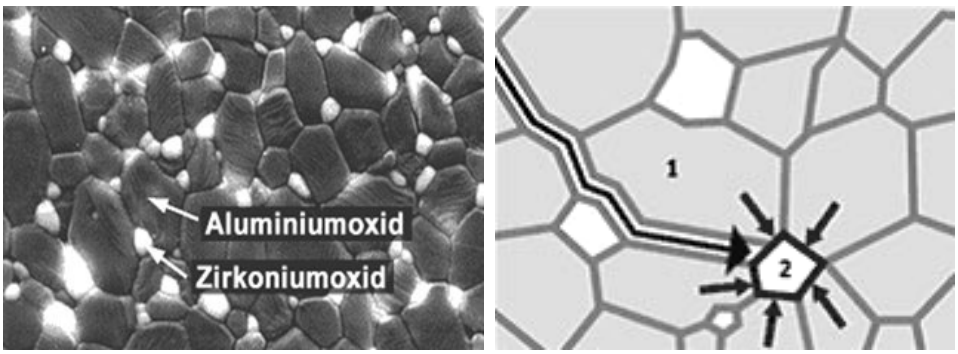

Figure 3-1: a) Microstructure of the zirconia toughened alumina (~ 20 wt% ZrO_2), b) Homogeneously distributed zirconia particles prevents the initiation or propagation of cracks [80, 81]

In research by Costa Oliveira and Cruz Fernandes [8] where they investigated thermal and mechanical properties of sintered cordierite-based ceramic matrix composites containing dispersed particles of monoclinic ZrO_2 (added up to 40 wt.%) and clay–talc–alumina mixtures, it was found that thermal expansion coefficient (CTE), elastic moduli (E) and flexural strength (σ_r) were critically dependent on the mixing/milling conditions, the ZrO_2 content and the retained porosity. Elsewhere, Sun *et al.* [82] showed that ZrO_2 additions into a cordierite matrix affect the densification behaviour and mechanical properties of the composites. By dispersing 25 wt% ZrO_2 into a cordierite mix, a densified (up to 98.5%) cordierite/ZrO_2 composite was obtained under an optimised sintering condition of 1440 ^oC / 2h. Both fracture strength and toughness were enhanced with increasing ZrO_2 content, and the toughening mechanisms were mainly attributed to martensitic transformation toughening.

There have been some discussions about the possible superiority of cordierite-zircon ($ZrSiO_4$) composite structure over the cordierite-zirconia composition. In all of those attempts that the dispersion of ZrO_2 phase in another ceramic matrix has been used to improve mechanical

properties, there was no significant improvement of mechanical properties and sinterability until the dispersed amount of ZrO_2 was more than 6 vol%. Moreover, since there is a large thermal expansion mismatch between ZrO_2 (10×10^{-6}°C^{-1}) and cordierite matrix (1.5×10^{-6}°C^{-1}), microcracks that are introduced to a matrix during the sintering process always link up during heating and cooling cycles; therefore, the addition of ZrO_2 is likely to have deleterious effects on the thermal shock resistance of cordierite. In view of the facts discussed above, Sun *et al.* [83] proposed a solution to the problem by dispersing minute amounts of zircon substituting ZrO_2 into the cordierite matrix. Zircon not only possess lower coefficient of thermal expansion (4.1×10^{6} °C^{-1}) than that of ZrO_2, but also has generally high thermal shock resistance and chemical stability as well as relatively high Young's modulus with respect to the cordierite matrix. Finally, they concluded that the formation of zircon as a secondary phase might also help in densification of cordierite provided it is homogeneously dispersed into the matrix. This latter effect on densification is partly due to the role of zircon in glass phase formation when it exists in relatively low concentration (~ 2.5 wt%) [84].

In an earlier research by Travitzky and Claussen [85], cordierite-ZrO_2 composites containing unstabilised and Y_2O_3-stabilized ZrO_2 were sintered at temperatures between 1200 and 1400 °C for up to 48 h. In most cases at 1200 °C and 1300 °C, both types of composites reacted to form zircon and spinel when sintered for more than 24 h. When Y_2O_3-doped ZrO_2 composites were annealed at 1400 °C for up to 48 h, hardly any compositional changes took place due to the formation of $A1_2O_3$-SiO_2-Y_2O_3 inter-granular phase which acts as a reaction barrier between ZrO_2 and the matrix. Travitzky and Claussen have stated that at temperatures between 1300 °C and 1400 °C diffusion of Y into the glassy phase is considered responsible for destabilization of t-ZrO_2 and formation of a eutectic phase in the $A1_2O_3$-SiO_2-Y_2O_3 system. In the cordierite matrix, this was confirmed with SEM-EDX study of the boundary

phase around ZrO_2 particles composed of Y, Si, and Al elements. This has been confirmed for Y-TZP and mullite/Y-TZP ceramics too [85]. The transformability of zirconia inclusions in a cordierite matrix would be expected to differ from those in an alumina matrix as a consequence of thermal expansion mismatch and the presence of an amorphous phase at the grain boundaries. Zirconia is said to be thermodynamically unstable in the cordierite matrix at temperatures above ~1280 °C due to the reaction resulting in formation of zircon [77].

Cerium oxide (CeO_2) has attracted much attention, because of its many practical uses, such as chemical mechanical polishing media, automobile exhaust catalysts, additives in ceramics such as zirconium-toughened alumina to enhance sintering properties, and solid electrolytes in solid oxide fuel cells. Ultrafine powder is particularly important for many of these applications, because of its small size, high surface area, and improved sintering properties. Ceria and ceria-containing materials have been extensively studied owing to their applications in catalysis, solid oxide fuel cells and ceramics. Ceria and ceria–zirconia solid solution are used as important components of automotive three-way catalysts for reducing exhaust pollutants. Compared to ceria, the ceria–zirconia solid solution shows enhanced thermal stability, oxygen storage capacity and catalytic properties [86, 87].

Shi and coworkers have published several research papers on studying the ceria-cordierite system and its preparation through different methods including co-precipitation from alkoxides [88] and nitrate solutions [89], sol-gel [90, 91] and solid-state synthesis of precursor oxides [26, 91]. Research by Shi *et al.* [26], in which DTA analysis of a mixture of cordierite precursor oxides containing different amounts of ceria (2-10 wt%) was investigated, showed that the diffusion of Ce^{4+} as well as other metallic ions was found quite important during sintering process. It has been shown that CeO_2 as an additive in small amounts (2-4 wt%)

improves the ionic diffusion in solid state, that finally promotes conversion towards cordierite composition.

According to glass structure theory [26], Ce^{4+} belongs to glass network modifiers; although located at the interstitial point of glass network, Ce^{4+} also has a strong attraction to O^{2-} in the network. An appropriate amount of cerium in the liquid makes ionic diffusion easier and therefore facilitates nucleation and growth of cordierite at lower temperatures. On the other hand, excessive additions makes the network compact and does not reduce the liquid viscosity effectively, therefore it results in resistance to the diffusion of Si^{4+}, Al^{3+} and Mg^{2+}, and the rise of crystallization temperature.

In the late 90's, cordierite-zirconia-ceria (ceria-zirconia and yttria-ceria-zirconia) composites were prepared by sol-gel process in a work by Senguttuvan *et al.* In that research where the crystallisation behaviour of the material was investigated, it was observed that the cordierite-zirconia composite powders are crystallized as α-cordierite and tetragonal zirconia when sintered at a temperature above 1200 °C in the presence of zircon in the cordierite matrix. A dense cordierite-zirconia composite was obtained by sintering at 1300 °C [92]. There is also evidence in the literature of studying the CeO_2–ZrO_2–Al_2O_3 nanocomposites for catalytic application, using co-precipitation or sol-gel method [93, 94].

In conclusion, none of the previous research discussed above was found to have investigated the effect of mechanochemical activation on the mixture of talc, kaolin, aluminum hydroxide and stabilised zirconia as a precursor for preparation of cordierite-zirconia/zircon composites. Moreover, to the author's knowledge, none of the work on application of ceria and its effects on cordierite ceramics has been concerned with combining the use of natural silicates (talc

and kaolinite) and application of mechanochemical processing during solid-state synthesis. Therefore, these mentioned factors were all considered in the current research.

4. MATERIALS AND METHODS

4-1- Materials

The main cordierite precursors (talc and kalolinite) in this study were selected based on the success of previous similar works using natural minerals. Boehmite was also considered for providing the alumina balance in the stoichiometric equation. The precursor powders in this research were used as-received, and they included highly pure talc (Talc N), Polsperse^{TM} 10 ultrafine kaolinite provided by Imerys Minerals Ltd., and Pural SB1® boehmite powder from Condea Chemie GmbH. Ammonium polyacrylate (Ciba Dispex A40) and Fisher Scientific nitric acid (S.G. 1.42, 70%) were used as dispersants in size distribution studies. Functional additives applied during activation processes included two high purity oxides: yttria-stabilised zirconium oxide (YSZ, ~3 mol% yttria) from Unitec Ceramics Ltd. and cerium oxide or ceria (<50 nm particle size (BET), >99.95% purity) from Sigma-Aldrich Co.

4-2- Methods

4-2-1- Processes

Appropriate proportions of the three constituent powders were used according to the stoichiometric reaction 4-1. Weight percentages of dry talc, kaolinite and boehmite powders were 38.7, 46.0 and 15.3, respectively. The individual powders were then mixed and milled/activated using laboratory grinding machines under atmospheric conditions (Table 4-1 and Figure 4-1).

$$4[Mg_3Si_4O_{10}(OH)_2] + 7[Al_2Si_2O_5(OH)_4] + 10[AlO(OH)] \longrightarrow 6[Mg_2Al_4Si_5O_{18}] + 23[H_2O] \quad (4\text{-}1)$$

Talc Kaolinite Boehmite Cordierite

To investigate the effects of mechanochemical activation process, non-activated mixtures of the precursor powders (henceforth with the prefix sample code: "MIX") were used as a reference and prepared by ball milling under non-activating conditions (running the mill with a much fewer media than optimum for a short time).

Table 4-1: Some milling conditions under which precursor powders were activated

Machine type (Alternate names)	Grinding condition	Grinding media	Mechanism of operation	Prevailing mechanisms of grinding	Approximate grams of powder activated in one test	Activation/milling time (minutes) and relevant coding
Ball mill (Jar mill)	Dry	Porcelain jar – alumina balls (Φ 26,18.5 & 13mm)	Tumbling (rotation) At ~75% critical speed	1- Impact 2- Attrition	100	60 , 300 , 600 BM1, BM5, BM10
Ring mill (Vibratory disk mill or pulveriser)	Dry	Tungsten carbide container and rings	Vibration/ Oscillation	1-Compression 2- Abrasion (shear)	25	2 , 5 , 10 RM2, RM5, RM10
Planetary mill (Planetary ball mill)	Dry	Alumina pots – zirconia balls (Φ 5mm)	Rotation and revolution ~265 rpm revolution speed	1- Attrition 2- Impact	50-60 (each pot)	10, 20, 50 PM10, PM20, PM50

Figure 4-1: Different types of laboratory milling machines used in the experiments; from left to right: ball mill, ring mill and planetary mill

As observed in Table 4-1 (grinding media column), none of the grinding machines was expected to contaminate the powders considerably, with respect to addition of metallic ions or oxides. Milling was performed in atmospheric conditions and no temperature control or check was considered during the process. Grinding time, variable in each milling system, was considered as a measure of powder activation. In those tests that aimed to investigate of the effect of functional additives on sintered structure, appropriate proportions of the oxide compounds (zirconia and/or ceria), based on the dry weight percentage of the mixed powder of the three basic ingredients (talc, kaolinite and boehmite), were added to the mill (in this case, the planetary mill only) and the whole assembly mixed, ground and activated at the same time. The amounts of additives used were determined according to the summary of previous similar studies' data on solid-state synthesis of composite cordierite ceramics (Section 3-3).

Powder compaction was performed prior to sintering using INSTRON 4467 Universal Testing Machine in which uniaxial loading at 1 kN (~20 MPa) was applied. Powders (about one gram in each test) were formed into cylindrical compacts measuring 10 mm (height) by 8 mm (diameter) in a steel die. Compression tests were undertaken on as-milled dry powders and no additives were introduced. Die wall lubrication using a light oil was necessary at some intervals between the tests to ease the movement of die parts and extraction of compressed sample, which found to be especially helpful in case of compacting higher activated (therefore more dehydrated) samples.

The compressed samples were then sintered in a furnace under atmospheric conditions at three temperature schedules with final residence temperatures of 950, 1000 and 1050 °C, in order to investigate phase transformations at different potential activation conditions. Later,

further experiments were undertaken with a higher temperature dwell (1300 °C) to study the formation of cordierite. The heating and cooling cycles were set at a rate of 10 °C per minute, but at the end of the cycle, furnace was effectively allowed to cool down naturally to the room temperature.

4-2-2- Characterisations

The extent to which the characterisation process was taken depended on the application. For advanced materials, detailed knowledge of the characteristics is required for adequate control of the microstructure and properties of the fabricated material. The initial powders as well as as-milled samples were subjected to a size distribution analysis using laser diffraction spectrometer. Initial experiments using a Beckman Coulter LS 230 machine did not prove consistent results particularly for the kaolinite nanopowder, and a Malvern Mastersizer 2000 was used for subsequent size distribution measurements. The machine was equipped with integrated ultrasound dispersion mechanism and used distilled water (RI: 1.33) as the bulk dispersion medium. The refractive indices (RI) and density values of individual powders were incorporated into the analysis according to mineralogical reference data, as presented in Table 4-2.

Table 4-2: **Materials specification data used in laser diffraction size analysis**

Composition	True density (kg/m^3)	RI
Talc	2650	1.59
Kaolinite	2600	1.58
Boehmite	3000	1.64

Each size analysis test was first evaluated without using any additive to assess the possible effect of dispersing agent. Later, ammonium polyacrylate (RI≈1.5, S.G.=1.16) was used as a dispersant based on 0.6-1% of the solids weight consumption. Particle shape, size and agglomerations in powders as well as phases and structures in the sintered bodies were

determined by scanning electron microscopy (SEM) using Philips XL30 SEM electron microscope. Although *secondary electron* imaging was mainly used for studying powder samples, sintered compacts were viewed under *back-scattered electron* imaging condition for better phase contrast; in the latter case, polished sections were prepared to allow this and qualitative observational analysis. The microscope was also equipped with Oxford Energy Dispersive X-ray (EDX/EDS) analyser which was applied as a chemical analysis tool for characterisation of both impurities and elemental content of the constituent phases.

Evaluation of the crystallinity and characterisation of different crystalline phases was undertaken by X-ray diffraction analyses using PANalytical Philips X'Pert machine, using Cu K_α radiation (40 kV, 40 mA), 0.02° (2θ) step size and counting time of 1s/step. The results were subsequently analysed using the integrated software X'Pert HighScore, as well as the Bruker DIFFRAC^{plus} EVA software, and finally using the materials diffraction database PDF-4+ provided by ICDD®.

Bulk densities were determined for powders (untapped) and for compressed samples (through dimension measurements). Powder specific surface area was measured for both initial and as-milled powders by nitrogen gas adsorption technique using Micromeritics ASAP 2010 BET apparatus. Previous heating of powder samples up to about 100 °C was performed to evaporate any volatiles from micropores before applying gas adsorption. Microporosity data for sintered compacts were obtained by mercury porosimetry using WIN9400 apparatus from Micromeritics Instrument Corp. Finally dilatometry tests were undertaken using NETZSCH DIL 402E apparatus with an alumina sample holder to study the shrinkage and thermal expansion in some samples.

5. RESULTS AND DISCUSSION

5-1- Characterisation of precursor powders

Advanced ceramics must meet very specific property requirements and therefore their chemical composition and microstructure must be well controlled. The size, size distribution, shape and state of agglomeration have an important influence on both the powder consolidation step and the microstructure of the sintered body. Both the densification rate and the reaction rate increase with decreasing particle size, but because of the stronger size dependence, the densification mechanism is more strongly influenced than the reaction mechanism [95]. Therefore, a reduction in the particle size increases the densification rate relative to the reaction rate (Figure 5-1).

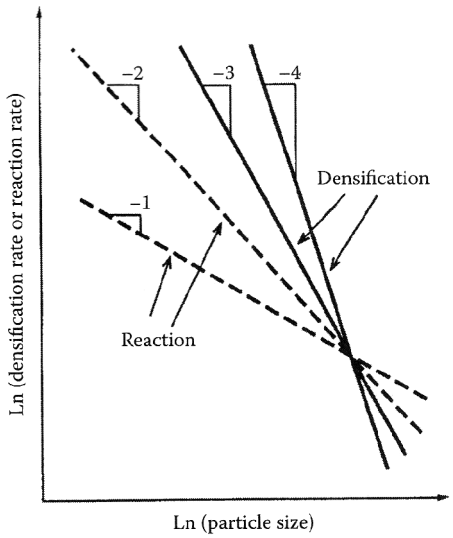

Figure 5-1: Effect of particle size on the rates of densification and reaction during reaction sintering of a powder mixture [95]

Results of particle size analysis for talc, kaolinite and boehmite are shown in Figure 5-2. The graphs show talc particle size falls within the micrometer range while kaolinite particles are in nanometer range. These two powders conformed to the manufacturer data, however for boehmite, a much finer particle size (a few nanometers) was expected than measured by laser diffraction analysis. Therefore, particle dispersion was prepared by a peptisation (acidification) method. For this purpose, a dilute solution (about 10 wt% solids) of boehmite powder was prepared in which the pH was adjusted to about 4 with appropriate amounts of nitric acid. This is the method usually practiced to produce colloidal sol systems [96]. As it is observed (Figure 5-2), acid peptisation resulted in a better dispersion of the apparently highly agglomerated boehmite powder. However, even under these conditions it was not possible to tell if de-agglomeration was complete. The kaolinite size distribution curve also showed that there was still partial coagulation of particles even after applying dispersant and mechanical shaking.

It is understood that unless an effective powder dispersion, commonly accompanied by particle surface charge measurements is applied, optical methods usually cannot measure particle size in a particular crystallographic direction and give an average size for aggregates of clay-sized materials [97, 98]. Further, it has been stated that for the non-spherical particles all sizing techniques give slightly different and the only referee for the laser diffraction will be the microscope [99].

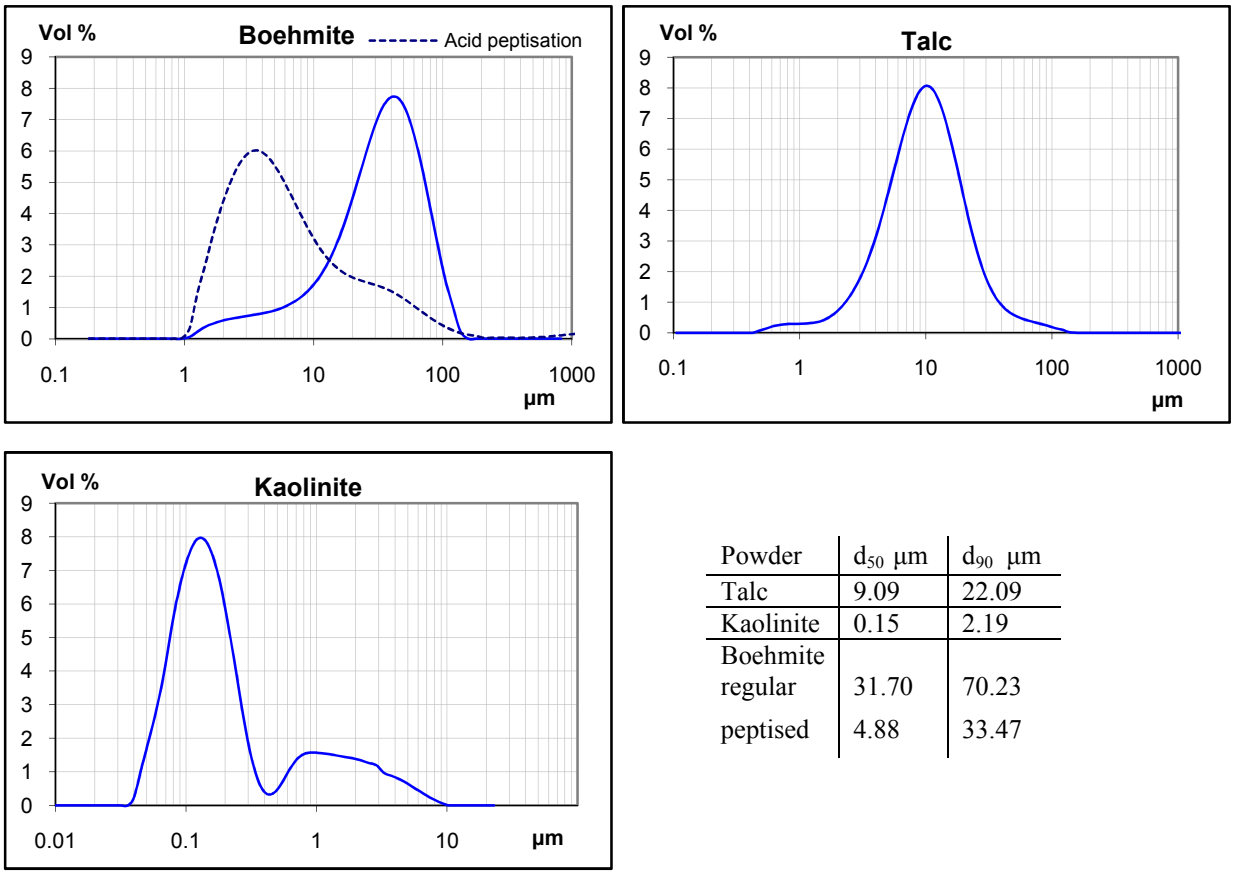

Powder	d_{50} µm	d_{90} µm
Talc	9.09	22.09
Kaolinite	0.15	2.19
Boehmite		
regular	31.70	70.23
peptised	4.88	33.47

Figure 5-2: Particle size distribution of the precursor powders

Powder specific surface area and aerated (untapped) bulk density values are reported in Table 5-1. The high BET value and relatively high powder density for boehmite represents its ultra-fine size distribution, which is usually the specific characteristic of boehmite prepared for applications such as catalyst supports and adsorbents [100].

Table 5-1: Measured BET specific surface area of the as-received individual powders

Composition:	Talc	Kaolinite	Boehmite
SSA (m^2/g):	4.31	10.82	257.79
Bulk density (kg/m^3):	363	267	757

Particle size, shape and aggregates were better evaluated and confirmed with scanning electron microscopy as shown in Figure 5-3. As observed in Figure 5-3(a), boehmite agglomerates are found as spherical bodies in some cases up to 45 µm and made of smaller

particles/aggregates. Such forms are indicative of spray drying being applied in the process of alumina/boehmite powder manufacturing. The mean kaolinite particle size was very small in the range of a few micrometers as observed in Figure 5-3(b), but large aggregates (larger than 10 μm) were also seen in the samples. Whether the smaller particles in the kaolinite sample were single plates or clusters of nano-sized particles was not distinguishable at the magnifications employed and the use of high resolution SEM or TEM is suggested. Talc samples were also made of differently sized particles, but the average particle size of about 10 μm (obtained in laser diffraction tests) could be confirmed.

Using energy dispersive X-ray analysis (EDX) during SEM studies, no foreign elements were found as impurities, except those associated with the sample mounts or coatings; an example of such observation (for talc) is presented in Figure 5-3(c).

a

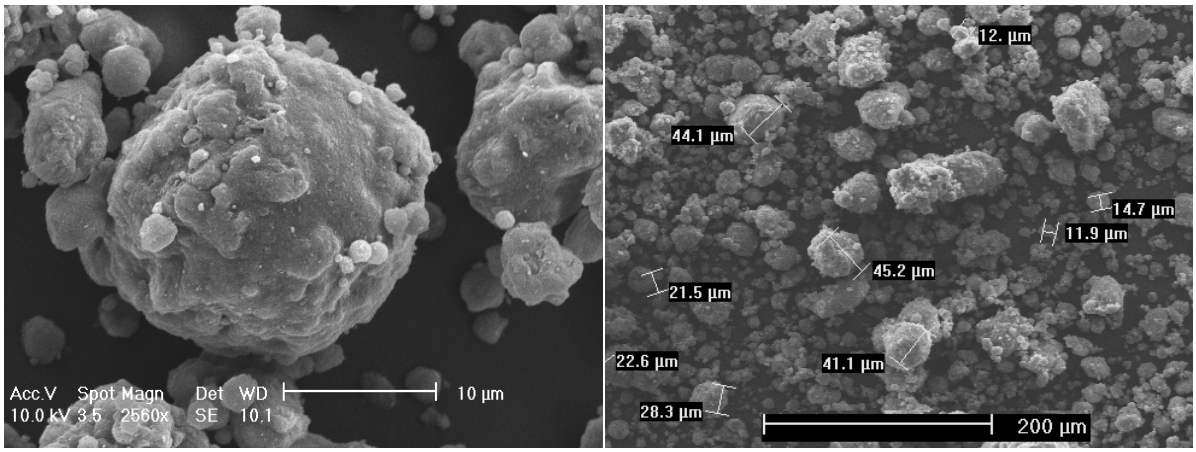

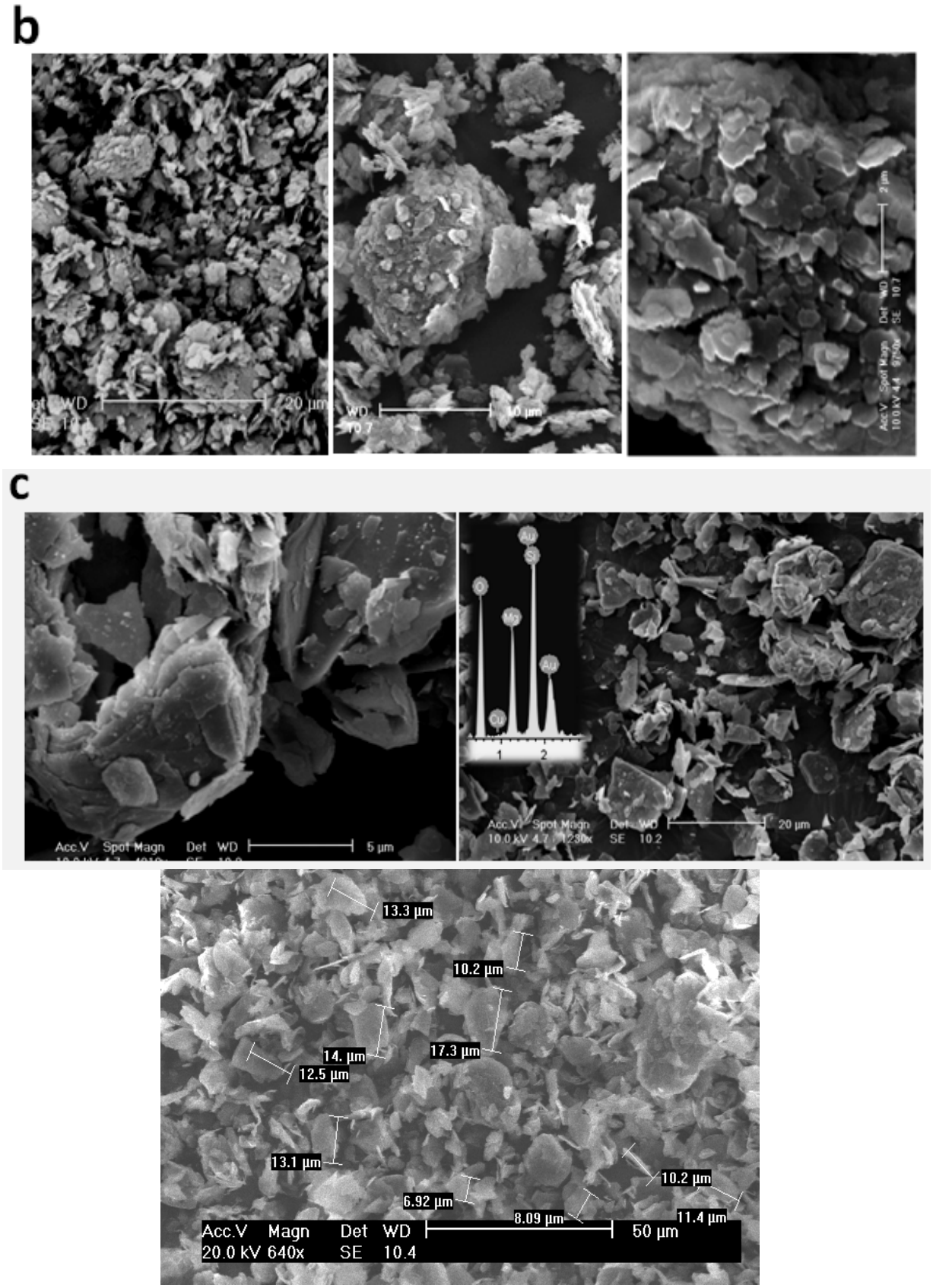

Figure 5-3: Scanning electron micrographs of the precursor powders; a) boehmite, b) kaolinite and c) talc

Graphs showing results of X-ray diffraction analysis of the precursors are presented in Figure 5-4.

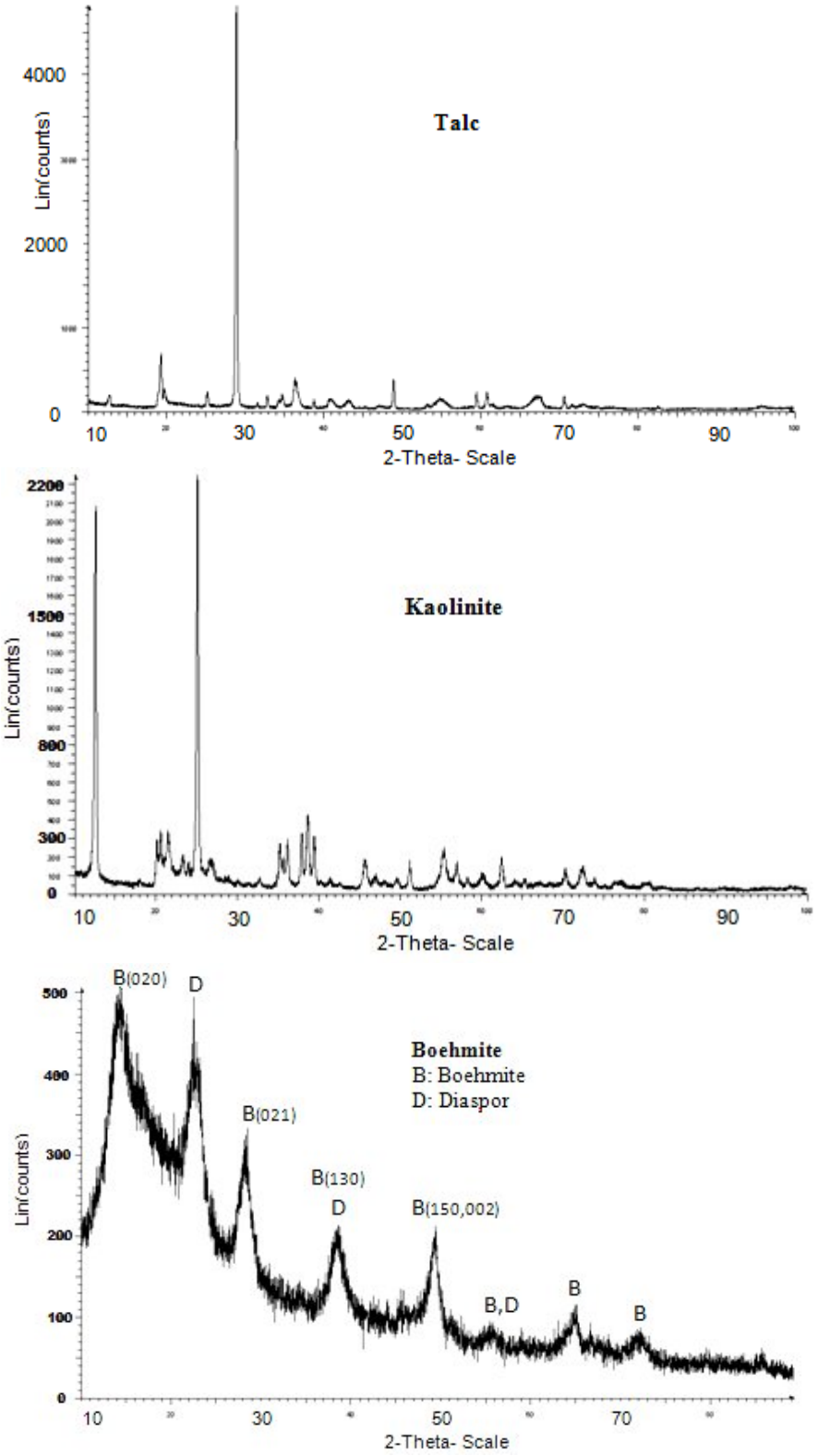

Figure 5-4: X-ray diffraction results of the precursor powders analysis

By reference to the PDF database -Powder Diffraction File available from The International Centre for Diffraction Data- the XRD results for the materials indicate that the initial powders are crystalline which match the following materials:

- Monoclinic talc, also called steatite or soapstone with the formula $Mg_3Si_4O_{10}(OH)_2$
- Triclinic kaolinite or kaolinite 1A, $Al_2Si_2O_5(OH)_4$
- Orthorhombic boehmite, γ-AlOOH (containing diaspore or α-AlOOH)

It might worth mentioning that diaspore and boehmite are polymorphs of the same mineral and differ in structural relationships by the packing of the oxygens [101]. One characteristic feature of boehmite X-ray powder diffraction data is significant peak broadness which is usually due to the degree of crystallinity and more probable here because of very small particle size; further, both experimental and calculated XRD profiles show that peak shifts and increased peak breadths are characteristic of fine-grained boehmite [102]. This clearly confirms the previous statements regarding difficulties in size distribution analysis of such material using optical method. Finally, it should be noted that one of the major peaks of talc ('002' crystallographic plane) at $2\theta \approx 9°$ is not included in the relevant pattern due to not falling within the measurement range of the experiment.

5-2- Mechanochemical dry milling of powders

Samples prepared from stoichiometric mixture of the three precursor powders were subjected to milling experiments and subsequently characterised with respect to particle size, shape, crystallinity and powder specific surface area. The results in this section are presented and discussed comparatively for the three milling methods applied.

5-2-1- Size analysis

Results of laser diffraction size analysis for the as-milled powder mixtures using three different milling methods and times are presented in Figure 5-5. Dispersion of the milled powders proved difficult and the laser diffraction size distributions do not appear to accurately represent the particle sizes observed by SEM studies.

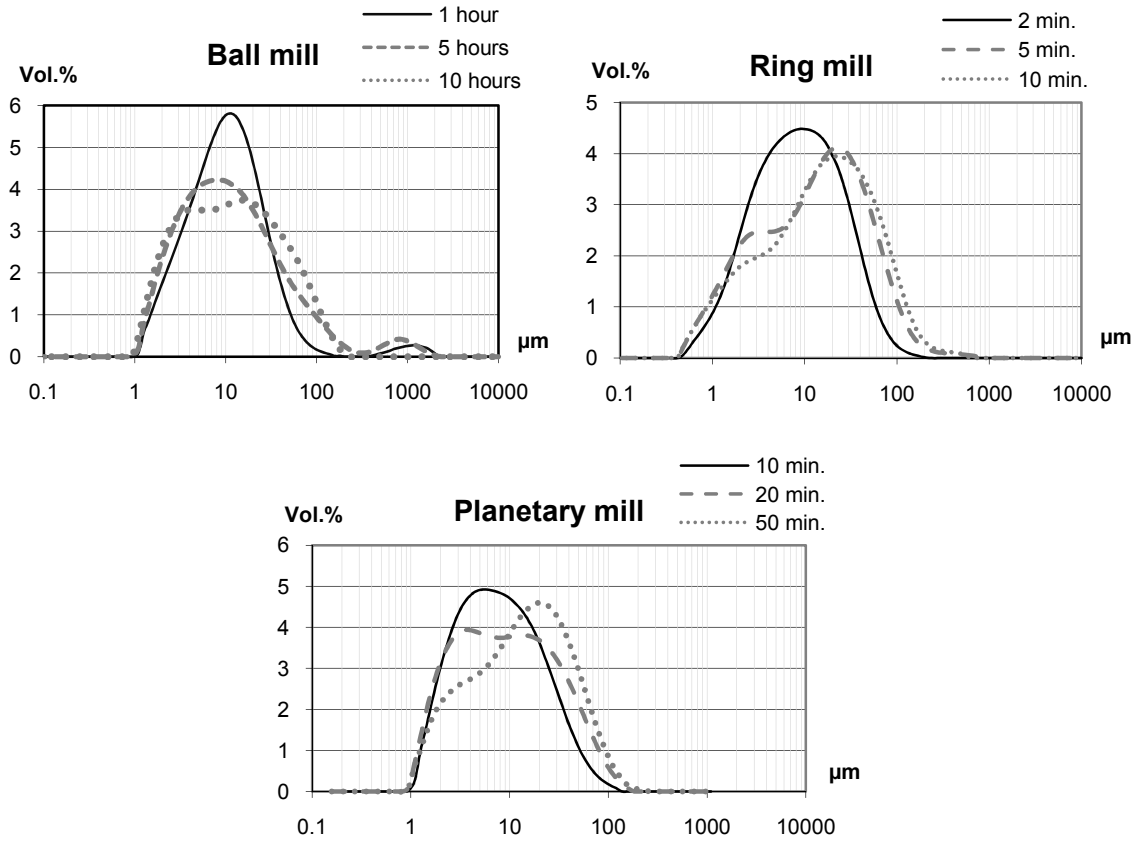

Figure 5-5: Size distribution graphs for differently milled/activated powders

There are some concerns about the efficiency of laser diffraction analysis under some specific conditions. First, determining an accurate particle size distribution of a mixture of materials (which is quite common in the ceramics industry) using this method could be difficult, knowing the fact that each individual material has a unique particle size distribution, as well as different particle shapes, densities and optical properties. Secondly, grinding processes

further alter the particle shapes and sizes [103]. For laser diffraction size analysis, Figure 5-6 shows the pronounced influence of particles' dispersion on the measurement error, as the particle size enters the nano region [99].

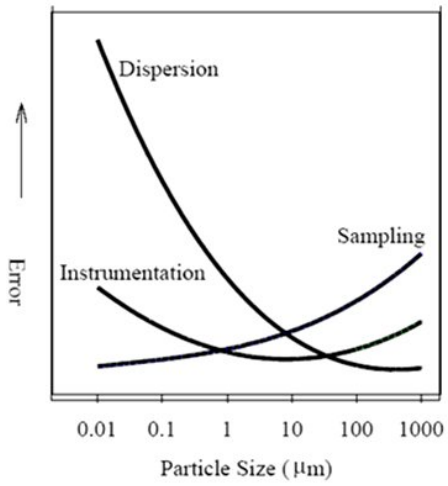

Figure 5-6: Effects of the major sources of error in particle size analysis as a function of particle size [99]

In this study, the ineffectiveness of the dispersant could be attributed to the changes in surface properties of the particles too. Apart from high degree of agglomeration in ultrafine milled powders, difference in particle shapes arising from different crystallographic systems (clay and talc compared to boehmite) and size (larger talc particles) have possibly had adverse effects on size measurements. One thing that might be realized from the shape of the size distribution curves is that increasing the milling time has resulted in moving toward a wider size distribution (curves with lower kurtosis) as aggregation continues (moving to larger particle size rage). Therefore, changes in optical parameters (mainly refractive index) as well as existence of agglomerated states alongside single particles in the submicron measuring range, are among the factors that have influenced the size distribution results when using laser diffraction [98].

5-2-2- Specific surface area and bulk density measurements

The results of BET specific surface area measurements for the as-milled samples are presented in Table 5-2. As observed, in most cases powder surface area has been increased with increase in activation/milling time. This is in agreement with propagation of microcracks and defects and reduction in particle size as grinding progresses. It is expected that further milling with planetary and ring mill beyond the times applied would result in a decrease of surface area values due to high degree of agglomeration as stated in similar works [13, 46, 104]. The slight decrease in the value of powder surface area after early stages of milling compared to the unmilled mixture could be attributed to the attachment of smaller flakes of kaolinite on the surface of larger talc sheets during that early stage of grinding. Such particle attachments has been observed with SEM (Section 5-2-4).

Table 5-2: BET specific surface area values for samples ground with different mills as well as the non-activated sample

MIX	**Ball-milled**		**Ring-milled**		**Planetary-milled**	
Surface area (m^2/g)	Activation time (min)	Surface area (m^2/g)	Activation time (min)	Surface area (m^2/g)	Activation time (min)	Surface area (m^2/g)
43.73	60	42.33	2	41.99	10	52.88
	300	42.53	5	60.21	20	58.16
	600	49.89	10	61.76	50	57.29

Bulk densities of dry milled powders were measured for each sample. Density values are on the basis of aerated (not tapped) powder density. As seen in Figure 5-7, the powders show higher density values as the milling time is increased in each method. Grinding of larger talc particles resulting in a more homogenous powder mixture with respect to size distribution,

together with the dehydration of the compositions are considered as possible causes of increase in the density of the mixture due to milling. However, changes in surface characteristics of the compounds, e.g. talc surfaces losing hydrophobicity after intensive dry grinding, could also affect the density of the mixture.

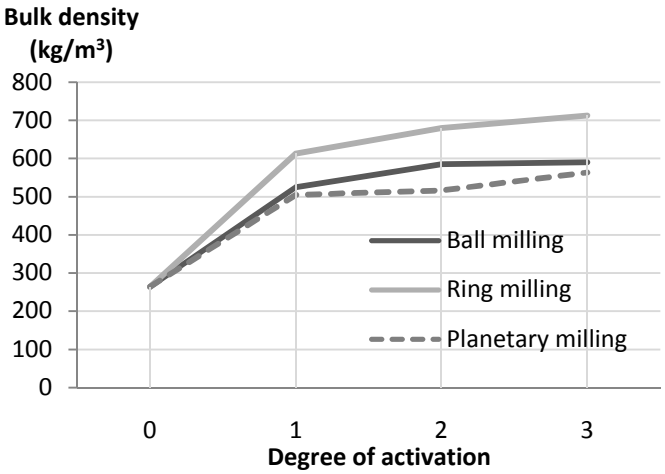

Figure 5-7: Effect of activation time on powder bulk density

5-2-3- XRD analysis

Effect of increasing the milling time is quite apparent on reduction of the X-ray diffraction peak intensities (Figure 5-8) which is considered as the direct result of degradation and/or rearrangements of crystalline structures and is well established in literature [13, 47, 105-107]. It is quite important to know that several different processing as well as material parameters affect the degree of crystal deformation and amorphisation in the process of powder activation in a mill. Further, it should be remembered that this is a mixture of three different mineral powders, each possessing a specific size distribution and particle shape, as well as individual bulk and surface structures and physicochemical characteristics. As a consequence, powder activation in a mixture of the compounds in different proportions might not follow the same route as when the individual powder compositions are activated. Therefore, the evaluation of

crystal degradation by comparing various XRD graphs must be performed with consideration of the interactions mentioned above.

What is quite apparent from the XRD patterns given in Figure 5-8, is that the boehmite diffraction peaks could not be distinguished in the patters; a possible reason for this could be the boehmite's inherent low-intensity broad diffraction peaks compared to the other two minerals. Moreover, boehmite's rapid dehydration and sensitivity to mechanical action, overlapping of its diffraction peak with other materials, and finally its lower concentration in the mixture compared to other components could all be considered as factors influencing the boehmite's characterisation in the X-ray patterns. Another interesting observation is that the talc particles seem to be more affected than kaolinite at high levels of activation degrees (lower XRD intensities in RM10 and PM50), which is a reflection of different properties of talc with respect to crystallography (double-layer or sandwiched structure – see Appendix), physical (low hardness) and surface properties compared to those of kaolinite.

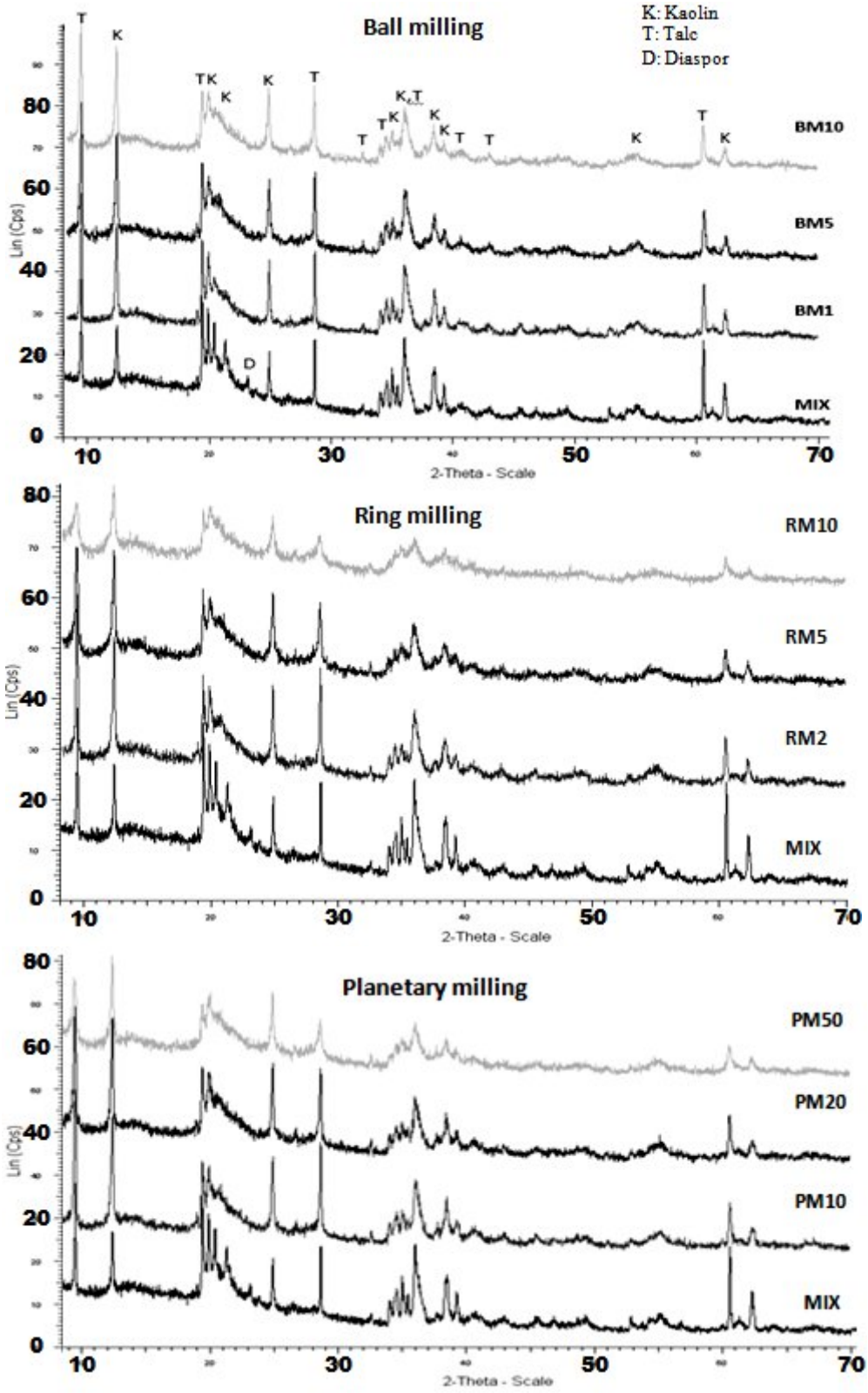

Figure 5-8: Effects of activation time on crystalline diffraction peaks for differently milled samples

5-2-4- SEM-EDX studies

Results of scanning electron microscopy of the as-milled powder mixtures from ball milling are presented in Figure 5-9.

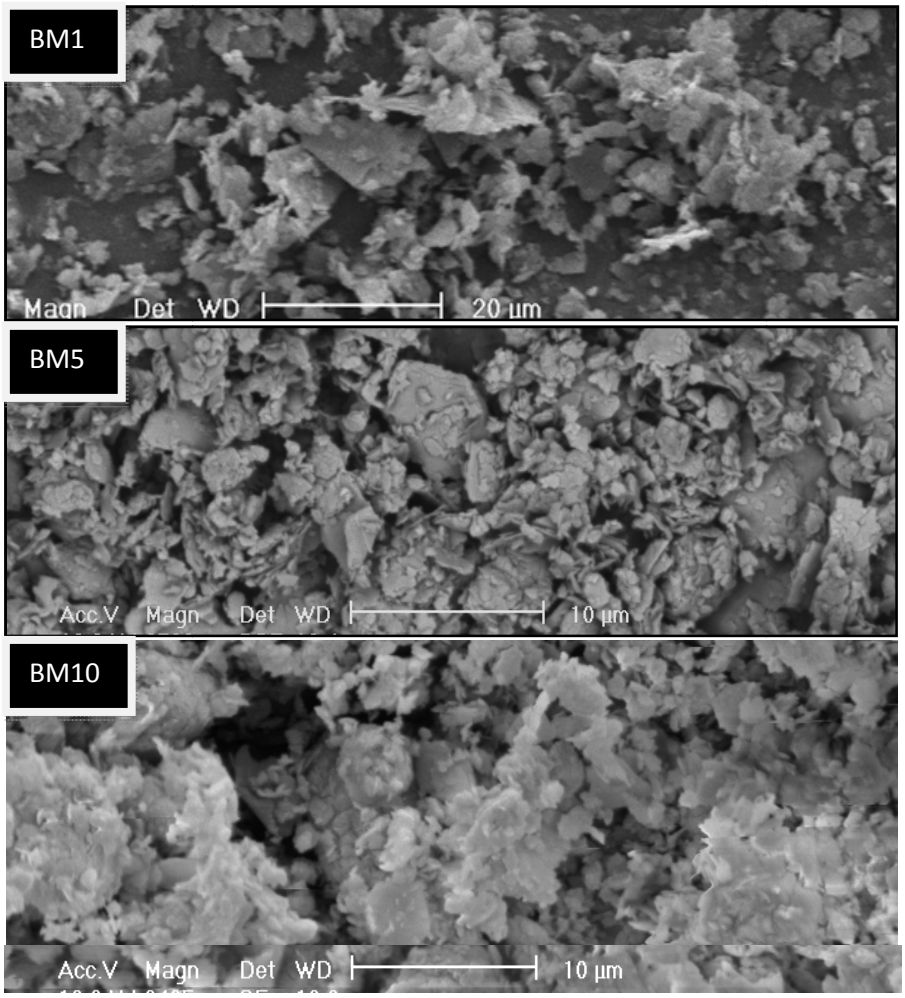

Figure 5-9: SEM micrographs of ball-milled samples; for sample BM5 it is in *backscattered electron (BSE)* view

As observed in the image related to sample BM5 in Figure 5-9, smaller (usually platy) particles or aggregates are attached to the surface of larger sheets (talc). This will dramatically influence the measurements by laser diffraction. On the other hand, agglomerates which quite readily form during extended milling of fine particles are clearly observed mostly in samples

with longer activation times, as shown in Figure 5-10a. There is also an inter-locking pattern observed for the sheet silicates, like pieces of jigsaw puzzle, Figure 5-10b.

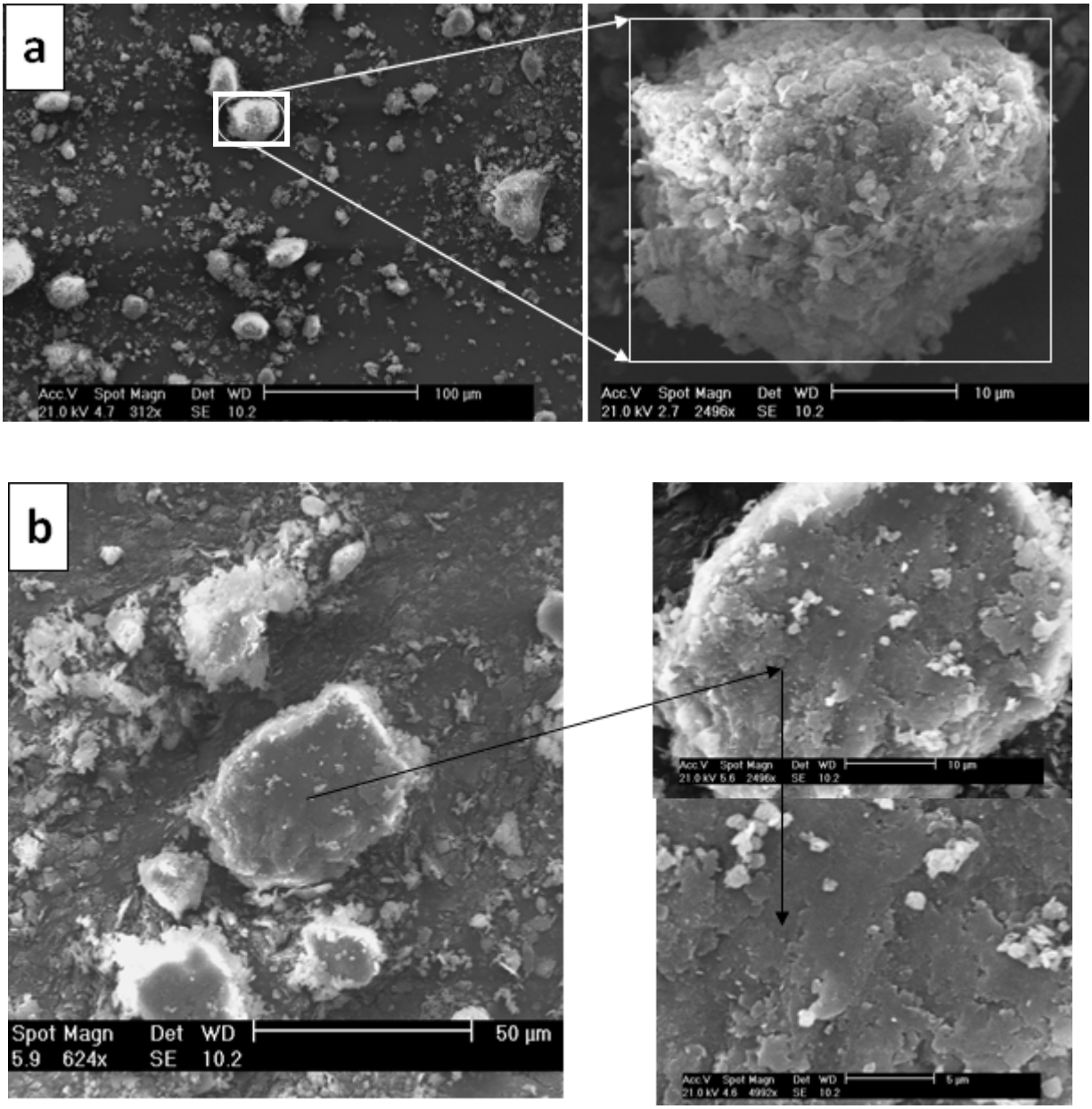

Figure 5-10: Agglomeration of fines after 10 hours of ball milling (sample BM10); a: an agglomerate of different particles, b: an agglomerate of sheet structures

Similar trends were observed after performing ring milling and planetary milling of powder mixtures, of which the results are shown in Figures 5-11 and 5-12 respectively. In Figure 5-11, agglomerate size is increased from RM2 to RM5; it is also noticeable that agglomerates look more rounded with smoother edges as particles are reduced in size and as defects spread through the crystal structure during intensive grinding (RM10 compared to RM5 or RM2). The same hypothesis is applicable when PM50 is compared to PM20 and PM10 in Figure 5-12. The average maximum particle size for RM5 sample evaluated in SEM images were in the range of 1-1.5 μm, while for sample PM50 it was 700-900 nm. These maximum values are attributed to talc, for the other two precursor minerals were already in nanometer size range before milling tests.

According to Holt [108], there is some agreement amongst different workers as to the characteristic shapes which are produced by comminution machinery; for example, it is generally agreed that roll mills produce angular products whereas the products of ball mills tend to be equidimensional and rounded. Although, there are debates over which of the factors between material characteristics and mill type is more influential on shapes of the product particles, it has been widely accepted that the latter has quite a marked effect. Even the choice of the grinding media within a mill (such as ball size in ball mill) has been found to be important in determining the product particle shape.

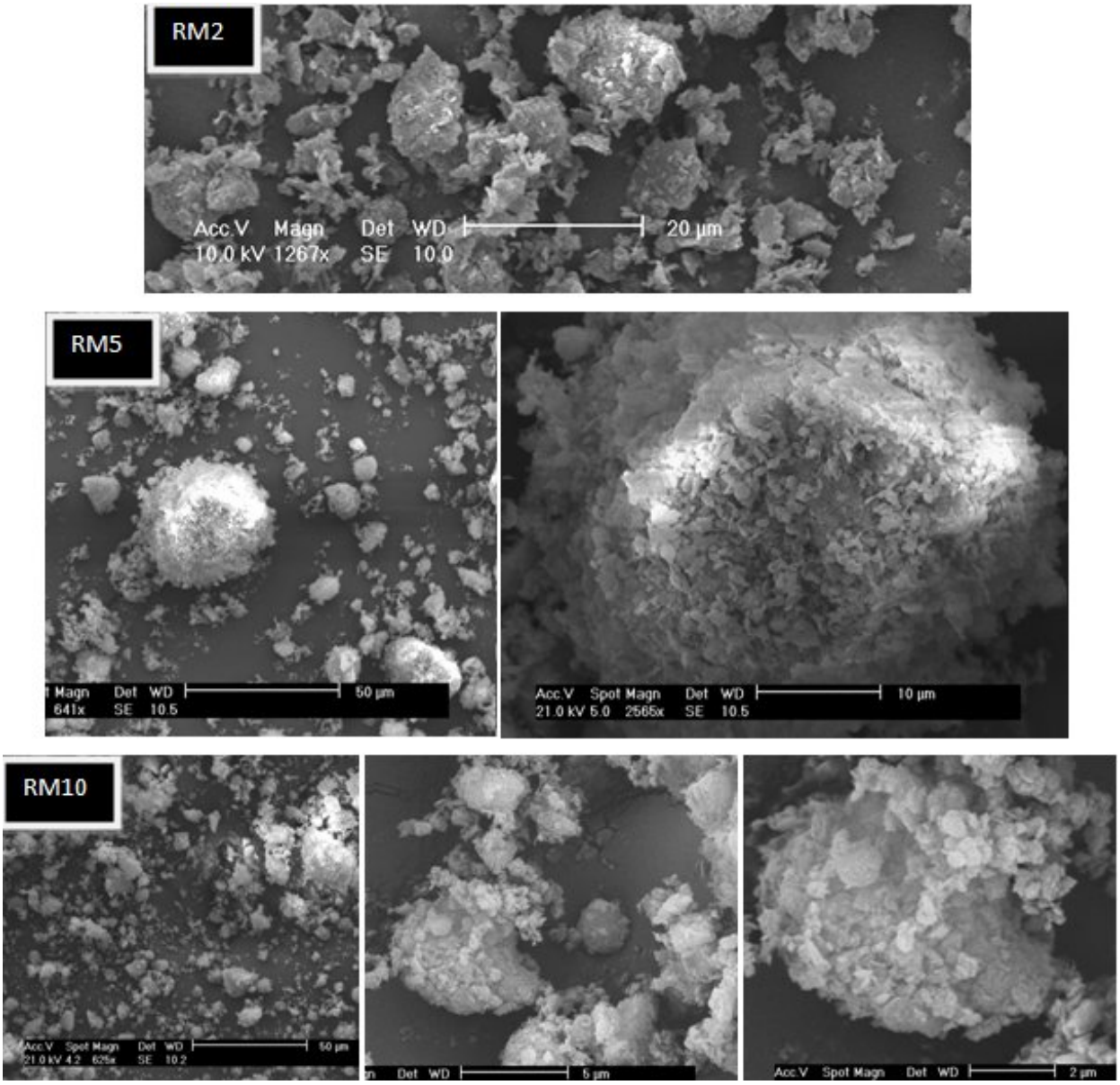

Figure 5-11: SEM micrographs of the ring-milled samples (magnifications increase from left to right for RM5 and RM10)

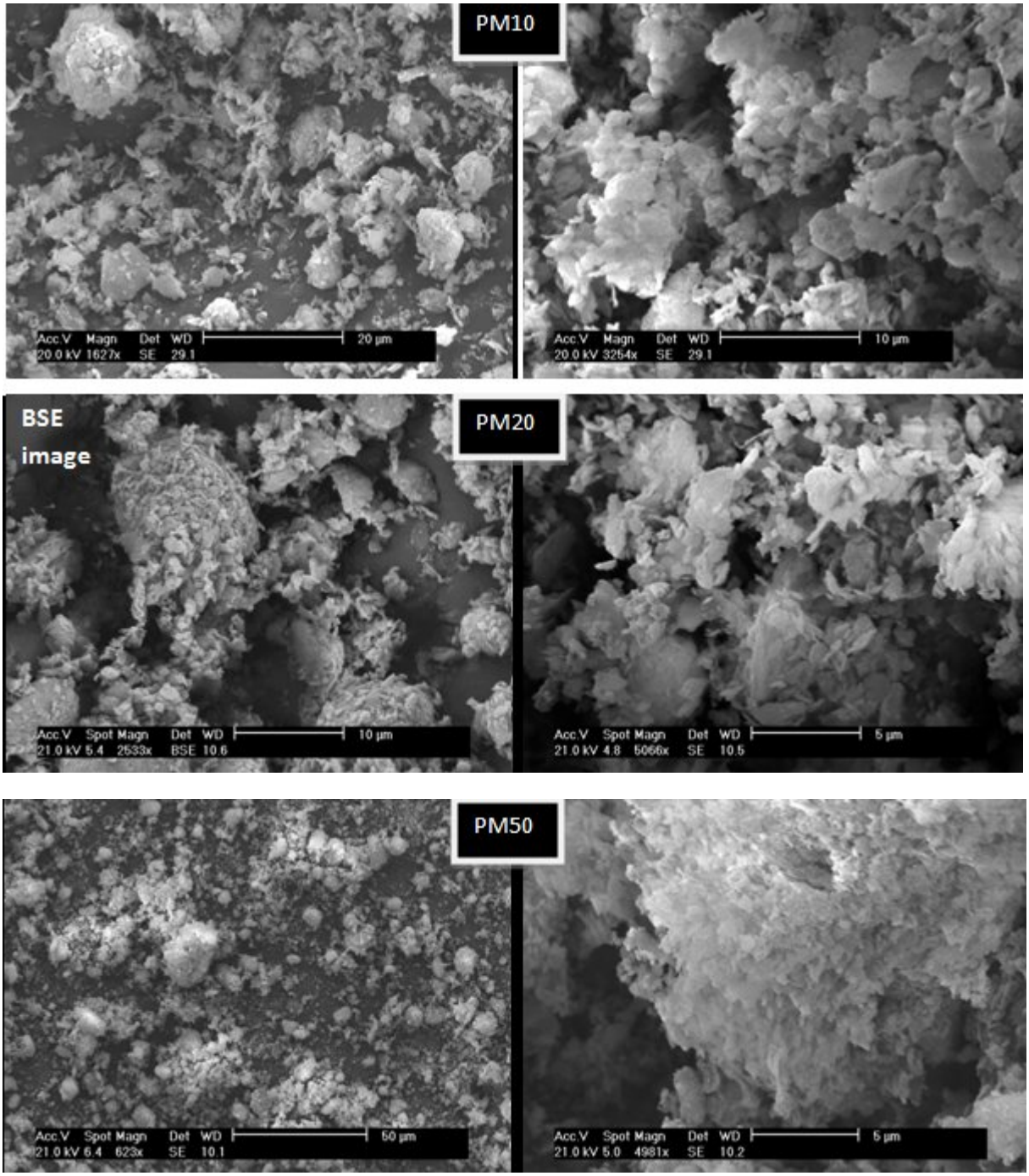

Figure 5-12: SEM micrographs of different planetary-milled samples at two magnifications; the backscattered image in PM20 well presents agglomerate conformed of smaller particles/aggregates

5-3- Powder compaction and sintering

The as-milled powders were subjected to uniaxial compression (die compaction) with an Instron Universal Testing Machine (UTM) to make compact green bodies ready for sintering. Although it is quite common to use a binder in the compaction process of ceramic powders in order to control final shape and packing uniformity [6], no such material were introduced in these experiments. This was because the main purpose of the current study was to investigate the effects of mechanochemical processing and phase formation during sintering. Moreover it was not the purpose of this research to fabricate a specific final ceramic structure or shape such as honeycombs, films or tubes which target specific industrial applications. Any foreign (commonly polymeric) material acting as binder or plasticiser must first be removed in a pretreatment prior to sintering. It was however necessary to perform a regular die wall lubrication so that the compact body could be released and ejected easily, without significantly damaging the delicate compressed sample.

Sintering experiments were undertaken for all the milled samples in which no sintering aids were applied. For this purpose, three different temperature schedules were selected: "*Low*", "*Medium*" and "*High*" at 950 °C, 1000 °C and 1050 °C respectively, based on major phase transformation and reaction steps during thermal processing of cordierite mineral precursors. Cylindrical compacts were put into the furnace and allowed to be sintered for two hours; heating and cooling rates were both set at 10 °C/min (Figure 5-13). Sintered articles were subjected to X-ray diffraction analysis, SEM-EDX analysis as well as density and porosity measurements. The specific coding used to denote different samples with respect to different processing conditions is shown in Table 5-3.

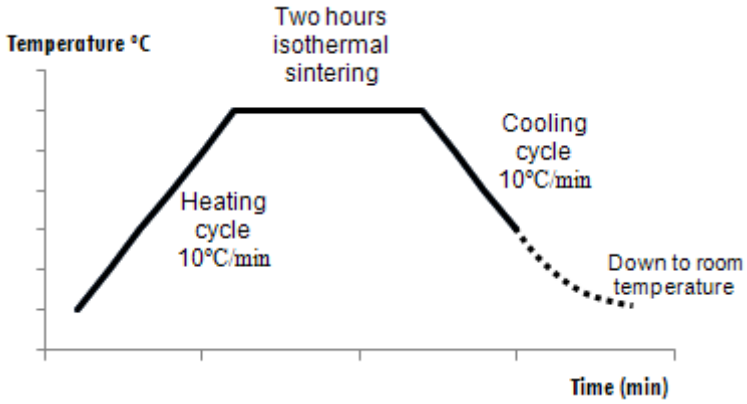

Figure 5-13: The heat treatment schedule applied for sintering of the samples

Table 5-3: Coding reference for the sintered samples at different sintering programs

	Low temperature (950 °C)	*Medium* temperature (1000 °C)	*High* temperature (1050 °C)
As-mixed	MIX-L	MIX-M	MIX-H
Ball milled 1hour	BM1-L	BM1-M	BM1-H
Ball milled 5hours	BM5-L	BM5-M	BM5-H
Ball milled 10hours	BM10-L	BM10-M	BM10-H
Ring milled 2minutes	RM2-L	RM2-M	RM2-H
Ring milled 5minutes	RM5-L	RM5-M	RM5-H
Ring milled 10minutes	RM10-L	RM10-M	RM10-H
Planetary milled 10minutes	PM10-L	PM10-M	PM10-H
Planetary milled 20minutes	PM20-L	PM20-M	PM20-H
Planetary milled 50minutes	PM50-L	PM50-M	PM50-H

5-3-1- XRD studies

The results of X-ray diffraction analyses of the sintered material are presented according to the sintering temperature applied. For each temperature schedule, three milling methods are discussed separately with respect to the XRD results. For each applied milling systems graphs are presented in two forms; the first gives a general unmodified pattern, useful for comparison, and the second, with the background effect removed, which shows the characteristic peaks relating to each crystalline phase in the sintered sample more clearly.

5-3-1-1- "*Low* temperature" sintering program

Referring to Figure 5-14, sintering of the material at 950 °C has resulted in formation of a more or less glassy phase which still shows traces of un-decomposed talc mineral. According to thermodynamic phase studies and data obtained by differential thermogravimetry (DTA-TG), a natural talc sample without impurities loses its structural water (dehydroxylates) over the temperature range 900-1000 °C. This reaction is accompanied by the formation of magnesium silicate mineral enstatite ($MgSiO_3$) and amorphous silica [37, 46, 48, 109]. Ball milling up to five hours promoted structural decomposition of talc and kaolinite during heat treatment toward enstatite formation and amorphous glassy phases (silica and metakaolin or pre-mullite). It has been demonstrated by Tamborenea *et al.* that the small exothermic effect at about 971 °C in the DTA analysis of similar samples, is due to the transformation of the non-crystalline structure of the kaolinite into a spinel or premullite phase. This peak, observed in the mixture without treatment, appears at lower sintering temperatures in case of highly activated samples [13]. Therefore, it seems the same intermediate phases are formed in the current study at about 950 °C. Further milling up to 10 hours appears to have slightly reduced the peaks of the glassy phases in the sintered material.

Activation using the ring mill even at short milling times has resulted in both complete decomposition of the remaining talc and reduction of glassy phases after *low* temperature sintering. Ultimately, it has resulted in formation of a magnesium aluminium silicate phase ("MAS" in Figure 5-15) as the only major crystalline phase present in the sample which is activated for 10 minutes (RM10-L). In the XRD powder diffraction files (*PDF* database) this latter phase in indexed as a hexagonal structure with a cordierite composition ($Mg_2Al_4Si_5O_{18}$).

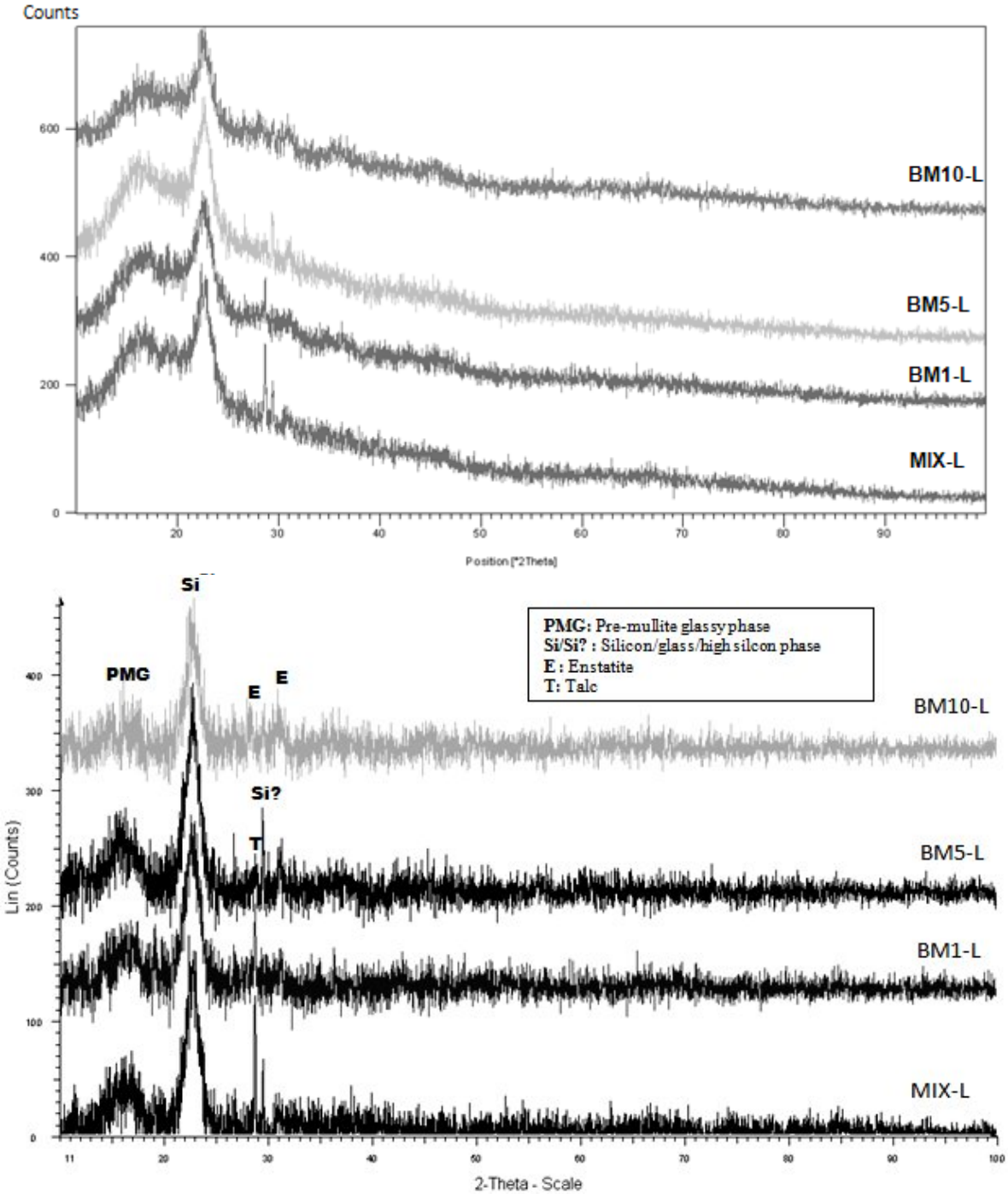

Figure 5-14: XRD pattern comparison for ball milling activation and *low* temperature sintering, top: general pattern, bottom: back-ground removed and labelled pattern

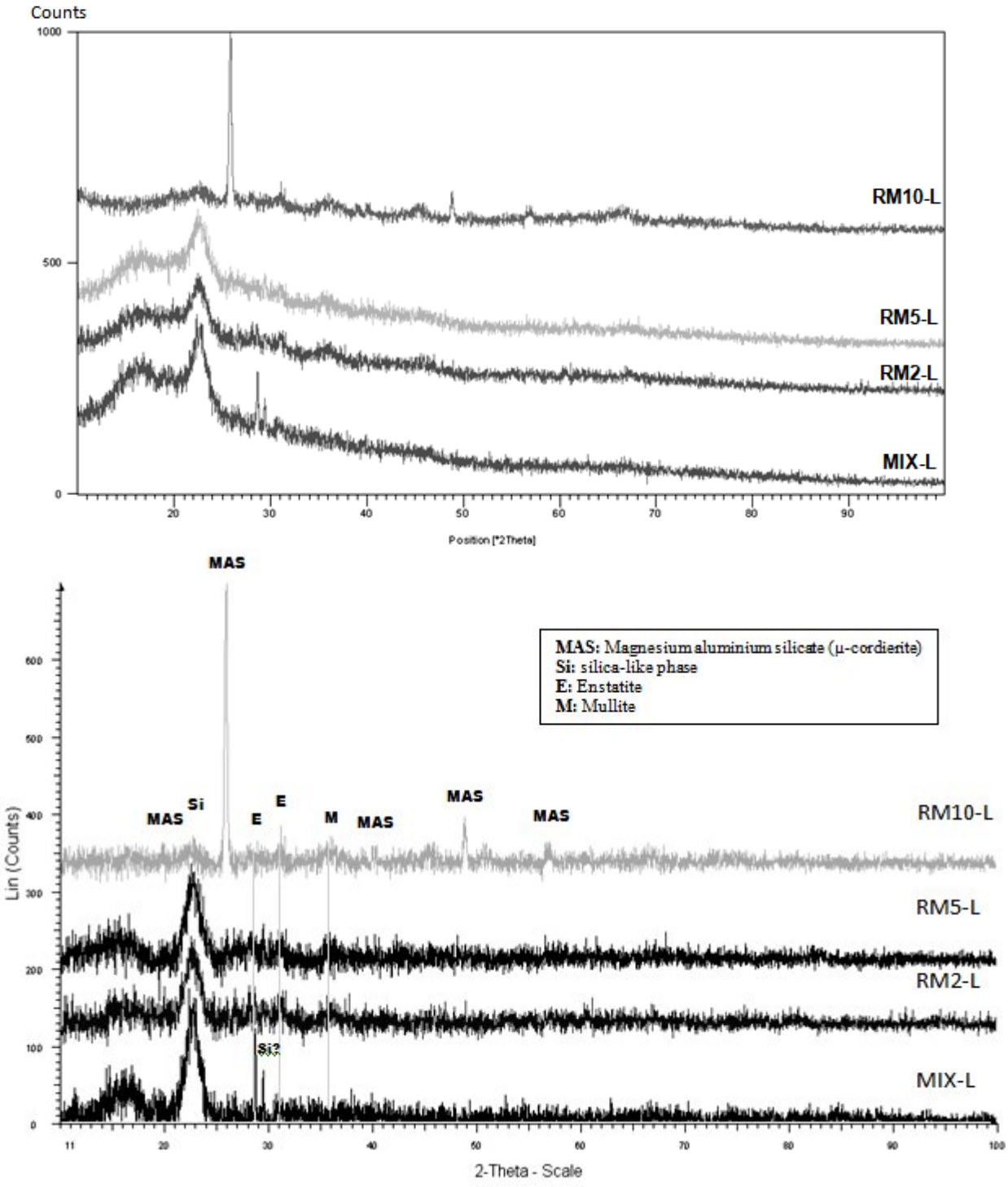

Figure 5-15: XRD pattern comparison for ring milling activation and *low* temperature sintering, top: general pattern, bottom: back-ground removed and labelled pattern

In research by Goel *et al.* [110] where a cordierite-composition glass prepared from a melt of precursor oxides was heat treated (DTA analysis), the phase which formed at 850 °C after 5

hours was recognised as “MAS”. This phase was characterised as a metastable solid solution of the quartz type which also produced the maximum peak height in X-ray diffraction patterns when the material was heated up to 950 °C for one hour. The “MAS” phase is also referred to as μ-cordierite (or occasionally β-quartz) which is considered as a metastable phase formed at such temperatures from a cordierite-stoichiometry glass [70, 92, 111-113]. Analysis of XRD patterns has indicated that μ-cordierite decomposes into β-quartz solid solution containing approximately 70 wt.% SiO_2 and spinel ($MgAl_2O_4$) at 1200 °C [114].

Sintering of the planetary-milled sample resulted in a slightly different XRD pattern. From Figure 5-16, it can be seen that the weak silica peak is removed in the long milled sample, but PM50-L shows the least degree of crystallinity at the applied sintering temperature. In PM50-L broad peaks presumed to belong to a spinel composition (or MgAl-oxide) can be seen; but this cannot be confirmed with a high confidence, for the whole pattern is like that of an amorphous mixture. When compared to corresponding patterns of other samples activated with other mill types, in particular the ring mill, the effect of the mechanism of milling on the structure of the sintered material becomes quite apparent.

Regarding the formation of spinel, something which is confirmed in the literature [37] is that the solid-state synthesis of spinel from magnesia and alumina, occurring by an inter-diffusional process of cations through the product layer between the oxide particles, needs high processing temperatures (>1400-1500 °C). However, it is possible to reduce the formation temperature of spinel down to about 1000-1050 °C by applying mechanochemical processing; something which is observed in the current study.

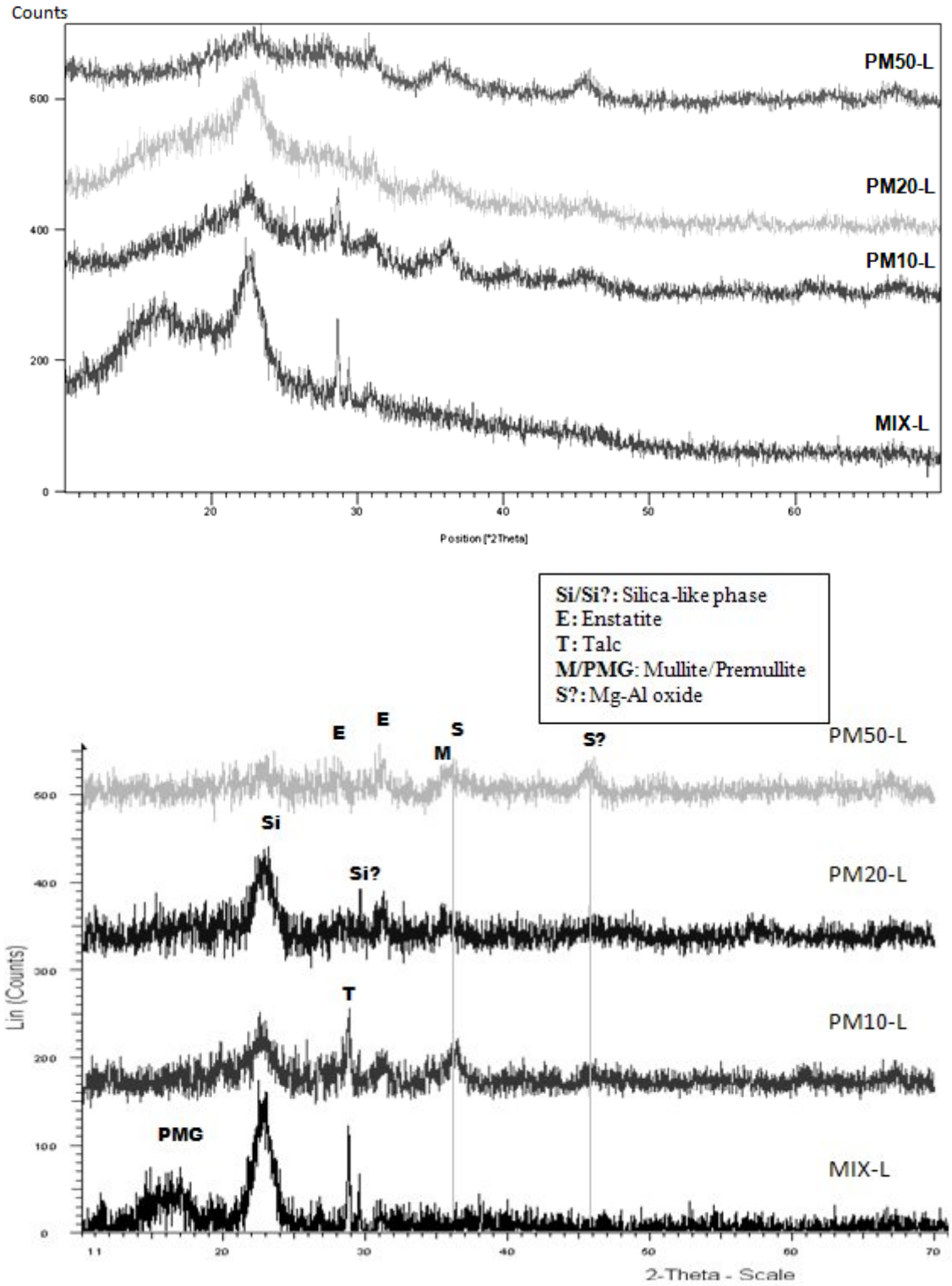

Figure 5-16: XRD pattern comparison for planetary milling activation and *low* temperature sintering, top: general pattern, bottom: back-ground removed and labelled pattern

5-3-1-2- "*Medium* temperature" sintering program

One of the main characteristics of material sintered at 1000 °C is the intensification of the X-ray peak related to enstatite and formation of crystalline mullite. According to literature [115], there are only two stable forms of $MgSiO_3$, orthorhombic enstatite up to about 985 °C and protoenstatite from 985 °C to the dissociation point. Clinoenstatite, although it occurs in nature, has been found to be only a metastable low-temperature phase formed during rapid cooling of protoenstatite, although in the binary system, a clinoenstatite solid solution may exist as a stable phase.

Glassy mullite and a silicon-aluminum spinel (phase with a spinel-type or cubic structure possibly with a γ-alumina solid solution) were identified as the main crystalline phases formed after heating ground kaolinite samples in a study by Sanchez-Soto *et al.* [43]. It is stated in their research that longer grinding times caused the transformation of the mechanically activated amorphous phase to mullite to occur at relatively lower temperatures. But, of course the current study is concerned with a mixture of three different mineral compositions and their interaction during milling and subsequent heat treatment.

Short-time ball milling resulted in an increase in the formation of enstatite (decomposition of talc) as well as a reduction of the amorphous silica phase; however, increasing the milling time to 10 hours has caused the reduction of the enstatite peaks (Figure 5-17). This phenomenon stems from the fact that the previous activation of powder mixtures has promoted phase transformations and reactions during heat process; once a phase composition have been decomposed, reaction of newly formed products makes new (crystalline/amorphous) structures. Additionally, the peak height of the amorphous (or possibly semi-crystalline) silica-like phase has increased in case of the sample BM10-M,

which supports the above hypothesis. As a result, there seems to exist a kind of balance between the degree of mechanochemical activation, sintering temperature and sequence of phase changes.

As shown in Figure 5-18, ring milling of the powders has resulted in the appearance of mullite peaks in the XRD data under the "*medium*" temperature sintering conditions. Intense activation of the material by ring milling for 10 minutes (sample RM10-M) produced a similar XRD pattern to the sample fired at the lower temperature, though more peaks are formed due to the formation of mullite and spinel-type structures. As discussed above, similar phase transformation trends have been demonstrated when ring milling is extended: first, an increase in the amounts of enstatite and mullite (as a result of decomposition products of talc and kaolinite respectively) at low activation condition (sample RM2-M), and later incorporation of these phases (decrease in relevant XRD peaks) to form new phases (magnesium aluminium silicate - MAS - and spinel). In similar research [13], the higher reactivity of the ring-milled mixtures has been shown to be responsible for the transformation of metakaolin into spinel during heat treatment, and said to be due to the lowering of reaction enthalpies.

XRD phase analysis of the materials milled by the planetary mill and sintered under "*medium*" conditions (Figure 5-19) showed similar behaviour to the materials milled in the ring mill. However, the difference at the highest activation condition in this case (sample PM50-M) is the increase of the proportion of mullite and spinel phases with respect to the MAS phase, which corresponds to less intensity (at least regarding the compressive forces) of the highest activation obtained with 50 minutes planetary milling in comparison to 10 minutes of ring milling.

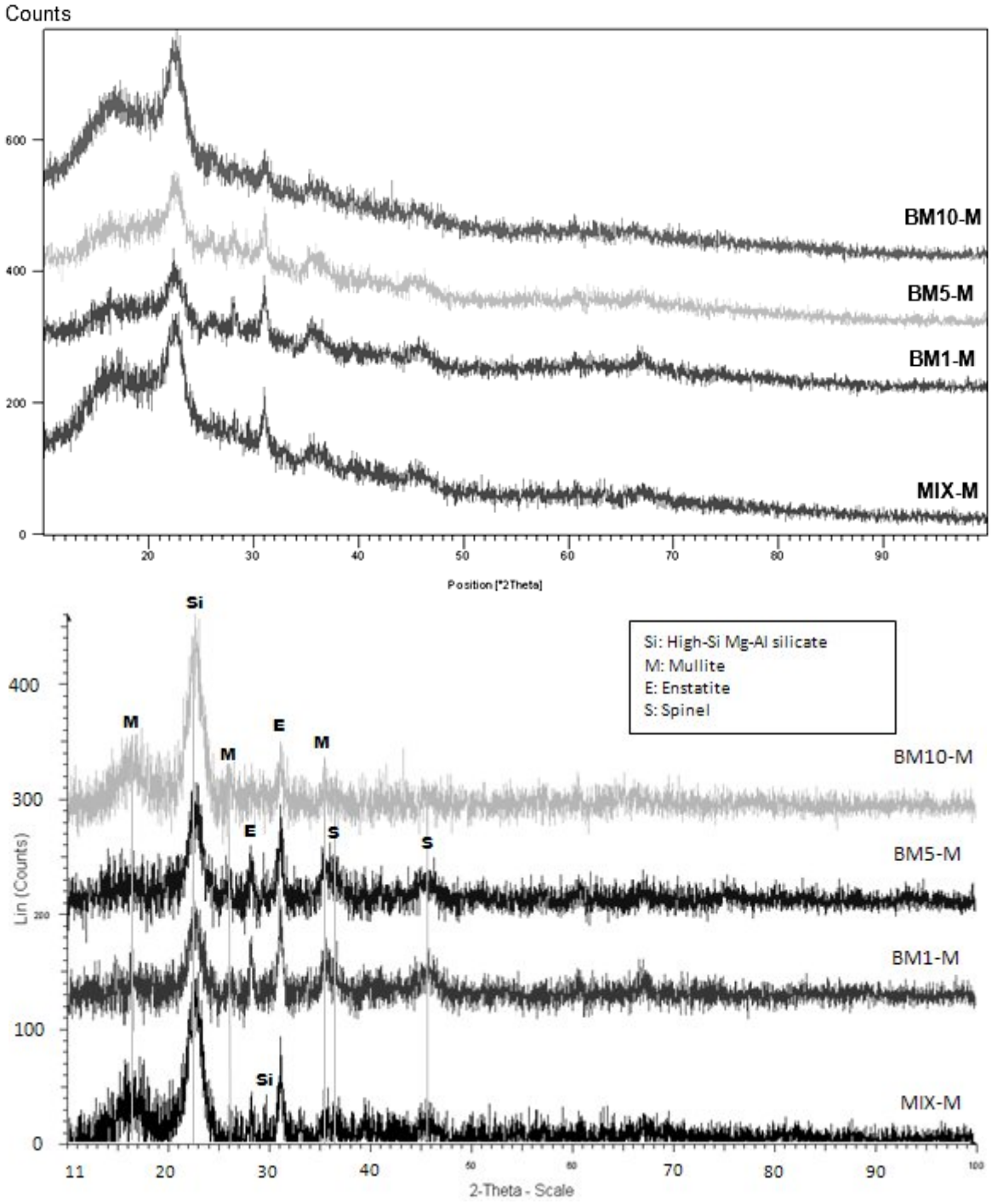

Figure 5-17: XRD pattern comparison for ball milling activation and *medium* temperature sintering, top: general pattern, bottom: back-ground removed and labelled pattern

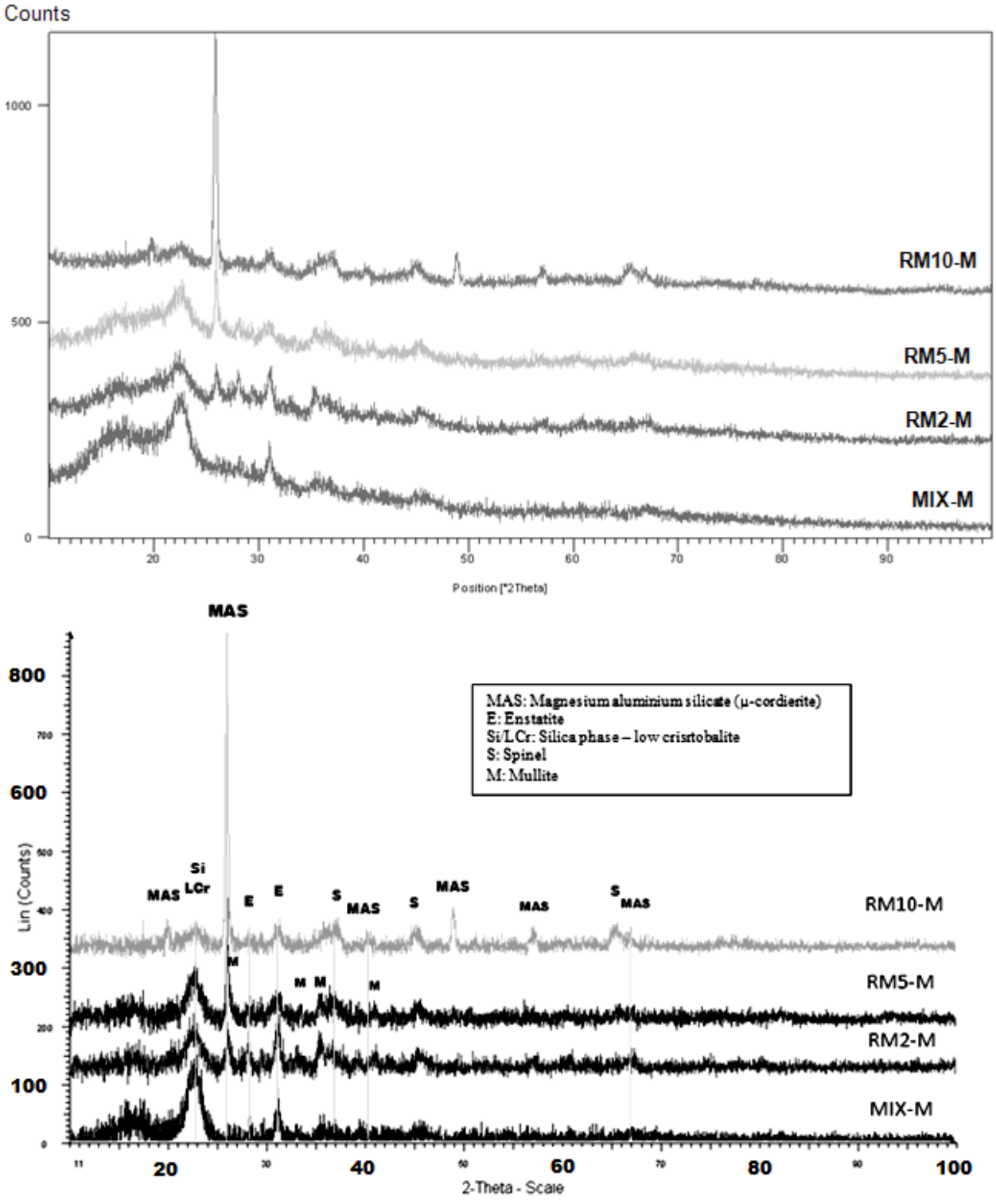

Figure 5-18: XRD pattern comparison for ring milling activation and *medium* temperature sintering, top: general pattern, bottom: back-ground removed and labelled pattern

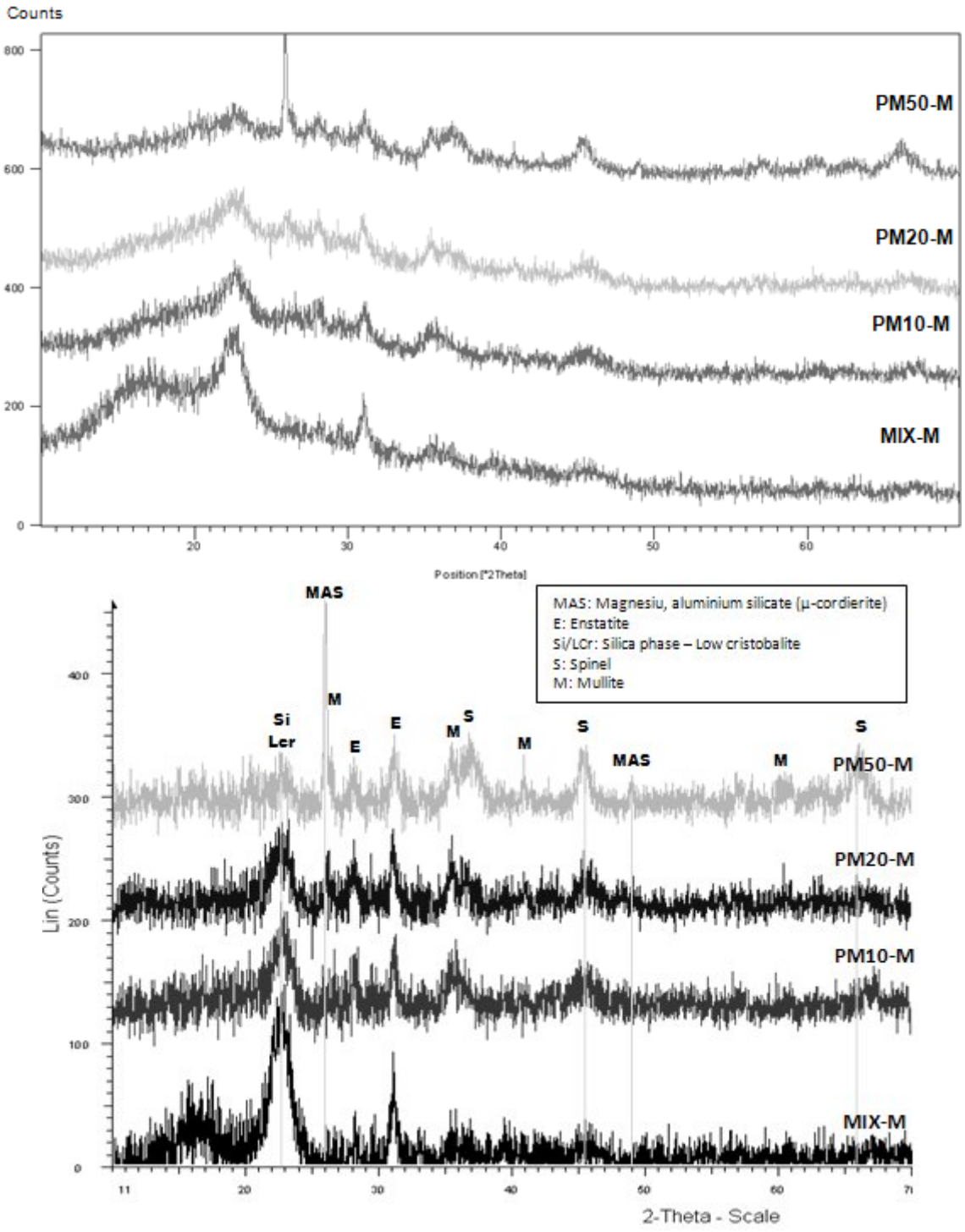

Figure 5-19: XRD pattern comparison for planetary milling activation and *medium* temperature sintering, top: general pattern, bottom: back-ground removed and labelled pattern

5-3-1-3- "*High* temperature" sintering program

By raising the sintering temperature to 1050 °C, the XRD data shows that the formation of mullite is increased. On the other hand, formation of cristobalite appears to be the direct result of the milling of the powders; for its major peak, related to (101) lattice plane, rises with the degree of activation (or increasing the milling time). It has been noted by works studying continuous (in-situ) X-ray diffraction of the phase transformations in silica-alumina-magnesia mixtures that when a mixture of talc and kaolinite is fired, there is a decrease in the formation temperature of cristobalite, but an increase in that of mullite of at least 50 °C, which is not the case when either of talc or kaolinite are fired alone [116].

In the ball-milled material (Figure 5-20) there is also an increasing trend with milling time in the amount of mullite formed, up to the point that in the sample BM10-H almost a complete XRD pattern of mullite composition is obtained. Similar patterns are observed in the RM2-H sample (Figure 5-21) and PM10-H or PM20-H (Figure 5-22); this fact shows the role of mechanochemical activation in modification of kaolinite mineral structure such that decomposition is easier or faster during heat treatment in the furnace. However, the previously mentioned trend follows the opposite direction as milling continues and activation intensifies. The amount of mullite in the sintered material at "high" temperature schedule falls after reaching a peak according to the degree of milling. This decrease occurs much more rapidly in case of such intense milling conditions as in the ring mill, and is accompanied by the formation of new phases such as those with high silicon content and magnesium silicate ("MS" in the figures). In the research by Tamborenea *et al.* [13], mullite was predominantly observed as an intermediate product in the non-activated sample, while activated samples contained more spinel, however, at temperatures higher than 1300 °C all samples produced similar products.

It seems the previous MAS phase formed at high activation degree and lower temperatures (e.g. in RM10-M) is replaced with the following phases at the higher temperature:

1- Cristobalite
2- Silicon oxide (quartz-like phase)
3- Enstatite (protoenstatite)
4- Spinel
5- Mullite
6- Corundum
7- Magnesium silicate (possibly an aluminum-bearing composition)

It should be noted that traces of corundum (α-alumina), a composition which is expected to be formed at higher temperature (≥1200 °C), was only observed in sample RM10-H. This occurrence could be regarded as an effect of intense mechanochemical action on reducing phase transformation temperatures during sintering process.

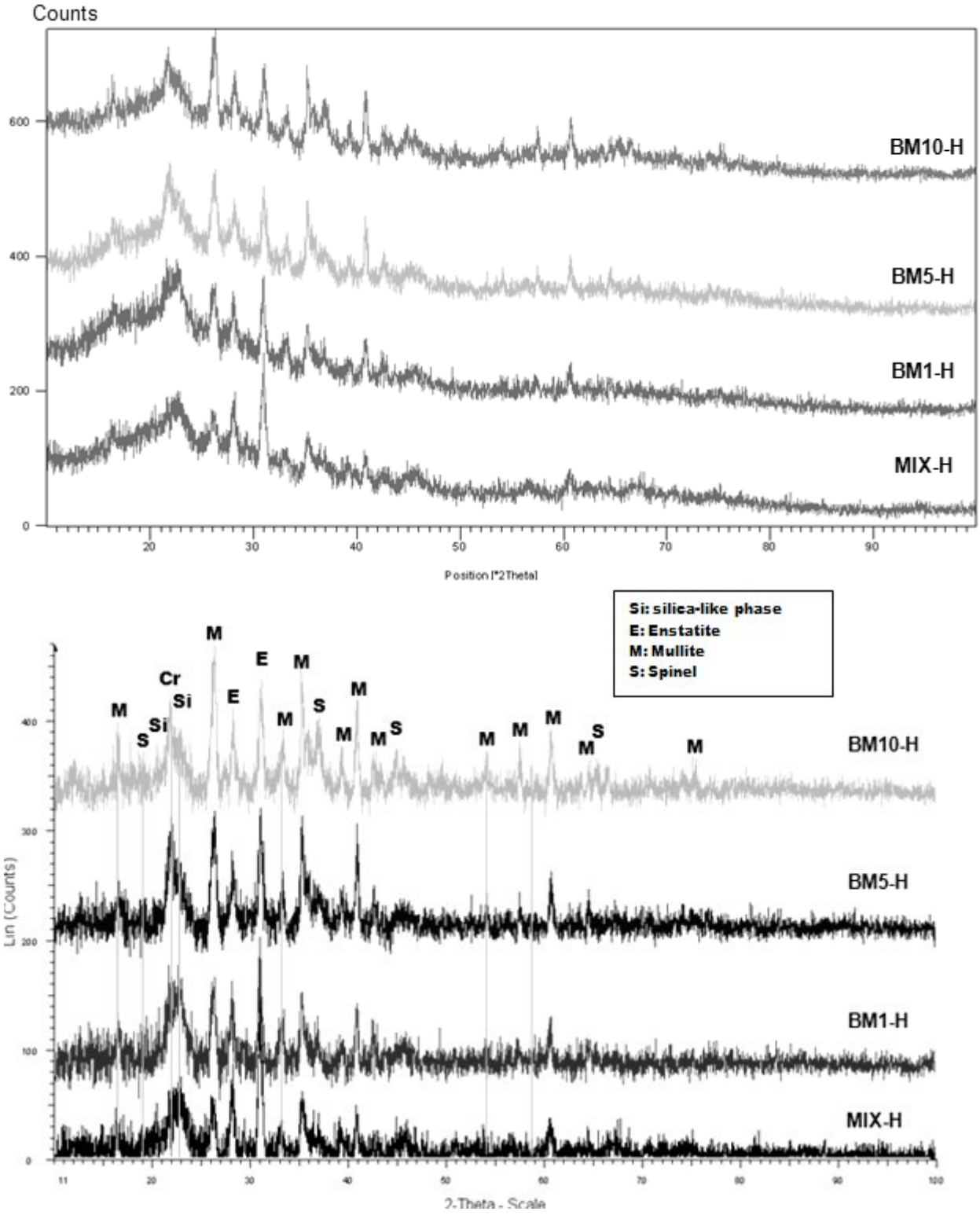

Figure 5-20: XRD pattern comparison for ball milling activation and high temperature sintering, top: general pattern, bottom: back-ground removed and labelled pattern

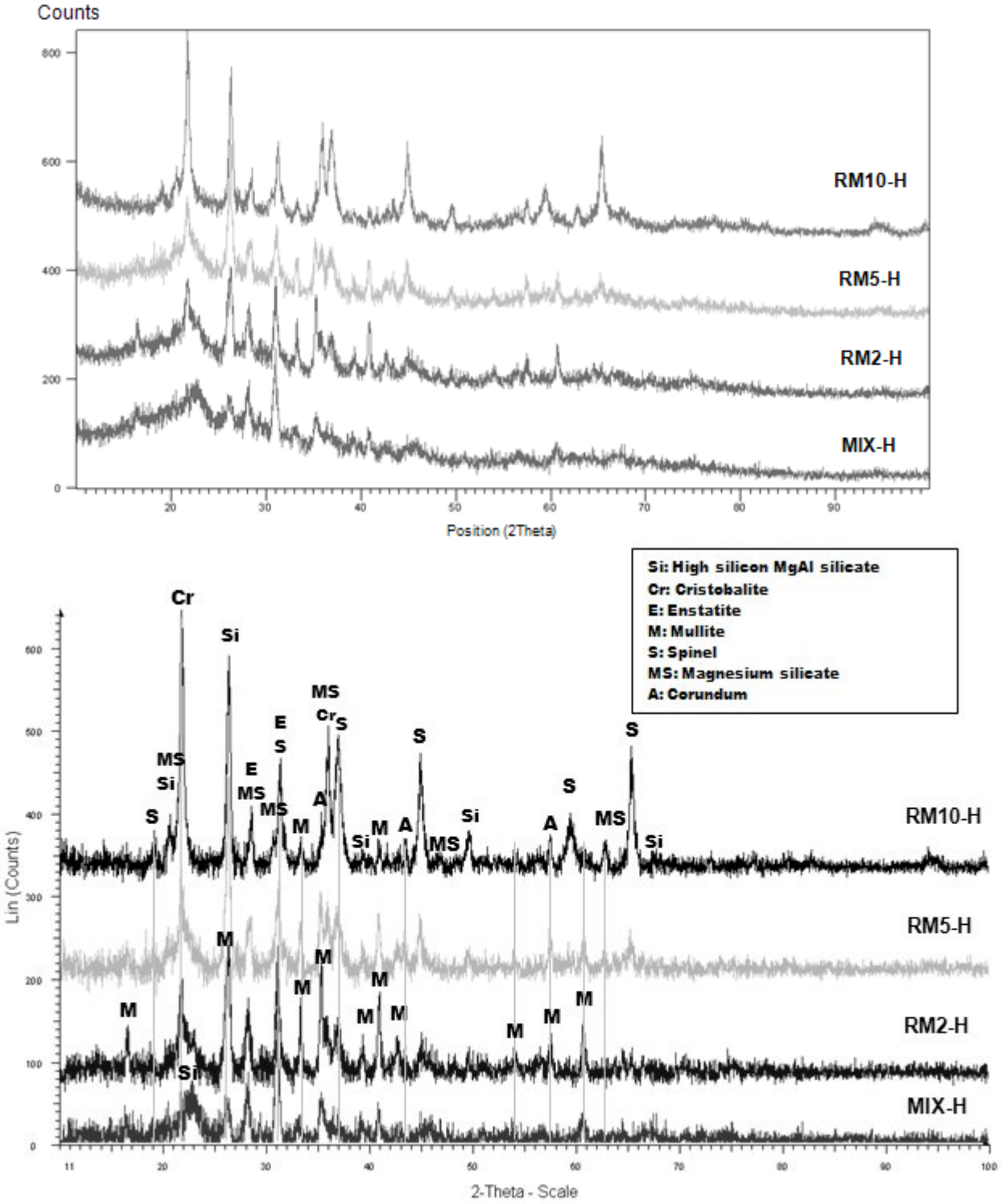

Figure 5-21: XRD pattern comparison for ring milling activation and high temperature sintering, top: general pattern, bottom: back-ground removed and labelled pattern

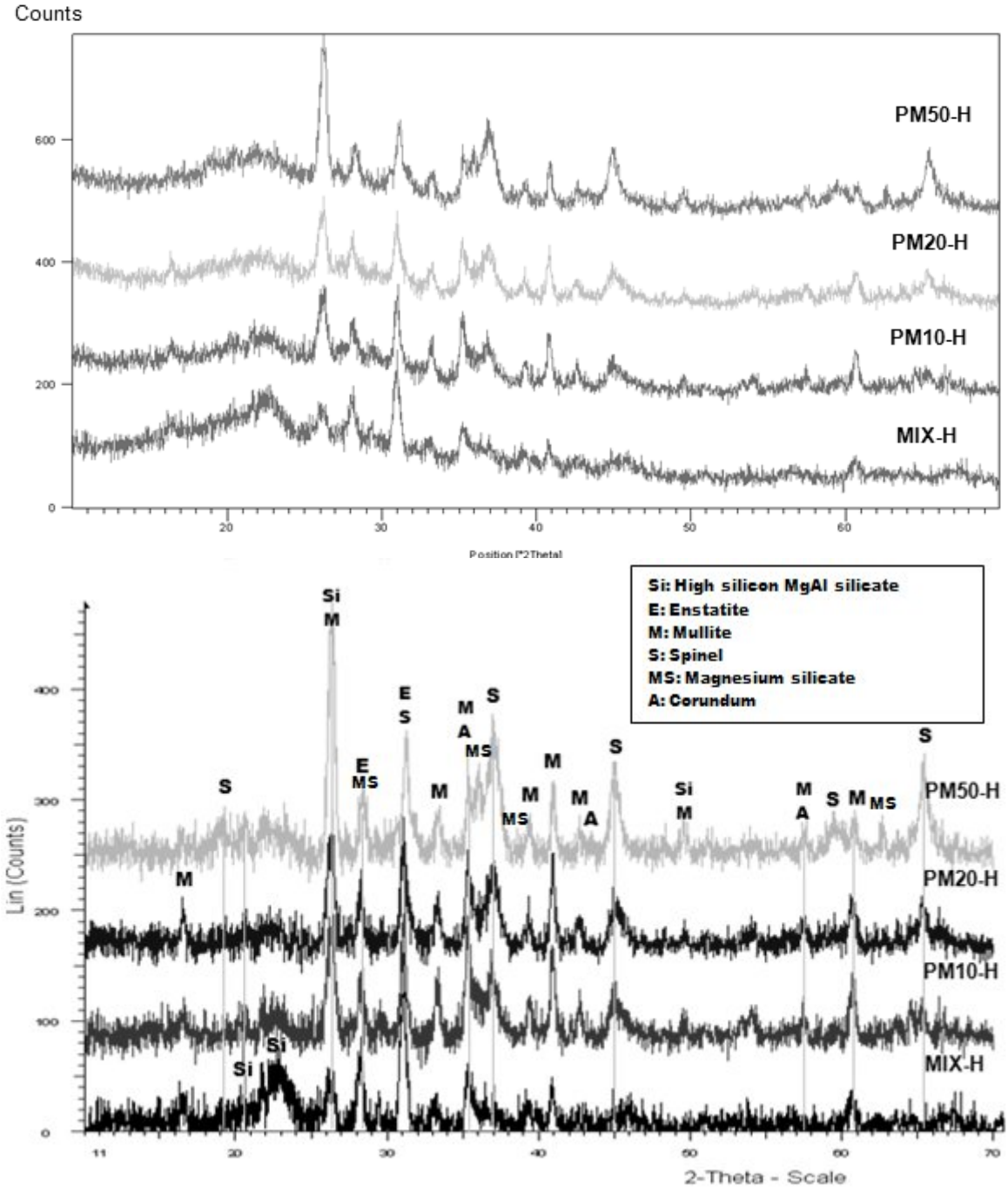

Figure 5-22: XRD pattern comparison for planetary milling activation and high temperature sintering, top: general pattern, bottom: back-ground removed and labelled pattern

In Figure 5-23, the effect of milling time (activation degree) on mullite content of different samples sintered at "high" temperature are presented as graphs showing relative XRD peak intensities for several major "d-values" of mullite crystal spacings. As is seen in the graph

related to ball-milled samples, the increase of activation time up to 10 hours (highest activation applied in ball milling) has just resulted in a continuous growing trend in the formation of mullite from decomposition of precursors. On the other hand, activation with either of the ring mill or the planetary mill first causes more mullite to be formed and later, as activation continues, production of mullite decreases; in other words, higher activation helps the dissociation of mullite which accompanies the formation of cristobalite and magnesium aluminate (spinel, $MgAl_2O_4$). Although such reaction and transformation has occurred after application of both ring-mill and planetary mill in activation of the mixture, effects have been presumably more intense in case of application of the ring mill, because at the highest degree of activation the sintered material (sample RM10-H) contains much less mullite than the similar material with maximum activation in the planetary mill (PM50-H). It is also noticeable that the latter does not show any evidence of the X-ray diffraction peak related to the formation of cristobalite in the sample.

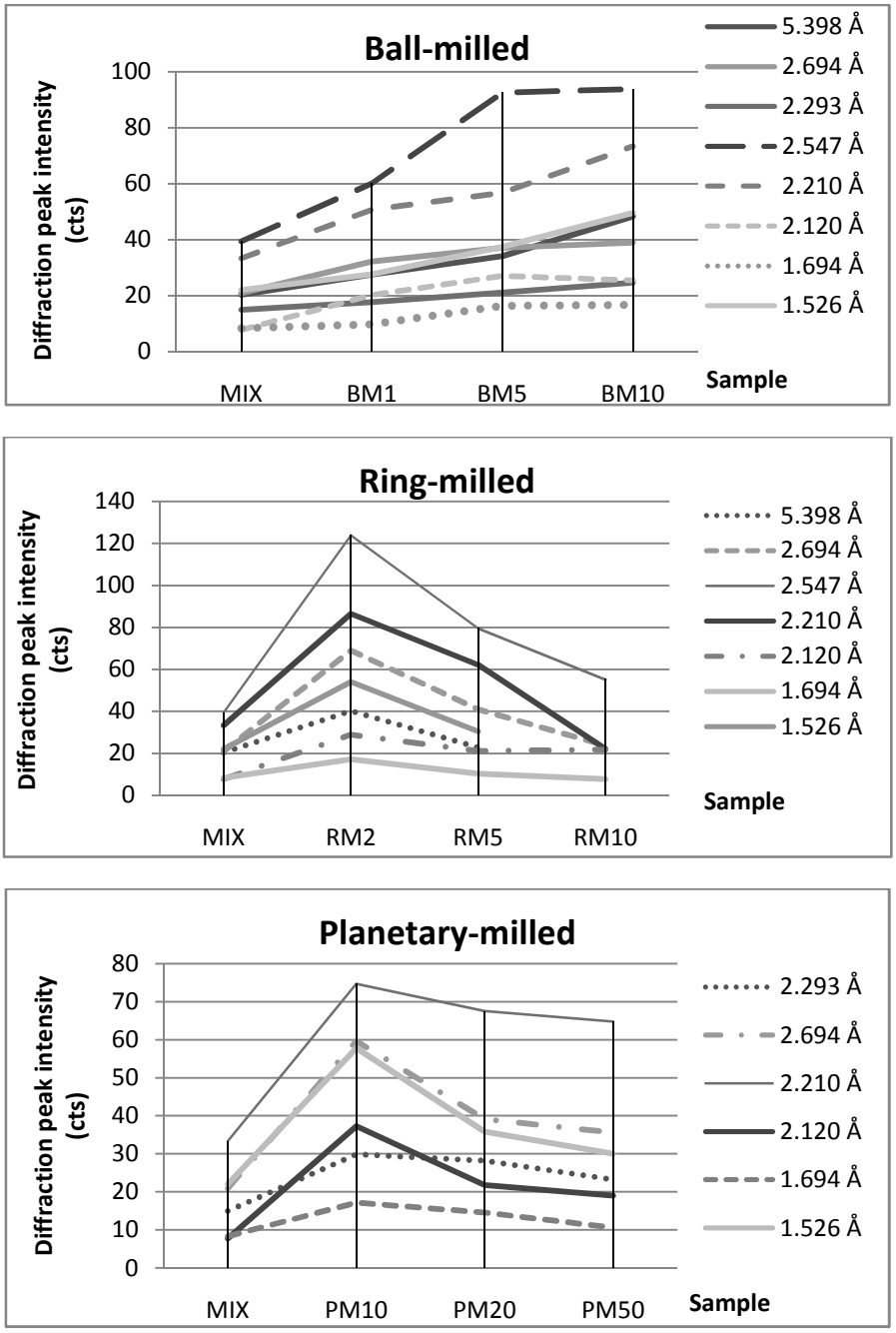

Figure 5-23: Changes of the mullite content in the samples sintered at "high" temperature schedule (trends are presented for several crystallographic d-spacings indicated with Angstrom values)

5-3-2- SEM-EDX studies

This section presents and describes the results obtained from scanning electron microscopy (SEM-EDX) studies of the polished sections prepared from sintered bodies. The observations at the three applied temperature schedules for the ball-mill and the ring-mill activated samples are discussed first. Then follows similar discussion about the results for planetary milled samples, which were not prepared at the same time in the powder activation procedure.

5-3-2-1- "*Low* temperature" sintering program

SEM images of the polished sections prepared from sintered bodies of non-activated as well as ball-milled samples at "*low*" temperature schedule are presented in Figure 5-24. It should be noted that, unless mentioned, all images are taken in the "backscattered" mode to make different phases distinguishable. As can be seen in Figure 5-24, talc particles (indicated with letter "T") still remain in the non-activated sample. These phases, which tend to decrease significantly after slight grinding (one hour ball milling), are almost completely removed after 5 hours of ball milling. Relatively large (in some cases larger than 50 μm) dark-coloured patches indicates alumina, "a" on images, (presumably amorphous) phases which did not contribute to any XRD peak. These are mainly intermediate products of structural changes in γ-alumina and decomposition products of kaolinite. Another noticeable phase is enstatite which is usually observed as needle-like bright light-coloured phases in the SEM micrographs.

As grinding progressed in the process of powder activation, the images of the sintered samples reflected the observed phase transformations. Even one hour of ball milling promoted the formation of high-silicon-bearing compositions at 950 °C. Large elongated phases are characteristics of more highly activated samples. The growth of apparently larger grains by

the consumption of smaller grains of different composition is evident. These newly formed compounds are high in silicon and contain aluminium and magnesium oxides as well ("Si" phase on images and XRD graphs). Sometimes, these large phases have a specific rectangular shape or at least two parallel sides and grow to different sizes, occasionally to larger than a hundred micrometers. But in general, at higher activation degrees, these large emerging compositions become purer with respect to the variety of phases in them, as seen in sample RM10-L (Figure 5-25) which can be considered as the most intensively milled sample in this study. Formation of pre-mullite phases around previously formed amorphous alumina compositions is also noticeable; such reaction is first enhanced with milling, and as activation continues, finally ends up in formation of high-silica compositions (corresponds to the rise and fall of the pre-mullite peak in XRD results). Figure 5-26 gives the result of EDX analysis for some of the selected points within the phase compositions in "*low* temperature" sintered bodies.

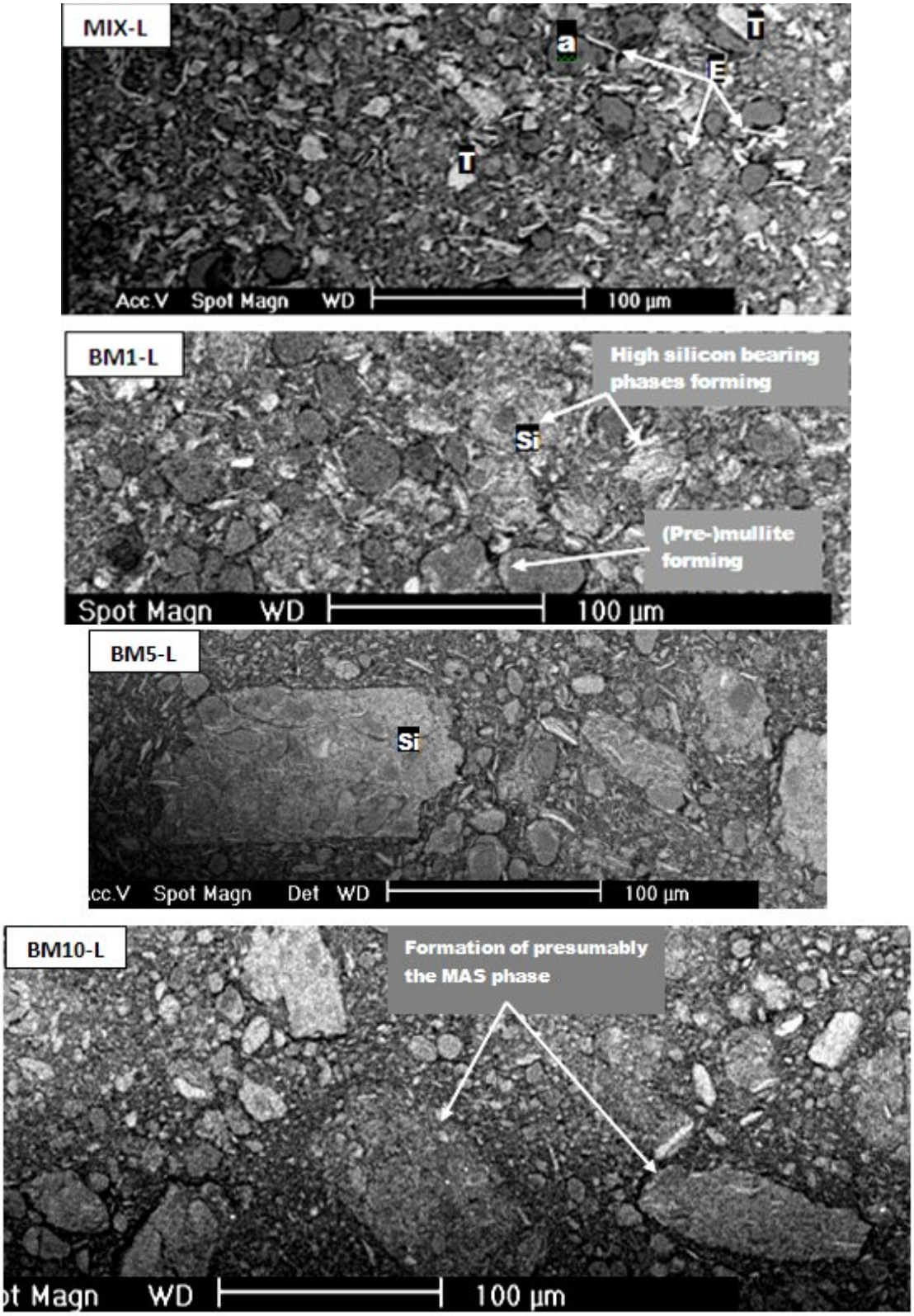

Figure 5-24: SEM micrographs of the non-activated and ball-milled compacts sintered at "*low*" temperature schedule; T: talc, a: alumina composition, E: enstatite Si: high silicon Mg-Al silicate

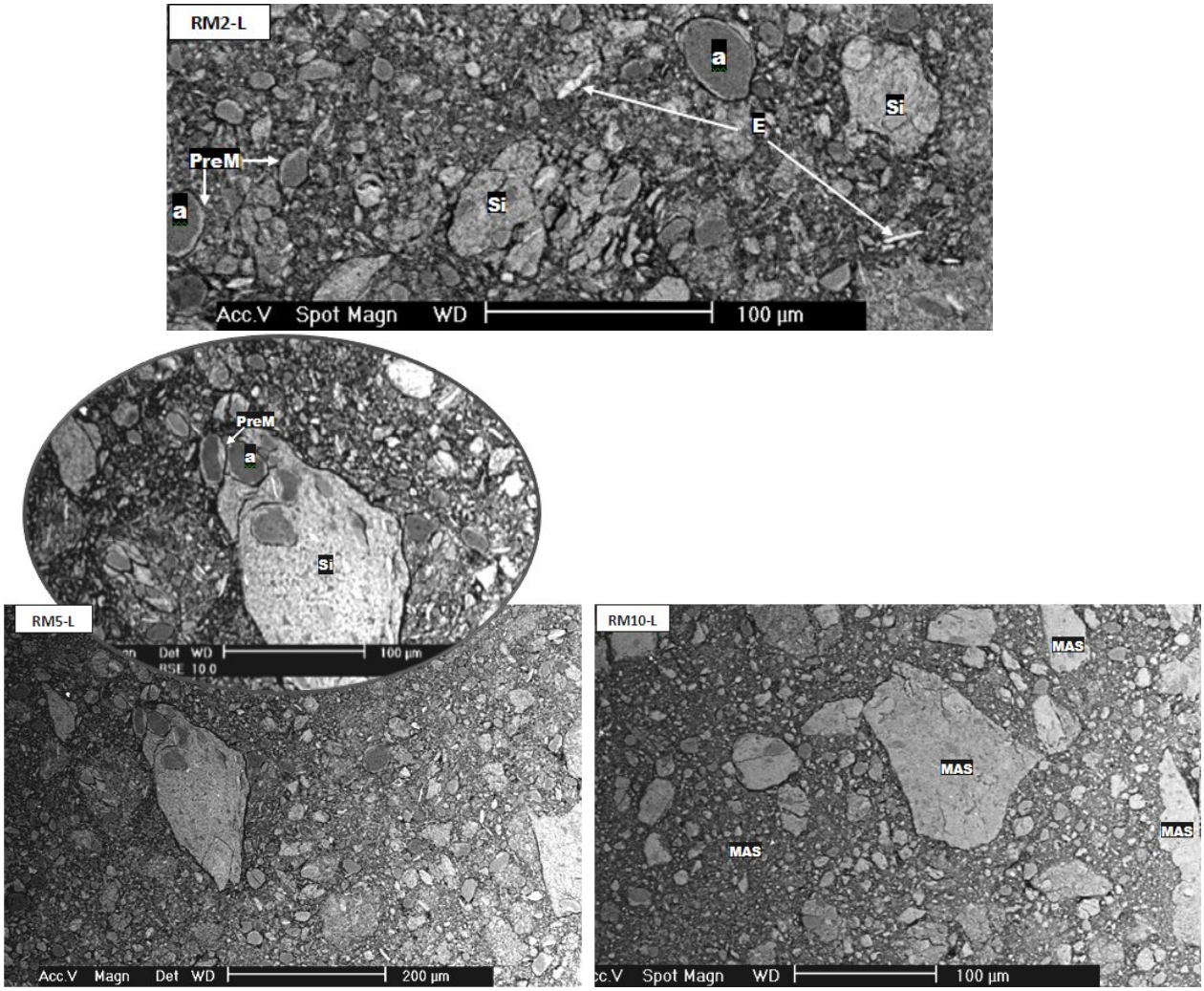

Figure 5-25: SEM micrographs of the ring-milled compacts sintered with the "*low*" temperature schedule; a: alumina composition, E: enstatite Si: high silicon bearing Mg-Al silicate, PreM: pre-mullite, MAS: magnesium aluminium silicate (cordierite composition)

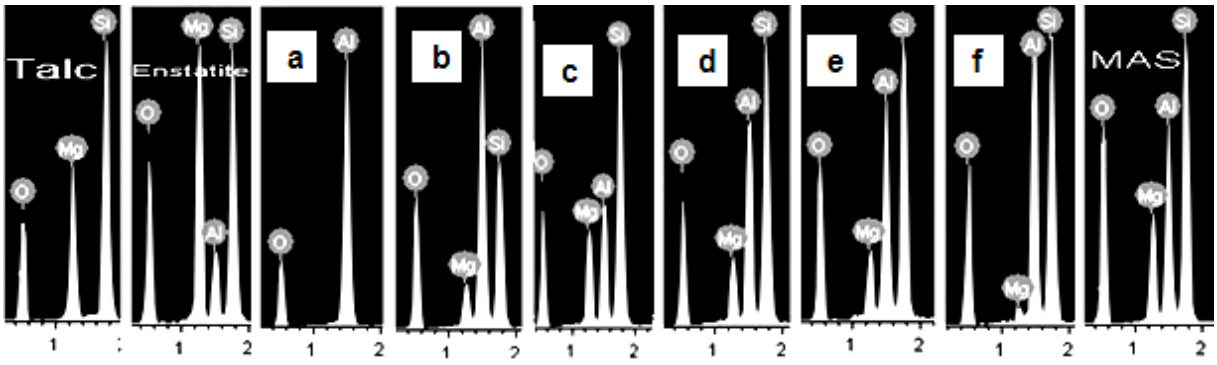

Figure 5-26: EDX analysis of some phases found in Figures 5-24 and 25; a: alumina (possibly amorphous), b: pre-mullite, c – f: High Si, variable Al/Mg phases (f is a rare case), MAS: magnesium aluminium silicate, the dominant phase in sample RM10-L with cordierite composition

5-3-2-2- "*Medium* temperature" sintering program

The results of SEM image analysis for the material sintered at 1000 °C are presented in Figures 5-27 for the ball-milled and 5-28 and 5-29 for the ring-milled samples. The most characteristic phase formation at "*medium*" temperature sintering, as previously mentioned in the XRD studies, is related to the formation of enstatite. Although this phase was also formed during sintering at "*low*" temperature experiments, its formation was mainly developed in the activated samples. At "*medium*" temperature sintering, there is first an increasing development of enstatite formed at early stages of milling (low-activation), this is most noticeable in case of ball milled and ring milled samples. Formation of high amounts of enstatite usually with high magnesium content in the two-minute ring-milled sample, confirmed by energy-dispersive X-ray (EDX) analysis (Figure 5-28), seemed to have resulted in high silicon bearing Mg,Al silicates being deprived of magnesium.

Formation of mullite from glassy phases in all samples is also noticeable. This is usually accompanied by changes colour of alumina phase ("a") to a lighter tone. High Si-bearing silicates are also formed in often regular shapes (rectangular or polyhedral) and grow in size, becoming more homogenous in composition with increasing the milling intensity/time (RM10-M in Figure 5-29). As further consequence of increasing the milling time is the development of larger pores in the sintered bodies. These pore spaces are created usually as a result of phase interactions and the merging of smaller pores; they are also formed along the boundaries of large and growing phases (as in samples RM5-M and RM10-M) as a result of shrinkage.

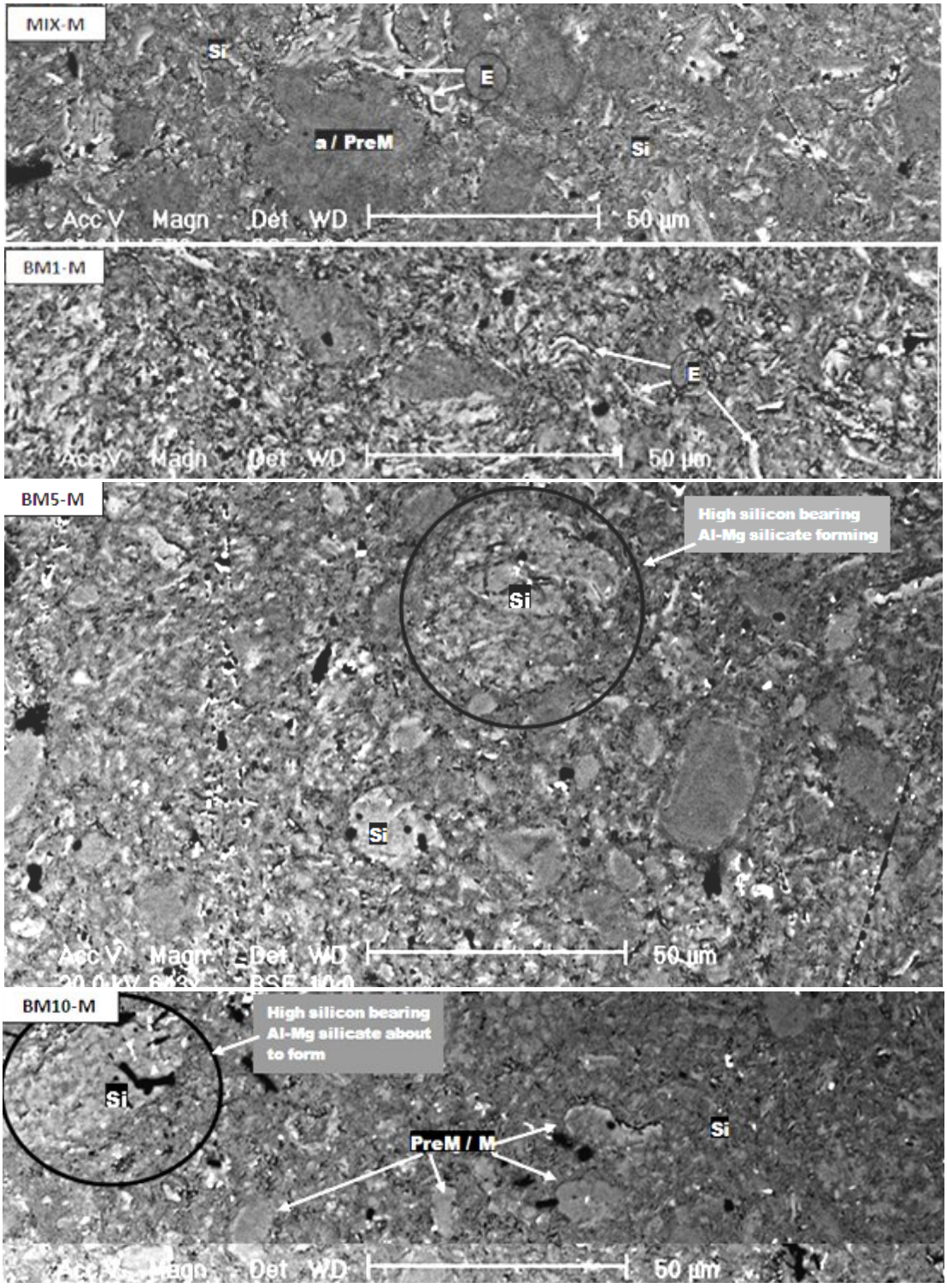

Figure 5-27: SEM micrographs of the non-activated and ball-milled material sintered under "*medium*" temperature schedule; T: talc, a: alumina composition, E: enstatite Si: high silicon Mg-Al silicate, PreM: pre-mullite, Black spots: pores

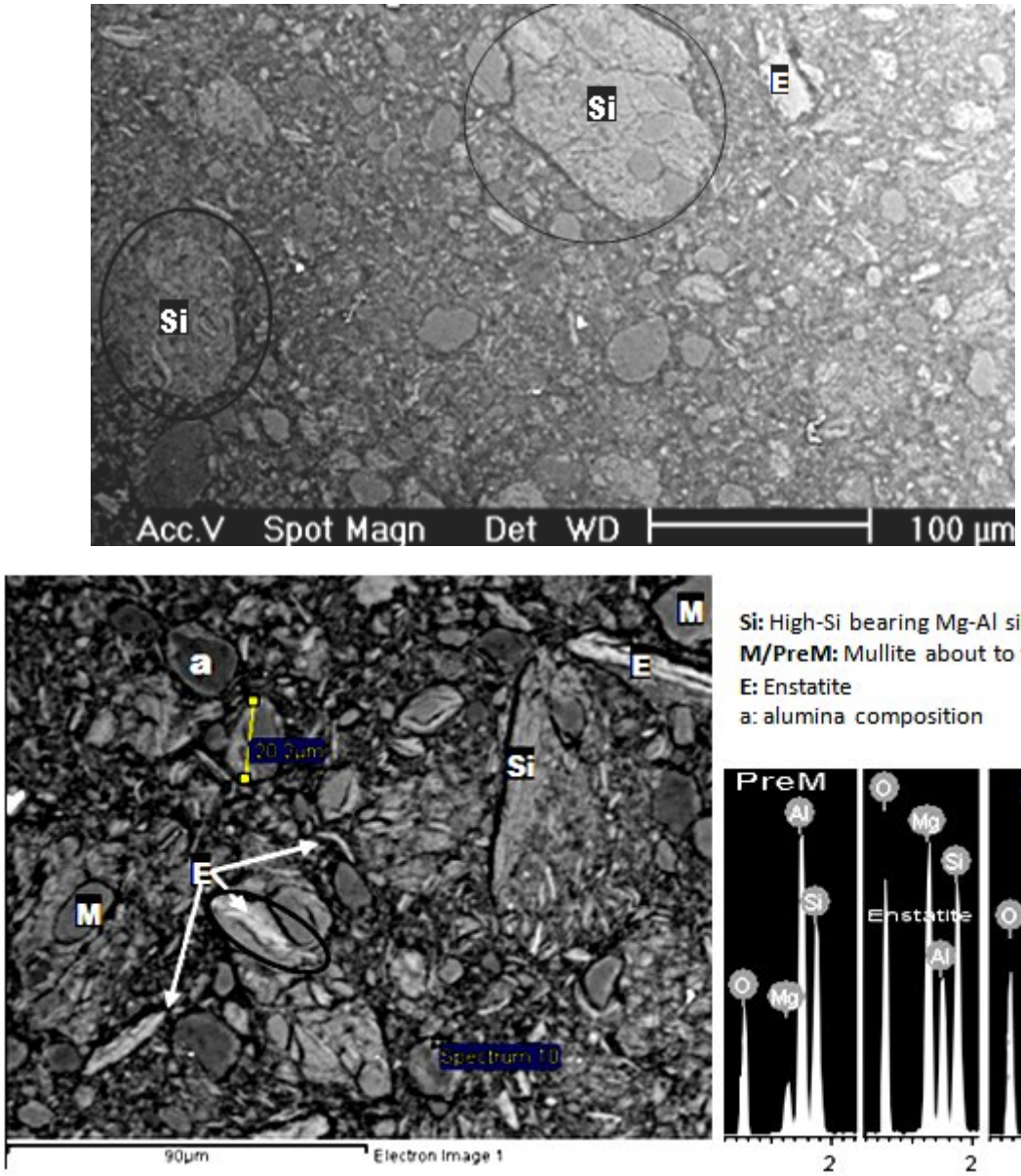

Figure 5-28: SEM micrographs and EDX spectrums for the ring-milled material sintered under "*medium*" temperature schedule; a: alumina composition, E: enstatite Si: high silicon Mg-Al silicate, PreM/M: pre-mullite/mullite

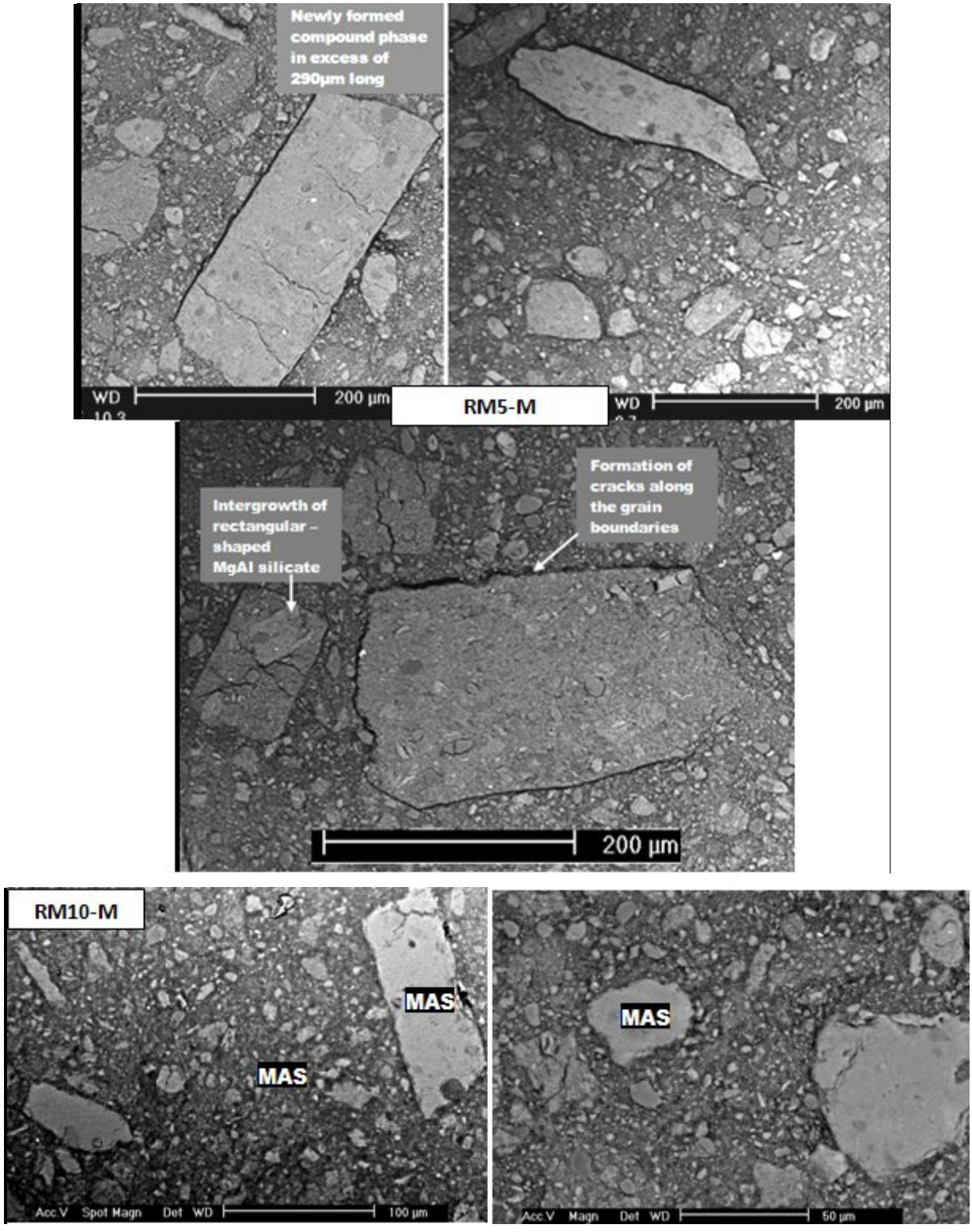

Figure 5-29: SEM micrographs for the ring-milled material (RM5 & RM10) sintered under "*medium*" temperature schedule; MAS: Magnesium aluminium silicate (cordierite composition)

5-3-2-3- "*High* temperature" sintering program

Results of increasing the sintering temperature to over 1000 ºC in development of larger pores in the ring-milled samples are observed in Figure 5-30 for different milling times.

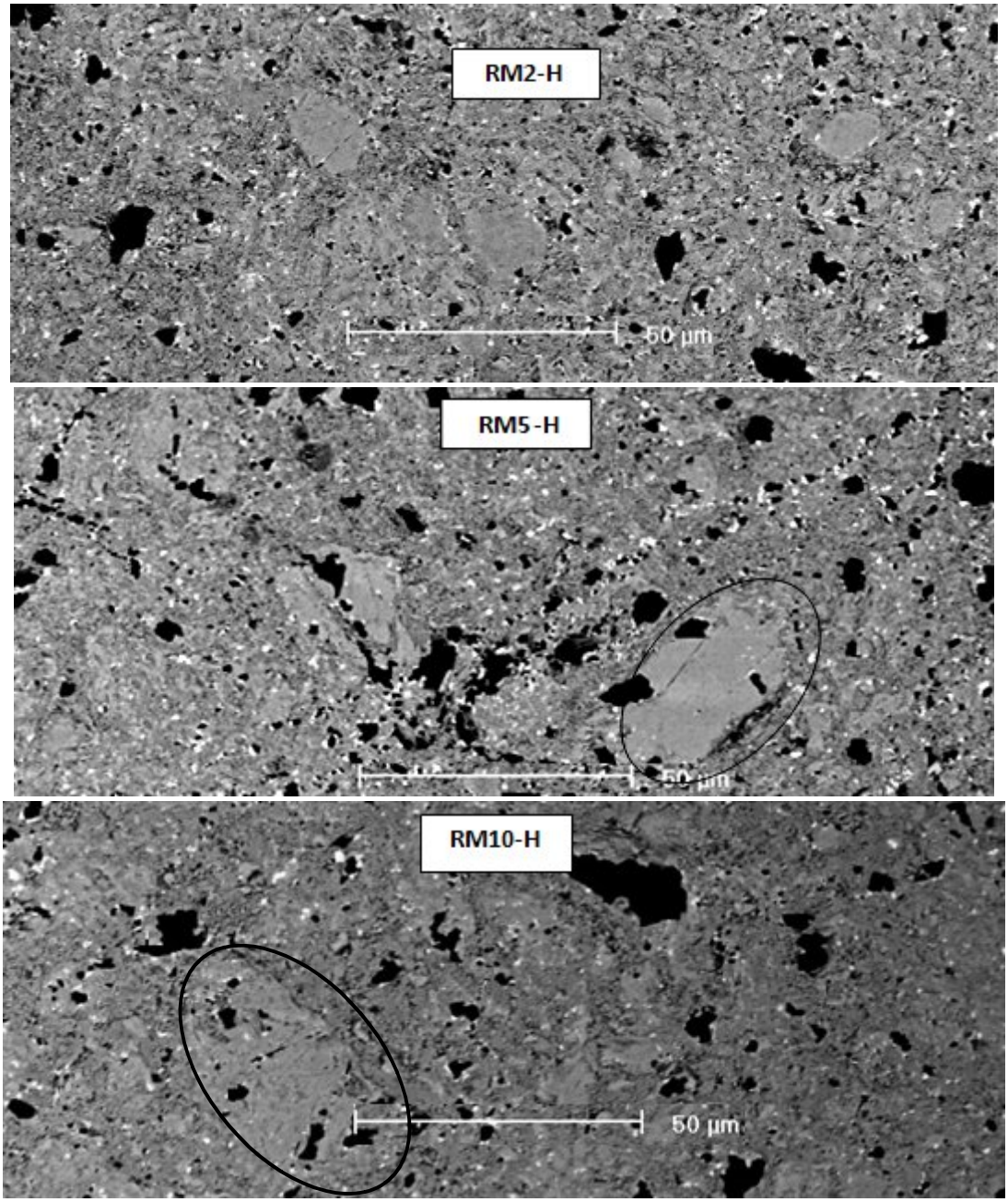

Figure 5-30: SEM micrographs for the ring-milled material sintered under "high" temperature; circled: large almost regular-shaped grains with a composition close to cordierite, black spots: voids (bright white spots are surface contaminations)

The increase in activation time has had an obvious effect on increasing the coarsening of the grains and pore size simultaneously. The large phases possess the characteristics of often hexagonal cross sections and a chemical composition close to cordierite (analysed by EDX). However, they are still considered as complex phases (as observed in grey-scale backscattered images in Figure 5-30). The matrix (generally with a darker shade) is made of almost similar composition, but contains more silicon in the Mg,Al silicate structure.

The changes in pore volume and shape during sintering process could be explained as following. When mass transfer occurs at the particles' contact points due to molecular vibrations activated by heating and high energy condition, consequently "necks" are formed at contact points that gradually grow thicker and result in removal of pores and shrinkage of the powder compact (stages 'a' through 'c' in Figure 5-31). The grain boundaries also become more distinct as the necks grow but do not migrate at this stage (i.e. most of the pores are interconnected). This is the point that the sintering process appears to have reached in the *high* temperature tests in the current study.

As sintering continues, the pores start to disconnect at thinner areas, and the material transport occurs on the pore surfaces in order to equalise the chemical potential and the pores gradually become spherical (stages 'd' through 'f' in Figure 5-31). Depending on the material characteristics, the densification at this intermediate stage might reach up to 85-95 %. As particle bonding and boundary migration progress, the number of particles around the pores decrease, the pores shrink in size and finally are trapped within the grains (stage 'g' in Figure 5-31). During the final stage of sintering the isolated pores also tend to be removed by heating [117].

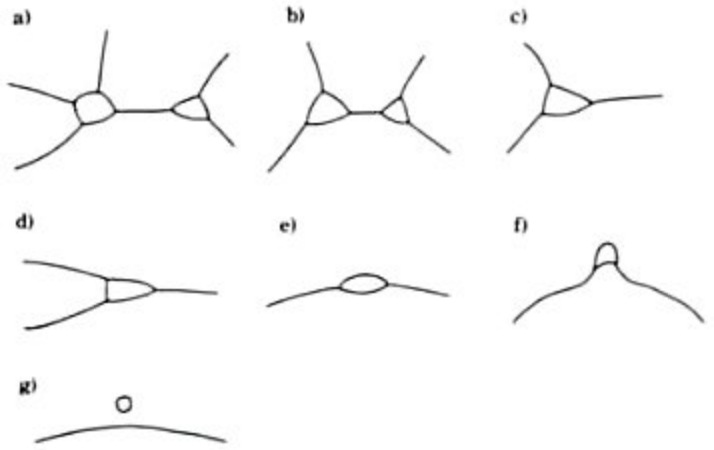

Figure 5-31: Pores merging and isolation as sintering of a green ceramic body progresses; curved lines indicate phase boundaries; different stages are explained in the text [117]

It is however important to emphasise here that in the current study, the intense mechanical action caused by milling the precursor powders has to some extent modified the temperature-affected densification process mentioned above. Therefore the mechanically induced structural defects and subsequent phase transformation during heat treatment, as discussed in the SEM results, have substantially influenced the coarsening-densification trend.

5-3-2-4- Planetary-milled samples

SEM micrographs related to planetary-milled samples sintered at different temperatures are presented in Figure 5-32. Major findings about these samples are summarised below:

- Similar to other milling methods grain growth and the formation of different phases specifically high silicon bearing compositions is observed as temperature increases
- More activation (longer milling) helps in consumption of previously formed phases, namely the alumina compositions (dark-shaded almost round grains)
- Activation using the planetary mill, in general, has resulted in formation of finer-grained phases in the samples compared to the other milling methods, however,

complex elongated phases such as those common in the ring-milled samples were also observed (PM10-H and PM20-H in Figure 5-32-c)

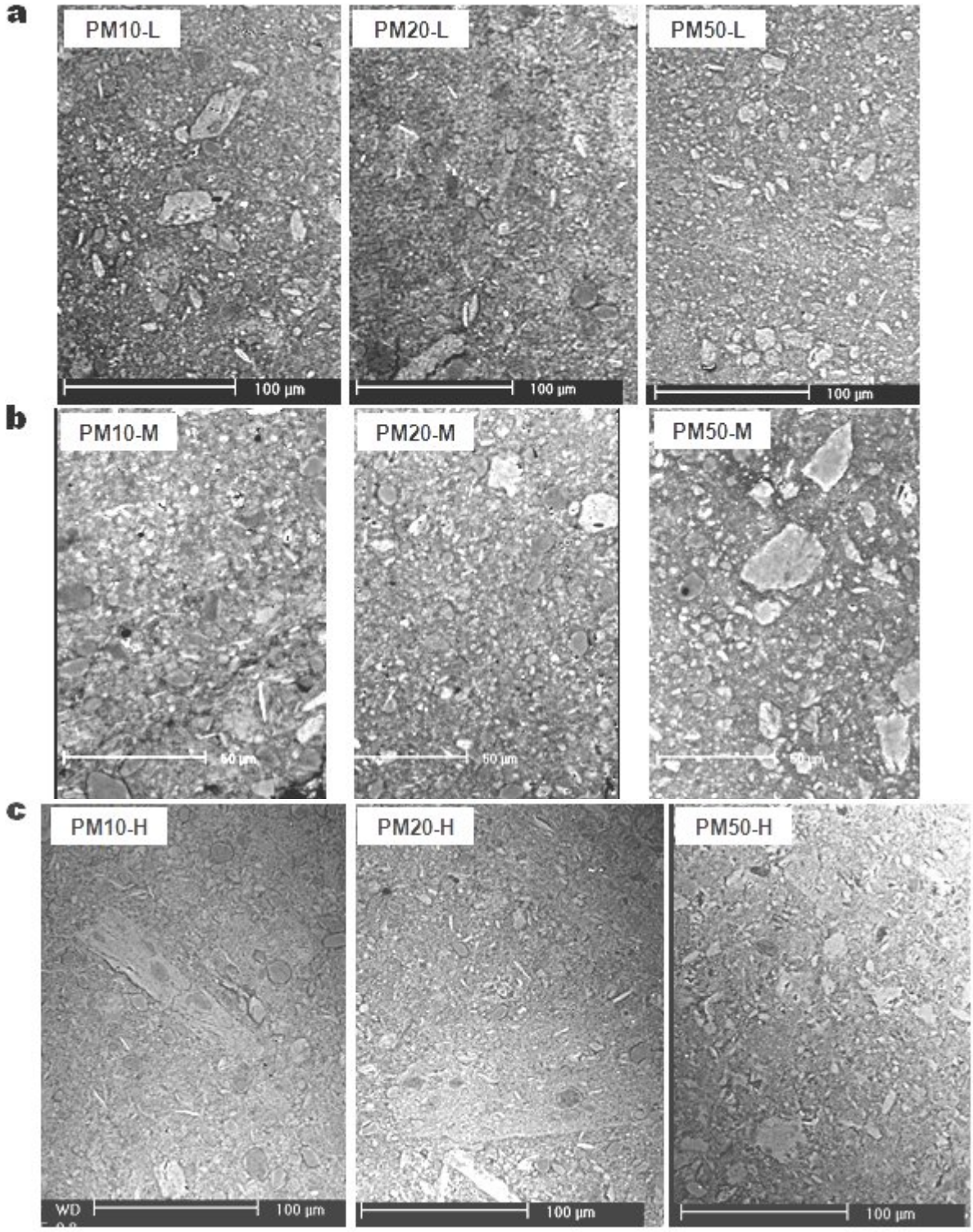

Figure 5-32: SEM micrographs for the planetary-milled material sintered at different temperature schedules; a: "*low* temperature", b: "*medium* temperature", c: "*high* temperature"

5-3-3- Density and porosity measurements

Before presenting the results in this section, it would be useful to give an introduction to densification process in solid-state sintering of materials. The driving force for sintering is the reduction in surface free energy of the consolidated mass of particles. This reduction in energy can be accomplished by atom diffusion processes that lead to either densification of the body (by transport of matter from inside the grains into the pores) or coarsening of the microstructure (by rearrangement of matter between different parts of the pore surfaces without actually leading to a decrease in the pore volume). The diffusion paths for densification and coarsening are shown in Figure 5-33 in an idealised situation. In fact, sintering involves a competition between densification and coarsening; depending on whichever dominates, the production of dense or highly porous body will be favoured [6, 95].

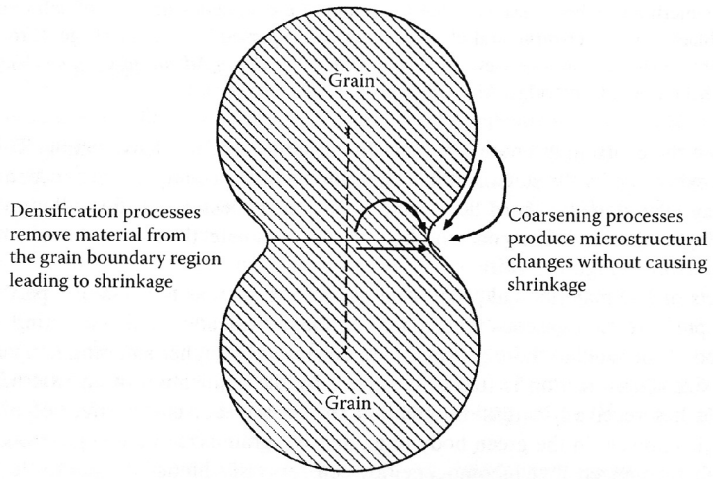

Figure 5-33: Schematic indication of the distinction between densification and coarsening microstructural changes during ceramics sintering [95]

Bulk density values obtained from dimensional measurements of the sintered cylindrical compacts are shown in Table 5-4. For the purpose of shrinkage evaluations, since the diameter of the non-sintered samples was the same and equal to the die diameter, the difference between the diameter of the sintered and non-sintered samples was considered as a

measure of the linear shrinkage which is provided as a percentage value according to the following equation:

Radial shrinkage of a cylindrical sintered body = $(1- \Phi_s/ \Phi_p) \times 100$

where, Φ_s= diameter after sintering, and Φ_p= diameter before sintering.

Table 5-4: Porosity and bulk density measurement data for cylindrical compacts

Sample	Bulk density (kg/m^3)	Shrinkage (%)	Sample	Bulk density (kg/m^3)	Shrinkage (%)	Sample	Bulk density (kg/m^3)	Shrinkage (%)
MIX	1410	-	RM2	1500	-	PM10	1560	-
MIX-L	1270	1.04	RM2-L	1440	2.43	PM10-L	1520	2.31
MIX-M	1300	2.43	RM2-M	1480	3.24	PM10-M	1580	2.78
MIX-H	1370	3.59	RM2-H	1720	8.45	PM10-H	1780	7.41
BM1	1540	-	RM5	1480	-	PM20	1530	-
BM1-L	1380	1.16	RM5-L	1490	4.17	PM20-L	1570	3.47
BM1-M	1420	2.55	RM5-M	1560	6.02	PM20-M	1630	3.93
BM1-H	1500	5.44	RM5-H	2020	14.12	PM20-H	1830	10.88
BM5	1550	-	RM10	1440	-	PM50	1480	-
BM5-L	1400	2.43	RM10-L	1630	9.72	PM50-L	1680	6.25
BM5-M	1450	3.24	RM10-M	1640	10.30	PM50-M	1820	7.41
BM5-H	1670	8.10	RM10-H	1960	14.70	PM50-H	2340	15.51
BM10	1480	-						
BM10-L	1420	3.59						
BM10-M	1470	4.74						
BM10-H	1830	10.76						

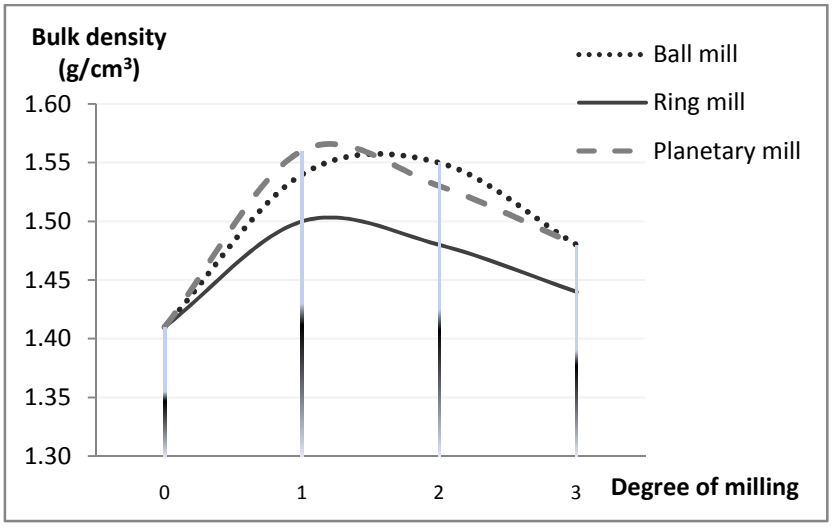

Figure 5-34: Change in the bulk density of the non-sintered cylindrical compacts according to the degree of activation

As seen in Figure 5-34, the density variations for the non-sintered cylindrical compacts made of differently milled powders tend to give more or less similar patterns. The compressed bodies of slightly activated material show an increase in the bulk density value, which could be a result of homogenisation of powder mixture with respect to particle size as well as its dehydration. As milling/activation continues (beyond preliminary stages), compaction of the powders with similar amount of load and compression rate, makes less dense bodies. This latter phenomenon is possibly the result of an increase in the degree of agglomeration that finally lead to creation of cavities and cracks in the compressed sample.

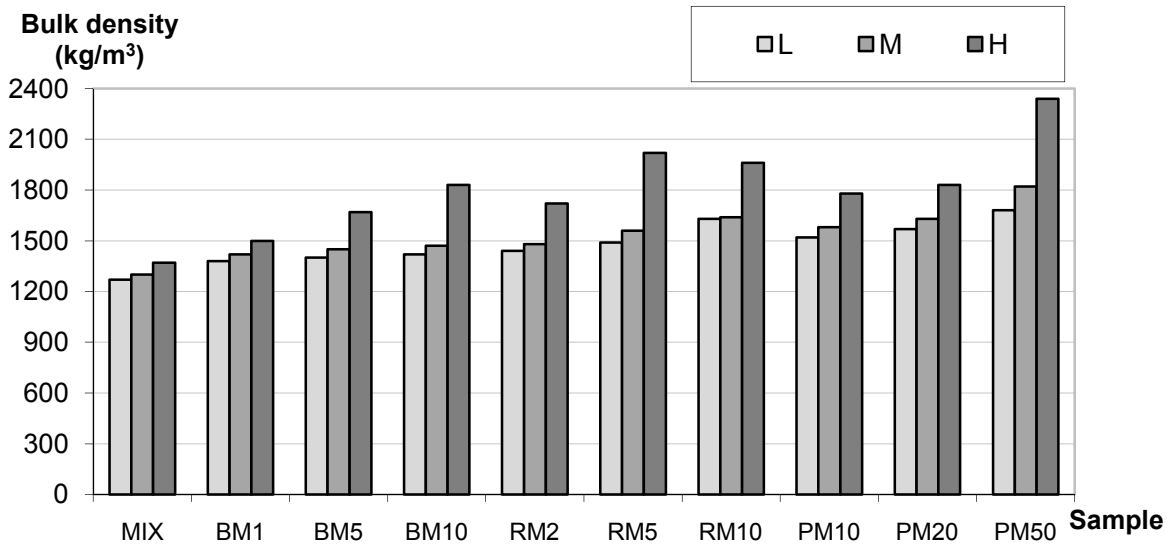

Figure 5-35: Bulk density of the sintered compacts for different samples (the legend shows the temperature profile; L=*Low*, M=*Medium*, H=*High*)

The data in Table 5-4 shows that for the sintered bodies an increasing trend is obvious in the bulk density value as the milling/activation progresses. This is observed in Figure 5-35 by comparing 3-bar sets of different activation degrees and methods with each other. Considering first the individual milling conditions, i.e. the 3-bar sets in Figure 5-35, the effect of sintering temperature could be investigated. Again, the trend (expected thermodynamically) is the

positive relationship between sintering temperatures and bulk density values of sintered samples, no matter if the previous activation (using any method) is applied on the samples.

The effect of milling/activation time on density when heat treated at the *high* temperature ("H") profile is clearly visible in Figure 5-35. This could also be attributed to the combined effect of high activation and high temperature. It can be concluded that more activation, at least to the limits applied in this research, resulted in denser bodies at relatively high temperature (in excess of 1200 °C). The maximum bulk density value (2340 kg/m^3) obtained in these experiments was found in sample PM50-H which is about 70% greater than the value obtained without activation (sample MIX-H). A further observation from Figure 5-35 is the decrease in bulk density value of the ring-milled sample sintered at *high* temperature (RM10-H); this sample is considered to have experienced the highest intensity of milling/activation from the results of structural studies (XRD and SEM). Whether the density tend to decrease or increase after this point at the applied sintering temperatures, could only be determined if ring milling time were extended beyond the current limit.

Results from linear shrinkage measurements for the sintered samples also support the density trend. As seen in the second graph (entitled RM) in Figure 5-36, the rate of shrinkage is decreased in sample RM10-H, though it still increases in the other two series of measurements (BM and PM). Considerable greater shrinkage is observed in those samples sintered under the *high* temperature profile ("H" curve) due to higher atom mobilities at higher temperature in the samples activated by different milling methods.

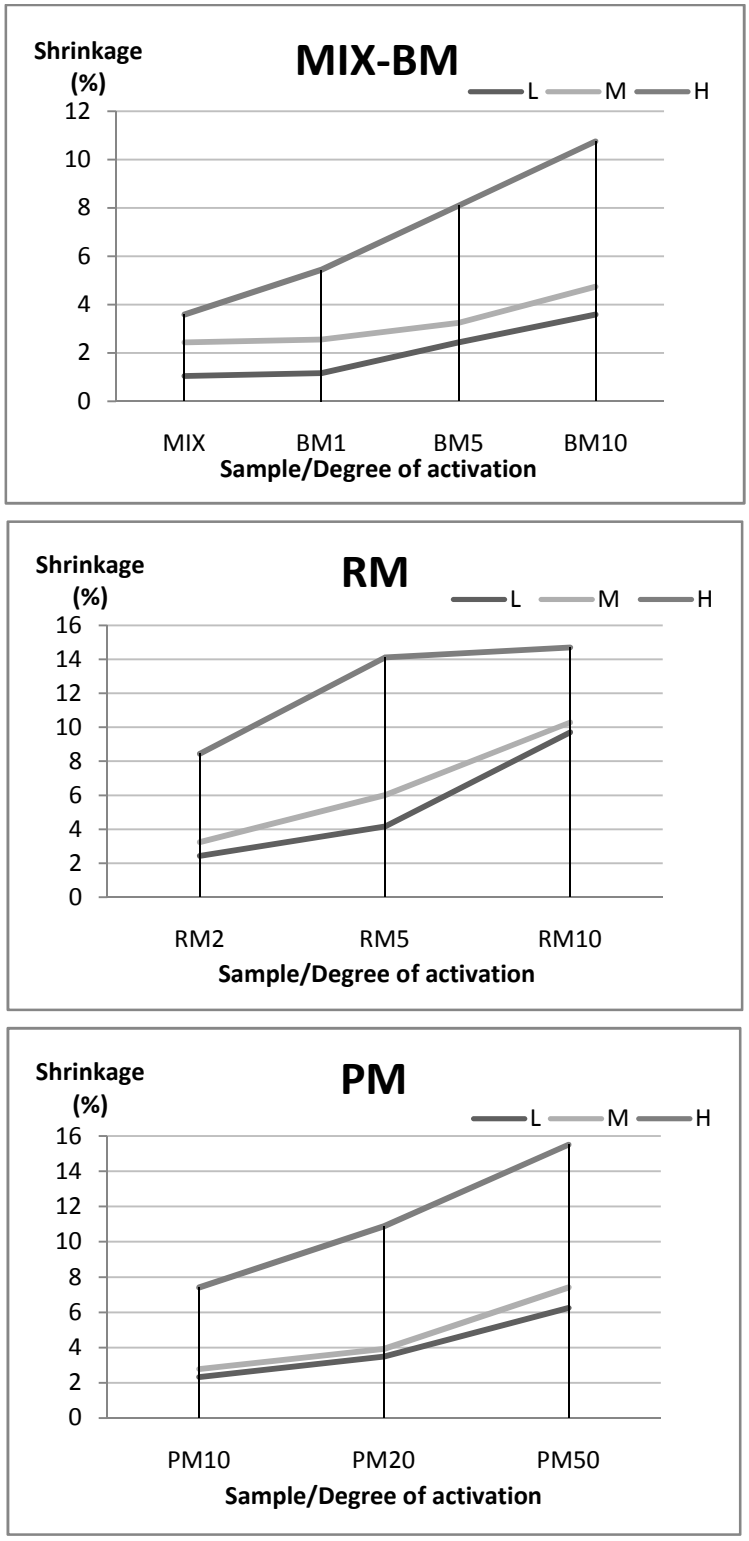

Figure 5-36: Linear shrinkage in sintered (non-activated and differently milled) samples

It is important to understand the mechanism by which higher temperature sintering has resulted in larger shrinkage (or higher densification). Although densification and reaction will

most likely occur by different mechanisms, they both involve diffusion and are, therefore, expected to be thermally activated, so the rates have an Arrhenius dependence on temperature [95]. The dependence of the densification rate and the reaction rate on the temperature is sketched in Figure 5-37, where it is assumed that the activation energy for densification is greater than that for the reaction. In this case, increasing the temperature leads to an increase in the densification rate relative to the reaction rate.

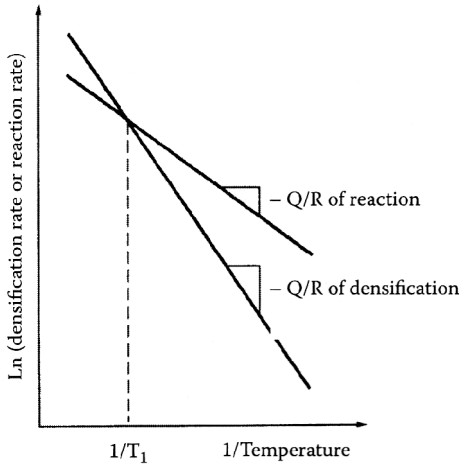

Figure 5-37: Effect of sintering temperature on the rates of densification and reaction during reaction sintering of a powder mixture [95]

To see how the activation affects the porosity of the material after sintering at the applied temperatures, the ball-milled as well as the non-activated samples were used for porosity evaluation by mercury porosimeter. Results are shown in Table 5-5 and Figure 5-38. This method (based on capillary law for liquid penetration into pores) is usually preferred [118] over other porosity determinations (such as BET gas adsorption) to give more accurate data on broader pore size distributions as well as bulk densities. Since the "*high* temperature" sintering profile was found to be of more interest with respect to the structures and phases formed, other relevant samples for this condition were also subjected to porosity analysis, of which the results are presented in Table 5-5 and Figure 5-39.

Table 5-5: Porosity measurement data (in percentages) for the sintered bodies

MIX-L	52.87	**B**M1-L	48.09	**B**M5-L	45.93	**B**M10-L	42.71	**R**M2-H	39.13	**P**M10-H	33.51
MIX-M	51.30	**B**M1-M	49.26	**B**M5-M	47.44	**B**M10-M	43.43	**R**M5-H	28.30	**P**M20-H	30.26
MIX-H	49.51	**B**M1-H	42.63	**B**M5-H	38.75	**B**M10-H	33.17	**R**M10-H	30.49	**P**M50-H	20.46

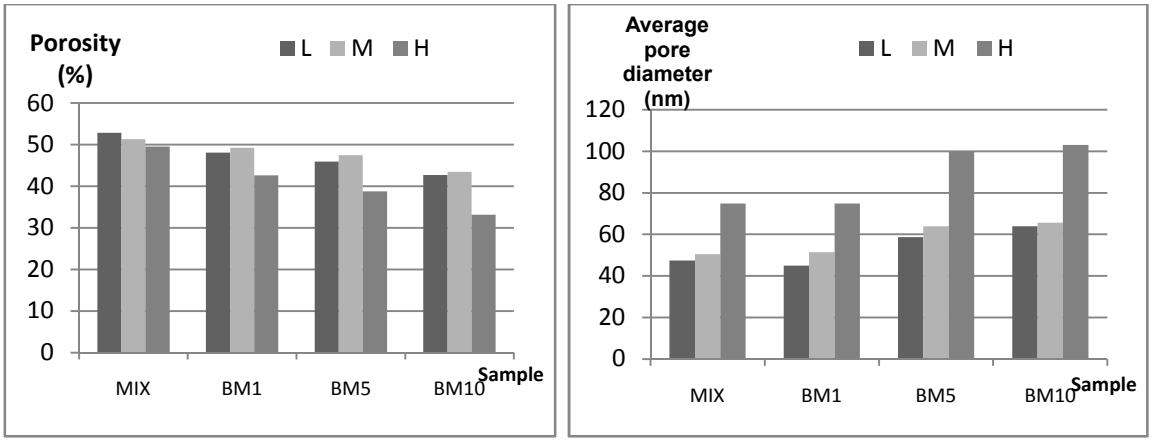

Figure 5-38: Changes of porosity (left graph) and pore size (right graph) in sintered bodies according to milling time and temperature

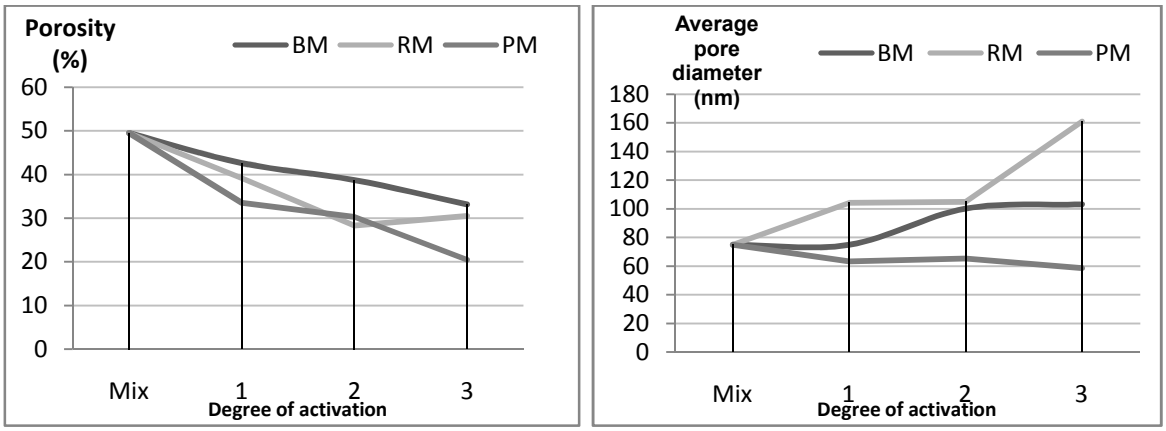

Figure 5-39: Changes of porosity and pore size in samples sintered at *high* temperature ("H") according to milling method and intensity

In Figure 5-38, the graph on the left shows how the porosity values in sintered compacts decrease with increase in milling intensity/time, however, there is a slight increase in the porosity value at *medium*-temperature sintering condition, "M", for the milled samples at shorter milling times.

As the milling conditions become more intense, larger pores tend to form in the sintered samples; this effect is much more pronounced under the *high* temperature condition (the right hand bar chart in Figure 5-38). Under the *high* temperature conditions ("H"), according to the graph on the left in the Figure 5-39, further activation process decreased the porosity in the sintered bodies, except for the sample RM10, where the porosity value increased again. This conforms to previous observation of decrease in density and shrinkage for the most intensively milled sample (RM10). There is also a noticeable increase in the pore size within the sample RM10-H (exceeding 160 nm) according to the right graph in Figure 5-39. The larger pore size specification of the RM10-H was also observed in the SEM analyses (section 5-3-2-3). Looking at the same graph, it appears that planetary milling in these experiments provided the maximum compaction of the powders which best reflected in the porosity measurements data for the sintered bodies. Porosity content of about 20.5% and average pore diameter of less than 60 nm are the specifications of sample PM50-H.

Apart from the milling procedure and methods, during the compaction procedure of the ceramic precursors other processing factors such as the addition of a binder or application of high compression loads (in excess of 100 MPa) could affect the density and porosity of the sintered material. Adjustment of sintering parameters such as heating rate could also result in significant modifications of the structure of the sintered bodies. On the other hand, while such processing parameters need to be best determined in the synthesis of ceramics, the effects of starter material properties must not be underestimated. For example the effects of particle size distribution on the packing and the compaction behaviour could cause a significant difference. A wider size distribution produces a higher packing density after die filling, but a narrow size distribution is found to produce a higher compact density after pressing [6].

According to the results of studies on the effects of particle size of precursor powders (especially talc) on densification of cordierite ceramics made of ball-milled and sintered mixture of kaolin, talc and alumina, it has been found that as the particle size of the mixtures becomes smaller, the raw material powders are mixed more uniformly and consequently the formation temperature of α-cordierite is decreased. Dense and pore-free sintered bodies are obtainable by firing ground mixtures with particle size smaller than 0.39 μm at temperatures as low as 1200 °C. Such fine (talc) particles are more easily decomposed by heating and contribute in the formation of new phases. Material bending strengths are improved and the thermal expansion coefficients of dense, high-strength cordierite bodies increase due to the lack of anisotropic thermal expansion. It is also understood that when the talc grain size is larger than that of kaolinite (which is the case in the current study) the sintering (diffusion) behaviour of grains becomes more complicated and greatly influence the pore formation within the sintered bodies. However, pre-grinding of talc to submicron size, helped to densify the fired material and high-strength cordierite ceramics obtained at lower temperatures. It has also been shown that although different talc particle size cause differences in thermal expansion behaviour of the final structures, mechanical and refractory properties are not remarkably affected by the particle size of talc [119-121].

Therefore, it can be postulated that in this research the initial difference (20 times) in the average particle size of the two major precursor components, talc and kaolinite, have had effects on reducing the densification degree of the sintered bodies, especially in case of the ring-milled samples (due to the mechanism of grinding). Therefore, for the purpose of size reduction of different minerals with sheet-like crystal structures, planetary milling mechanism is preferred for production of more uniform mixtures and also denser final microstructures.

5-4- Increasing the sintering temperature – formation of cordierite

In the previous sections the phase development has been observed in cordierite precursor mixes at sintering temperatures well below that required for full cordierite formation. In this section the sintering temperature is raised to 1300ºC in which cordierite formation is significantly enhanced and the densification process becomes completed. This is the temperature that is quite frequently reported in literature about formation of cordierite during heat treatment of powder precursors [71, 109]. Ball milling was not studied in these experiments as previous studies (section 5-3) indicated relatively poor activation. The codes allocated to the sample set are given in Table 5-6.

Table 5-6: Coding of differently activated samples sintered at 1300 °C

Sample code	Activation conditions
MIX-T	Not activated
PM10-T	Planetary-milled for 10 min.
PM50-T	Planetary-milled for 50 min.
RM10-T	Ring-milled for 10 min.
RM15-T	Ring-milled for 15 min.

5-4-1- Increasing the ring-milling time

Further milling with the ring mill (extended to 15 minutes) was undertaken to evaluate its possible effects on changing the phase transformations and microstructure of the sintered material. The as-milled powder, RM15, though not significantly denser than the similar less activated sample (RM10), showed a significant increase in the BET surface area value (88.87 m^2/g) which was about 30% higher than the value for RM10.

5-4-1-1- XRD results

The most significant characteristic of the sintered samples at 1300 °C was the formation of cordierite and/or its hexagonal polymorph, indialite. Orthorhombic (cordierite) structure differs from hexagonal indialite in the presence of disorder in the SiO_4 or $A1O_4$ tetrahedral occupancy, otherwise in both hexagonal and orthorhombic forms, the aluminosilicate framework is identical (Figure 5-40). Cordierite formation was expected according to the thermodynamics of the reactions and the stoichiometric composition of the mixture. Results of DTA analysis by Rodrigues Neto and Moreno [12] who studied the effect of planetary milling on the sintering behaviour of slip cast samples obtained from a suspension of talc, kaolinite and alumina, suggest that milling accelerates the reaction of formation of cordierite at 1280 °C that starts immediately after the mullite formation.

The most significant impurity phase found in the non-activated sample (MIX-T in Figure 5-41), was corundum, although traces of (proto)enstatite were also observed. On the other hand, the activated samples presented an X-ray diffraction pattern of an almost pure cordierite composition.

5-4-1-2- SEM-EDX results

The SEM images presented in Figure 5-42, show that possibly the most important effect of ring milling activation for both RM10 and RM15 on the sintered material at 1300ºC has been the densification of the structure. As observed, the large network of inter-connected voids in the non-activated sample (darker grey spaces in MIX-T) are significantly reduced and mostly replaced with isolated round pores in the activated samples.

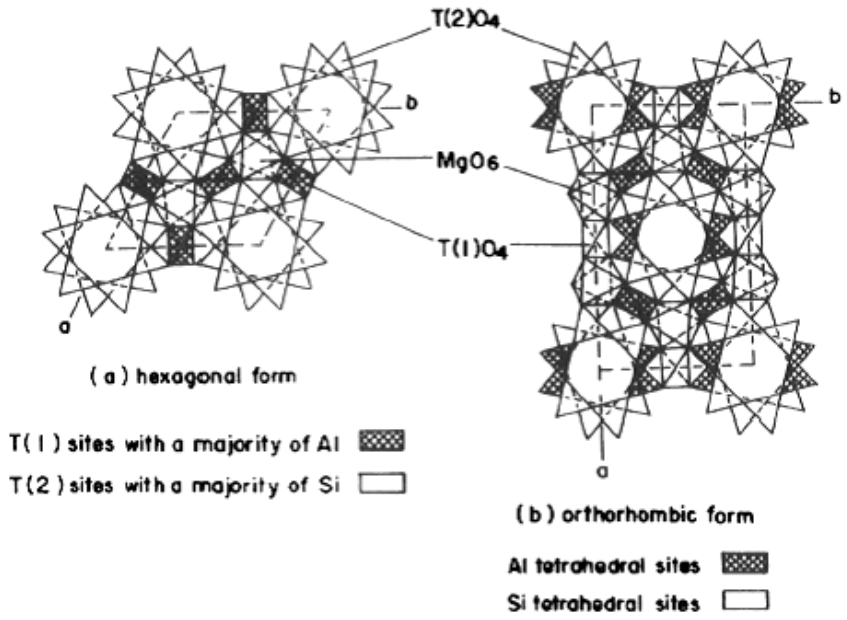

Figure 5-40: Crystallographic structure arrangement in the two cordierite forms [92]

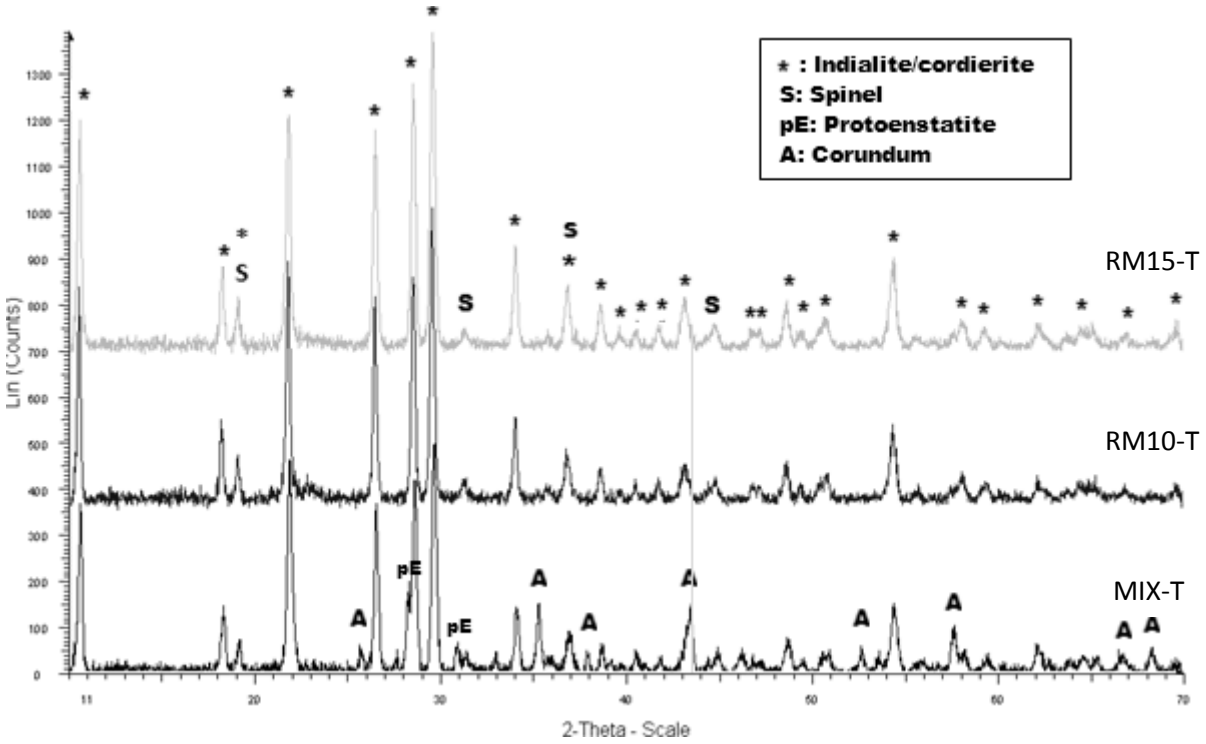

Figure 5-41: X-ray diffraction pattern of the ring-milled as well as non-activated sample after sintering at 1300 °C

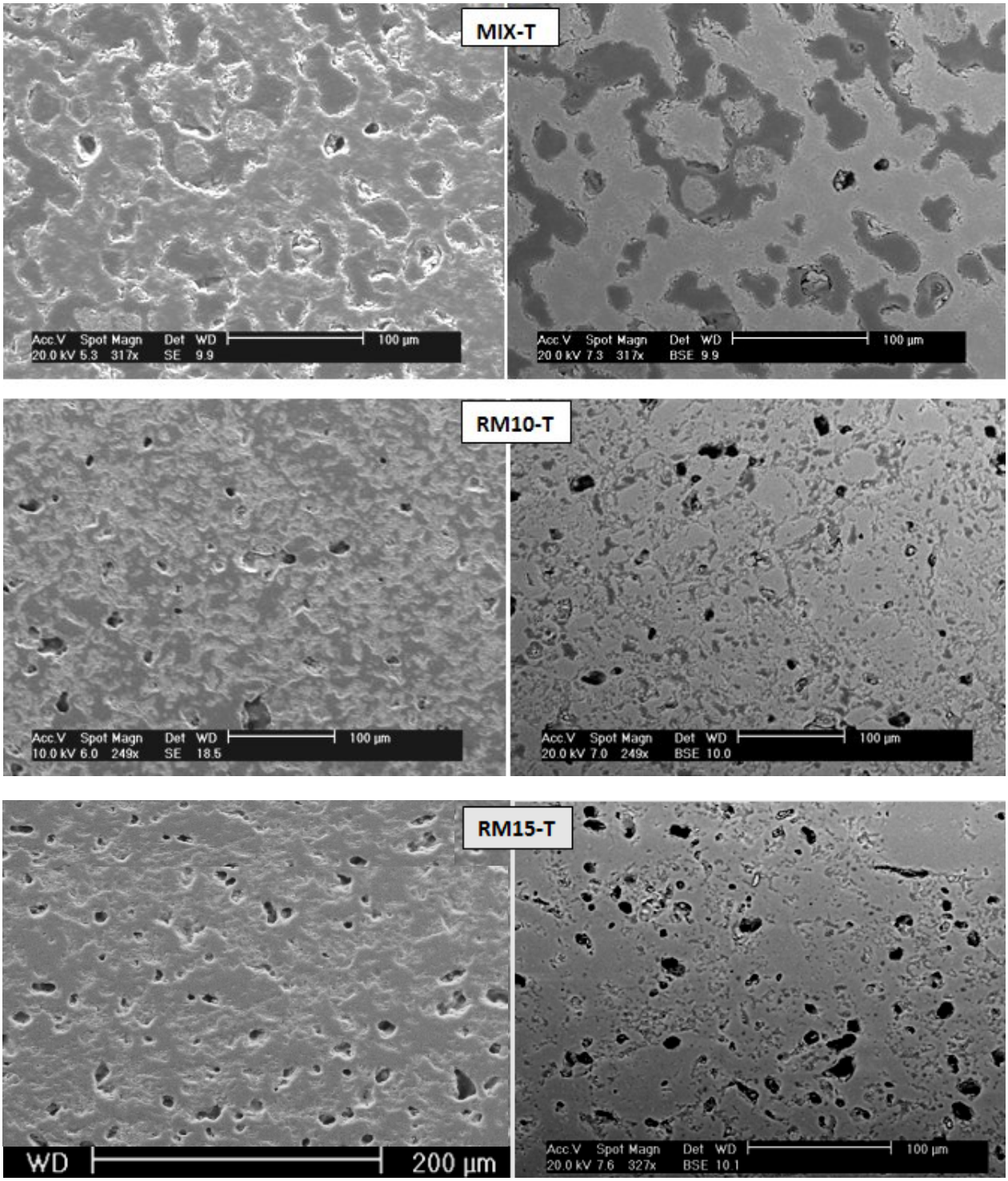

Figure 5-42: SEM micrographs of the ring-milled compacts sintered at 1300 °C; Left: Secondary Electron images, Right: Backscattered Electron images

5-4-2- Planetary milling – effect of additives: zirconia and ceria

To evaluate the influence of zirconia and ceria, certain amounts of these dopants were applied during activation milling. On the basis of the data from similar literature, weight percentage values (based on the total sample weight) were selected at *low* and *high* amounts for oxide additive contents. Planetary milling experiments were also undertaken at low (10 minutes) and high (50 minutes) intensities. Sintering temperature for this series of tests was 1300 °C (10 °C per minute heating/cooling rate and 2 hours dwell time). Although the effects of the addition of zirconium and cerium oxides was mainly investigated through phase analysis (XRD) and structural studies (SEM), evaluation of density/porosity and thermal expansion data for some of the samples was also performed. The results of experiments are presented and discussed with particular emphasis on the simultaneous effects of mechanical activation and oxide doping on phase transformation and densification in the sintered bodies. The sample nomenclature is according to Table 5-7.

Table 5-7: Sample coding in additive-contained experiments

Sample Code	**Additive types and amounts (wt %)**		**Activation degree/ milling time** (minutes)
	Yttria-stabilised zirconia	Ceria	
PZ10	15	Nil	10
PZ50	15	Nil	50
PZC10	12	3	10
PZC50	12	3	50
PC10	Nil	4	10
PC50	Nil	4	50
PCZ10	3	12	10
PCZ50	3	12	50

5-4-2-1- Bulk density and shrinkage measurements

Measurement of the densities of sintered composite materials revealed some interesting information. The theoretical density value for cordierite is about 2600 kg/m^3, while the densities for the two additive oxides are reported to be about 6000 and about 7600 kg/m^3 for yttria-stabilised zirconia and ceria respectively. Due to the density difference between the functional oxide additives and the matrix, one can expect the rise in the density of the doped systems in proportion to the amount of oxide added.

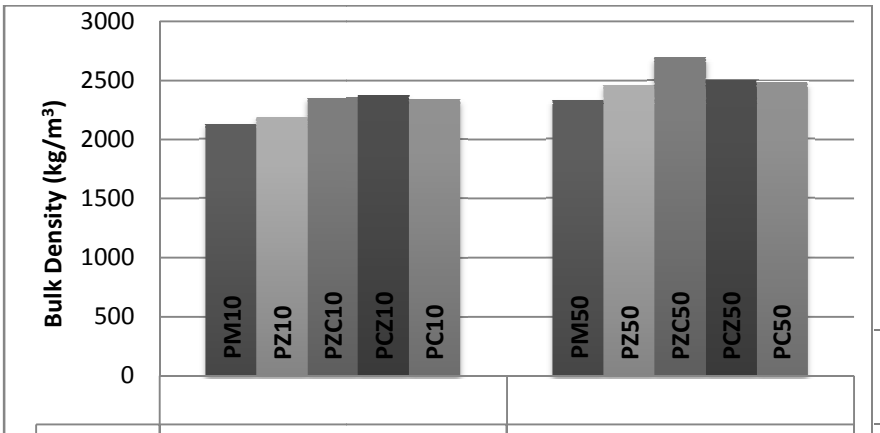

			Calculated theoretical values for zero porosity (based on proportions)
PM	2130	2330	2600
PZ (15)	2190	2460	3110
PZC (12-3)	2350	2690	3160
PCZ (12-3)	2370	2500	3300
PC (4)	2340	2480	2800

Figure 5-43: Bulk density values for planetary-milled samples sintered @1300ºC; the table shows density data (digits beside the sample codes give the additive proportions (wt%) in order)

As can be seen in Figure 5-43, the positive effect of activation time on densification is quite apparent; as the bars on the right indicate higher densities compared the ones on the left. While the relatively higher density of ceria-contained samples could be mostly due to higher density of cerium oxide, the effect of activation on the high-zirconia samples is better reflected in the data, especially for the PZC sample, in which longer milling has increased the

bulk density considerably. At low activation, oxide additives have caused a decrease in shrinkage of the samples sintered at 1300 ºC, 2 h; as shown in Figure 5-44. However, at higher activation (50 minutes milling), generally there has been an increase in the amount of shrinkage in the sintered material containing the additives with respect to the sample without them (PM50). Sample PCZ50, the sample with high (12 wt%) ceria content, has undergone the most shrinkage.

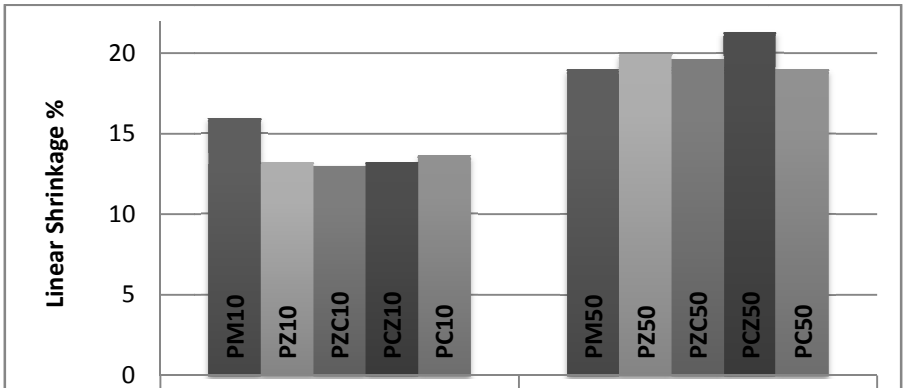

	Low	High
PM	15.97	18.98
PZ (15)	13.19	19.91
PZC (12-3)	12.96	19.68
PCZ (12-3)	13.19	21.30
PC (4)	13.66	18.98

Figure 5-44: Shrinkage of planetary-milled sintered samples with and without additives; the table shows shrinkage data (digits beside the sample codes give the additive proportions (wt%) in order)

5-4-2-2- XRD analysis

As previously shown (section 5-4-1-1), the heat treatment of activated samples at 1300 °C resulted in formation of nearly single-phase cordierite bodies containing some residual porosity. Figure 5-45 shows that the planetary milling of the precursor powders has resulted in similar sintered material with respect to the phase composition, however, the amounts of the cordierite formed is slightly different from the samples with no additives, activated by the

ring-mill (Figure 5-41). Most of the major XRD peaks of cordierite in PM50-T have a higher intensity compared to those of RM15-T.

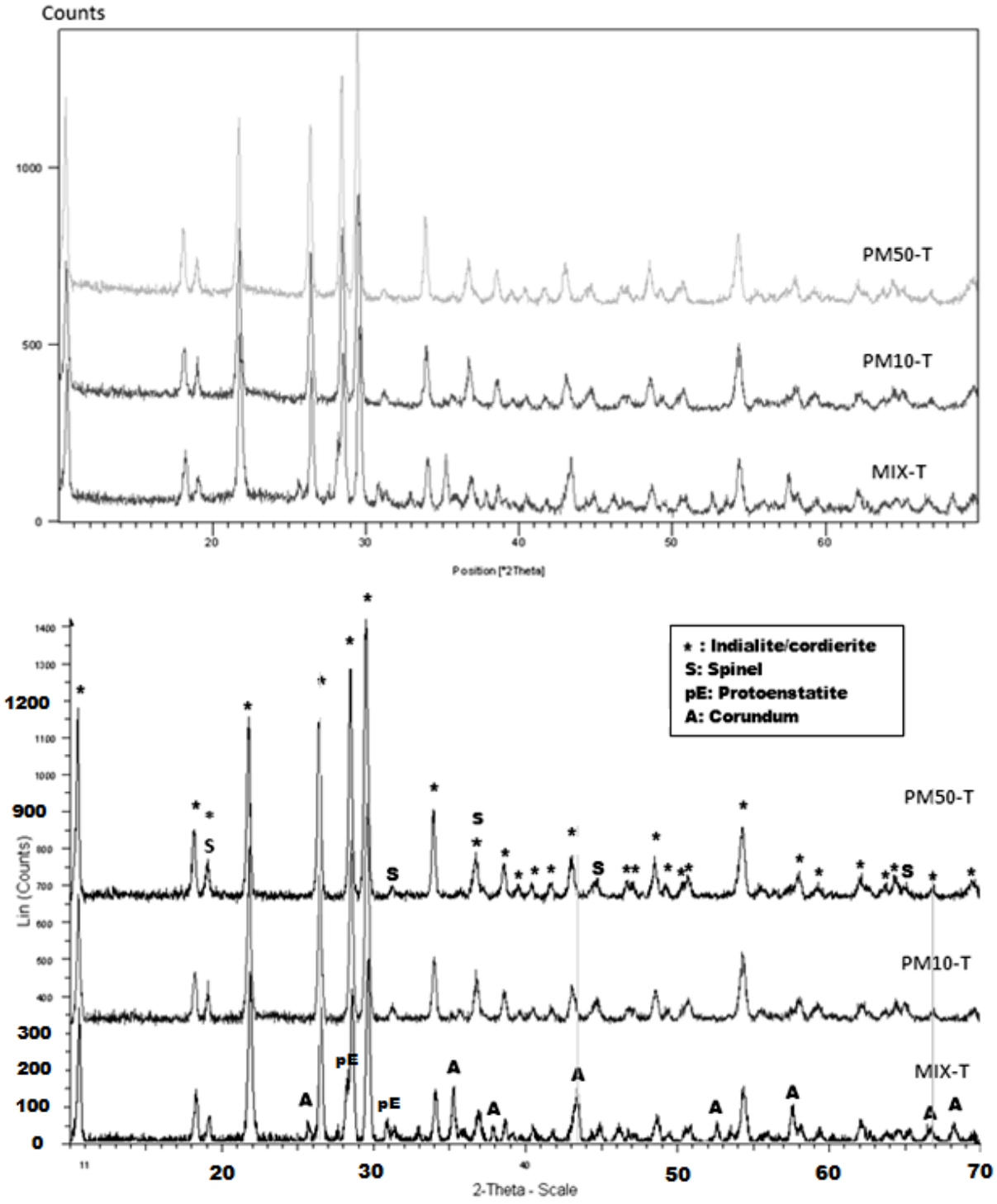

Figure 5-45: X-ray diffraction pattern of the planetary-milled and non-activated sample after sintering at 1300 °C; Top: general pattern, Bottom: background-removed and labeled pattern

X-ray diffraction patterns of those experiments in which yttria-stabilised zirconia (YSZ) was added as the major additive (PZ and PZC codes) are shown in Figures 5-46 and 5-47. Formation of zircon ($ZrSiO_4$), indicated with "*Z*" in the figures, is the most important phase transformation within these samples. Such a reaction suppresses the availability of SiO_2 for stoichiometric formation of cordierite. It has been generally observed in similar researches that the formation of zircon is a result of the reaction of (silica in) cordierite matrix with zirconia which is added either as a monoclinic ZrO_2 [8, 77, 82, 83] or as individual components together with ytrria, Y_2O_3 [24, 92]. It is also important to know that in none of those works, the mechanochemical milling of the precursors had been applied, however, in one study [8], wet attrition milling resulted in formation of more zircon due to reaction of non-stabilised zirconia with cordierite.

Although sintering of the non-activated mixture with additives was not tried in the current experiments, it seems the activation of the powder mixtures has promoted the reaction of zirconia with cordierite which is reflected in the direct (increasing) relationship between the XRD peak height of zircon with milling time (Figure 5-48a). A reasonable answer to this phenomenon might be the destabilisation of YSZ by the diffusion of yttria into the glassy phase during heat treatment possibly due to the mechanical stress applied on precursor oxides in previous activation process. The very low intensity of the major XRD peak related to (101) plane of the tetragonal zirconia crystal (indicated with "*YZ*" in graphs) also confirms the dissociation of the YSZ structure. Similar results, in case of no mechanochemical activation being applied, are reported by Travitzky and Claussen, only at higher sintering temperatures (~1400 °C) and long retention times (48h) [85].

The amount of zircon in the samples with 3% ceria addition (PZC) has decreased considerably in comparison to sample without ceria (PZ). Considering the lower initial YSZ content (12 wt%) in these samples, there are two other possible factors responsible for the decrease in zircon peak intensities: first, the formation of a new compound (zirconium cerium oxide, "*CZ*" in the graphs) and secondly the milling process. The evidence for the latter is found when the XRD patterns of PZC samples at low and high activation degrees are compared (Figures 5-48b). There is a significant decrease in the intensities of major X-ray diffraction peaks of zircon in PZC sample at high activation degree. This is not unrelated to the other factor which is the formation of a combined zirconia-ceria phase; however, higher activation has slightly reduced the amount of this new phase too, i.e. longer milling has possibly caused a slight reduction in the crystallinity of the sintered mixture. The zirconium cerium oxide characterised by X-ray diffraction analysis is recognised to have a chemical formula $(Zr_{0.20}Ce_{0.80})O_2$ and a cubic crystal symmetry, which usually forms at ambient temperatures.

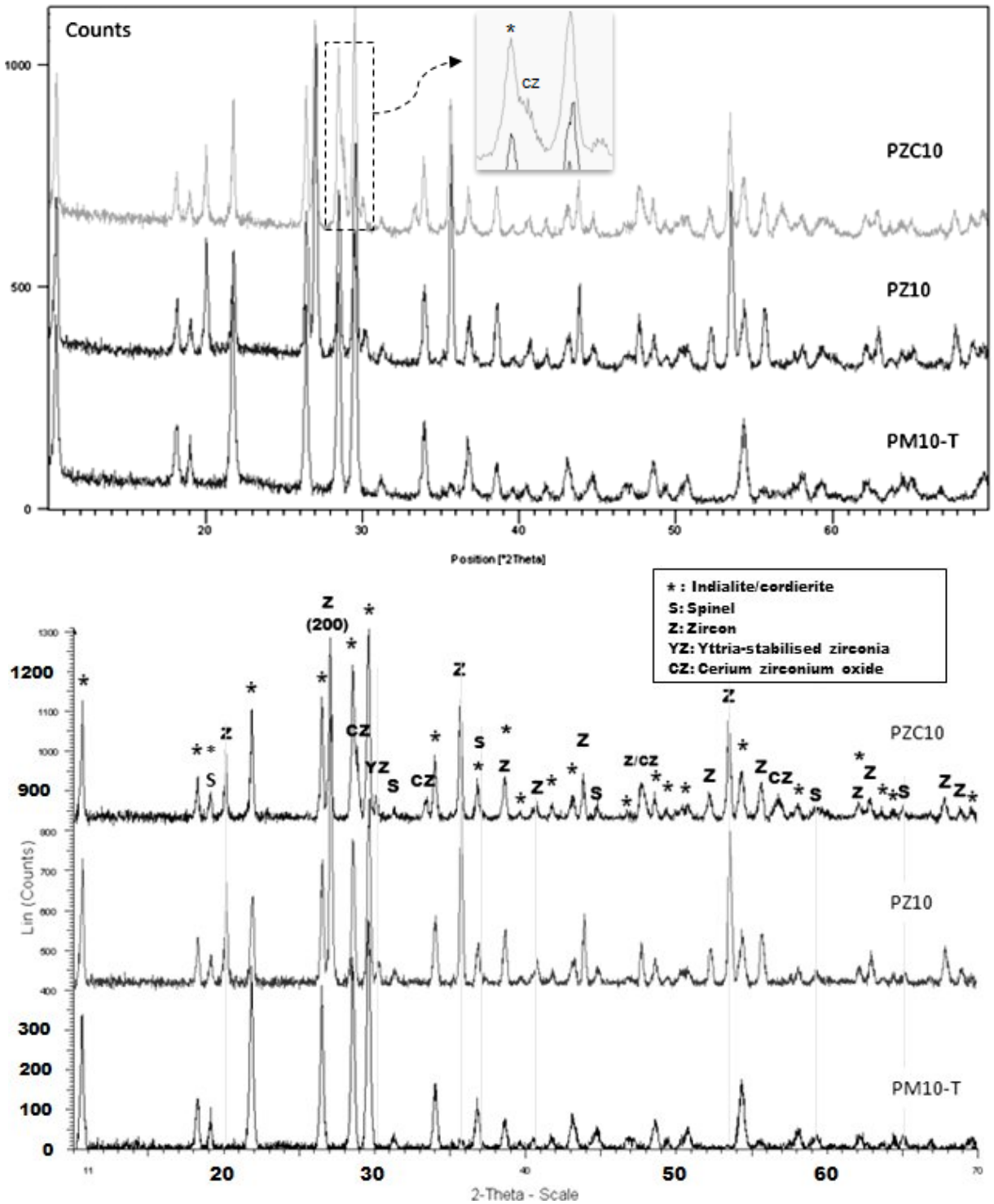

Figure 5-46: Comparison of X-ray diffraction patterns of samples of low activation degree, containing no additive and zirconia as the major additive (magnified view shows the overlapping peaks)

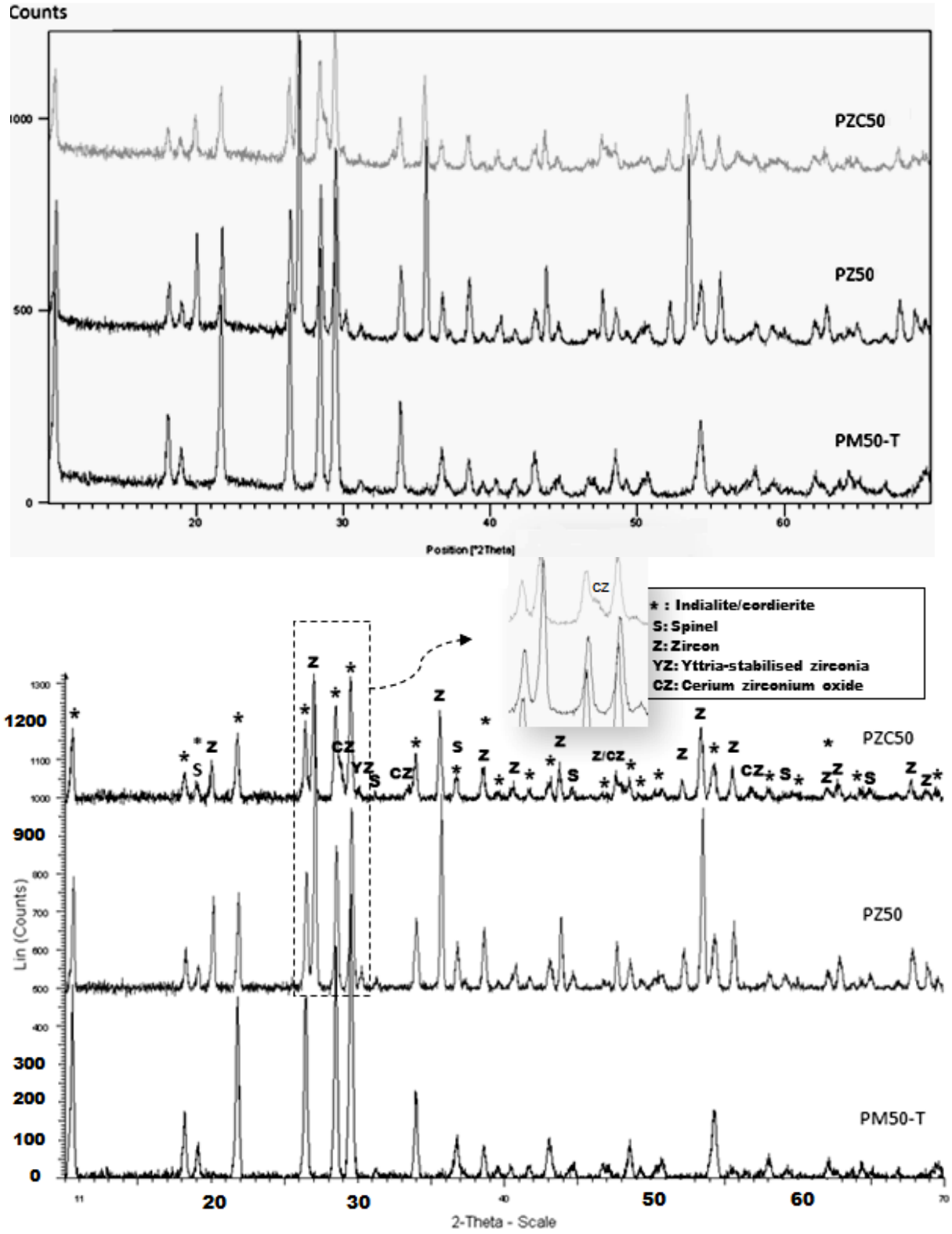

Figure 5-47: Comparison of X-ray diffraction patterns of samples with high activation degree, containing no additive and zirconia as the major additive (magnified view shows the overlapping peaks)

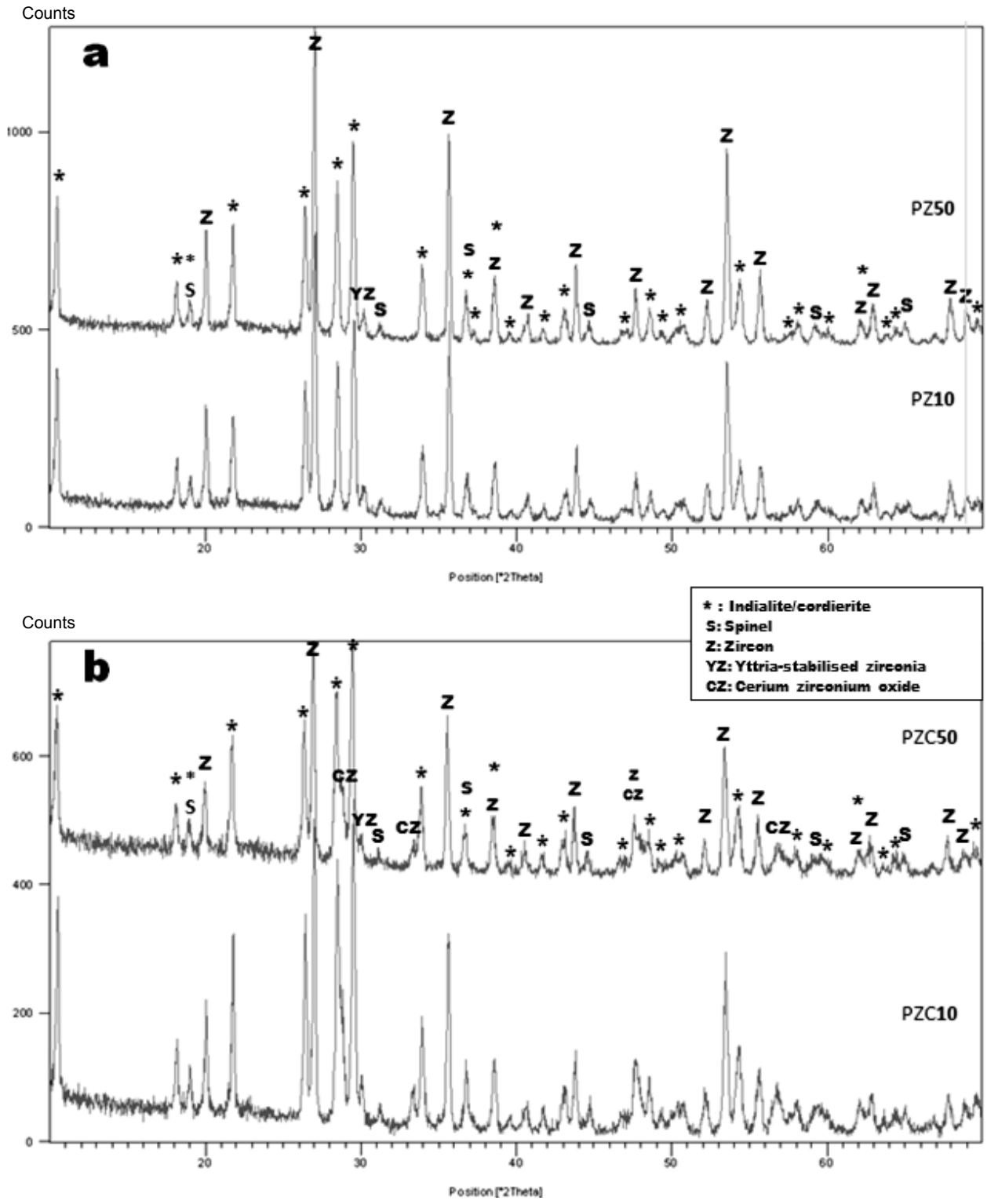

Figure 5-48: XRD graphs showing the effect of milling time (activation degree) on phase formation and proportions within the sintered samples of PZ (a) and PZC (b)

The effect of cerium oxide addition on the cordierite precursors during mechanochemical process and after sintering at 1300 °C is shown in X-ray diffraction patterns in Figures 5-49

and 5-50 for low and high degree of activation respectively. Comparing the graphs/plots in Figure 5-49, at low activation degree, the sample containing only 4 wt% ceria (PC10) shows decrease in the diffraction peak intensities related to cordierite, though the decrease is more pronounced for some peaks relative to others. Without the formation of a new composition after addition of ceria, the only additional compound to be found in the system is the cerium oxide itself, which is also known as cerianite (CeO_2), possessing a cubic crystal structure and indicated with "Ce" in the figures. It is also emphasised by Montorsi and co-workers that CeO_2 lines are very sharp in the XRD patterns even for cordierite doped with 2.5 wt% CeO_2 [122].

The sample PCZ10, has moved toward a non-crystalline or a glassy structure according to the XRD pattern with significant reduction in the diffraction peak heights. In this sample, which contains relatively high ceria (12 wt%) and low stabilised zirconia (3 wt%), less zircon is formed with respect to cordierite when compared to PZC10 (containing 12 wt% zirconia and 3 wt% ceria) in the previous tests. As with the latter, PCZ10 sample also contains the combined oxide phase of ceria-zirconia. It is shown that room-temperature high-energy ball milling is effective for the synthesis of nanophase CeO_2-ZrO_2 solid solution in a wide compositional range [123]. In the current study, the possible compositions according to the X-ray diffraction database (PDF) for the so-called alloyed ceria-zirconia compound are as follows, with the last composition recognised as a better match for samples with low ceria content (PZC).

Composition	PDF reference number	Crystal system
(Zr0.20 Ce0.80) O2	01-074-8064	Cubic
(Zr0.10 Ce0.90) O2	01-074-8065	Cubic
Ce2 Zr2 O7.04	00-054-0016	Cubic

This observation indicates there is an interaction between YSZ and ceria that is possibly initiated or enhanced during activation process. In the case of no mechanochemical processing being applied, such as in the work of Tompsett *et al.* [124], who studied the solid-state synthesis of ceramic composite made of doped CeO_2 ($Ce_{1-x}Gd_xO_{2-y}$) and YSZ, heat treatment at 1300 °C did not result in formation of ceria-zirconia solid solution. Only after sintering for 72 h did the zirconium ions diffuse into the ceria via solid-state reaction between the ceramic discs in intimate contact. It is also mentioned that firing temperatures in excess of 1600 °C are usually applied to make such a reaction occur. In their research, the main product of reaction between gadolinium-doped ceria and yttria-stabilised zirconia was determined from XRD and Raman spectroscopy to be a cubic like modification of the original CeO_2 material.

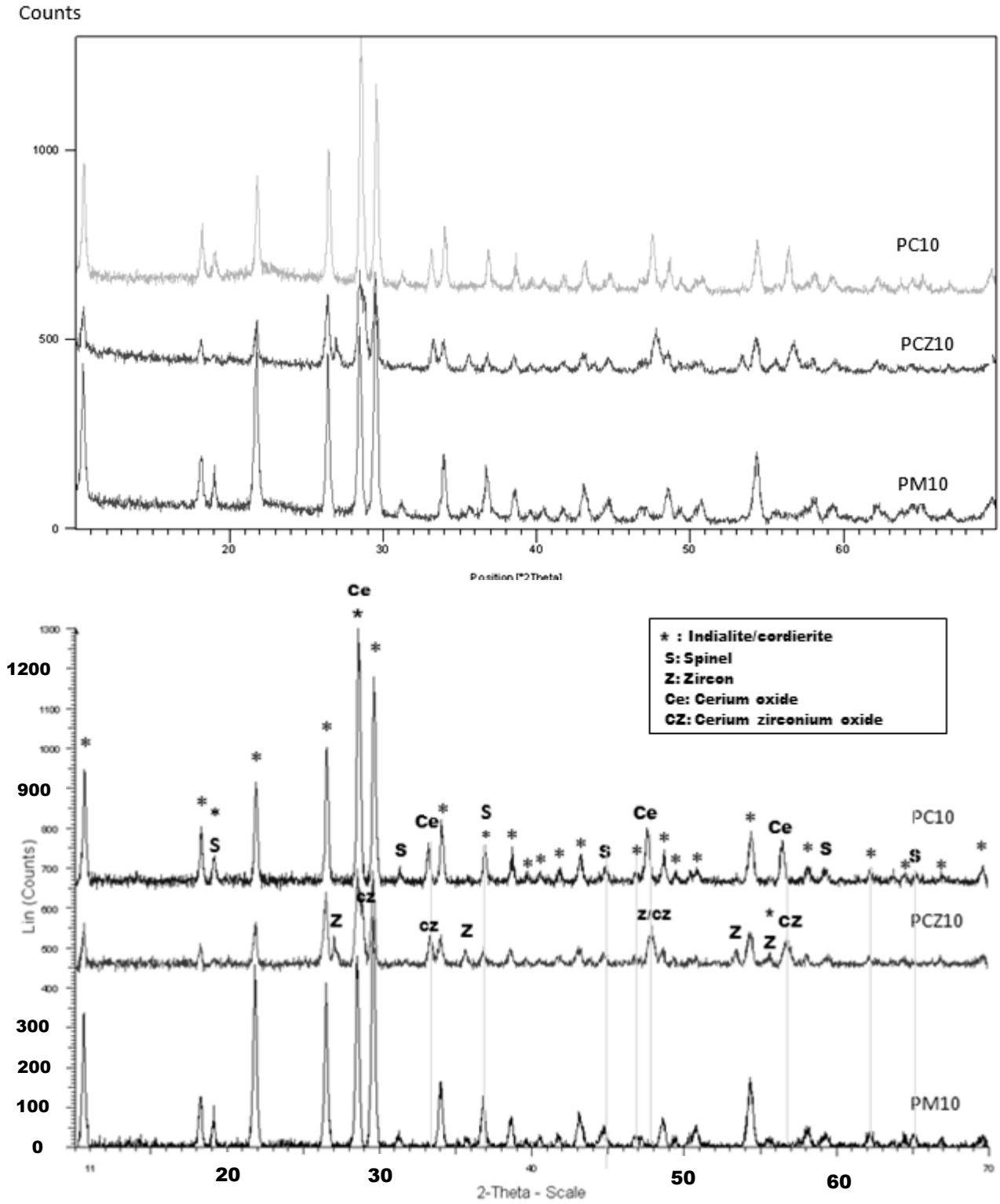

Figure 5-49: Comparison of X-ray diffraction patterns of samples with low activation degree, containing no additive and ceria as the major additive

Increasing the activation time to 50 minutes in the sample PC50 has resulted in a decrease in the cerianite phase content, Figure 5-51a, when major XRD peaks relating to (111) lattice plane of CeO_2 at $2\theta \approx 28.5°$ (indicated with dashed brackets) are compared for the low and high activation conditions. It is noticeable that this diffraction peak for ceria overlaps the diffraction peak due to (202) plane of indialite. Evaluation of other diffraction peaks of indialite such as the immediate peak at $2\theta \approx 29.5°$ (belonging to (211) plane), confirms that the transformation toward increasing the indialite content of the material has continued as a result of increasing the milling time. On the other hand, comparison of the patterns in Figure 5-51b, reveals that the milling at longer time has resulted in a sintered structure of a composite material generally with a higher degree of crystallinity when compared to the same composition with less activation. Therefore, mechanical activation could compensate for some of the increase in the glass viscosity and fluxing properties induced by adding relatively high amounts of cerium oxide to the mixture. It is worth remembering that sample PCZ50 had undergone the most degree of shrinkage among all doped samples, which could be attributed to such a transformation from a glassy state to a more crystalline structure.

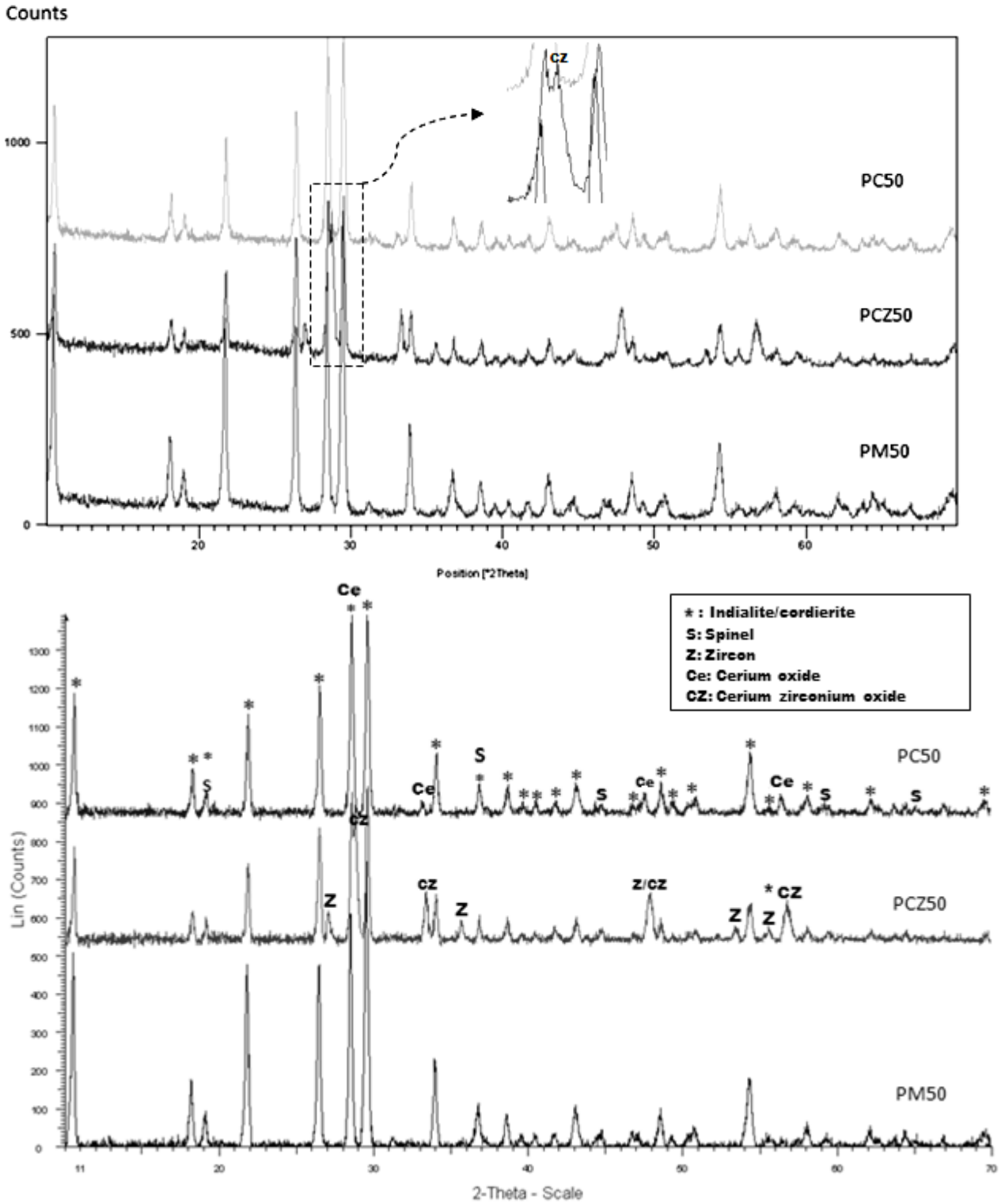

Figure 5-50: Comparison of X-ray diffraction patterns of samples of high activation degree, containing no additive and ceria as the major additive (magnified view shows the overlapping peaks)

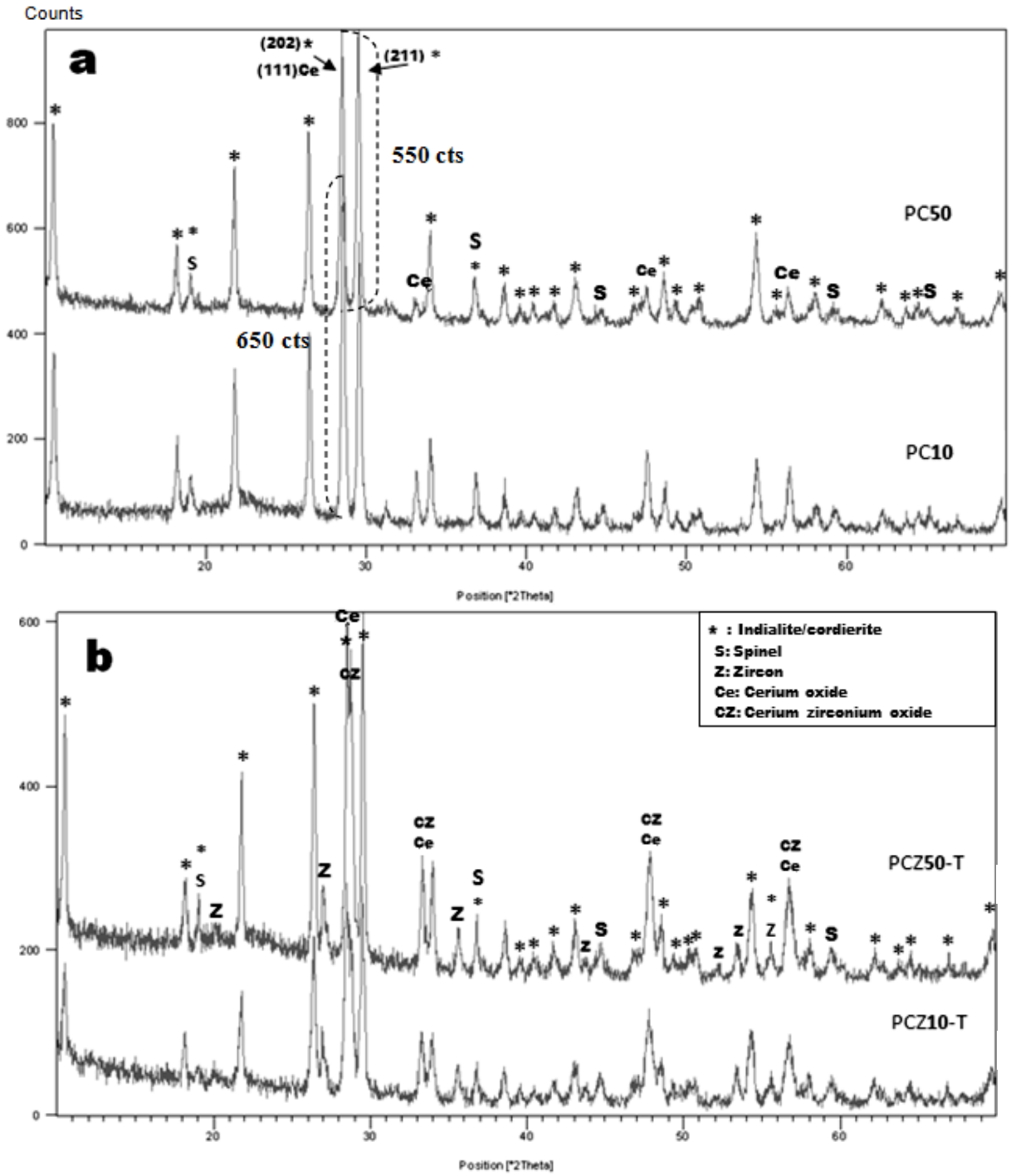

Figure 5-51: XRD graphs showing the effect of milling time (activation degree) on phase formation and proportions within the sintered samples of PC (a) and PCZ (b)

Finally, to find a semi-quantitative measure for the variation of the amounts of cordierite within different samples in these experiments, eight major X-ray diffraction peaks related to

cordierite/indialite crystal system were selected for such a comparative study in the sintered samples. The diffraction intensity/height (in counts) of the selected peaks/d-values were then ranked for all 13 samples in the experiments from 1 (the lowest) to 13 (the highest), the result of which is shown in Table 5-8. Before studying Table 5-8, one should remember that the degree of crystallinity of a sample influences the XRD peak intensity values; therefore, low crystallinity will result in lower ranks in peak heights.

Table 5-8: Ranking of XRD peak intensities of major cordierite d-values for samples sintered at 1300 °C

Average d-value (Å)	Samples' XRD peak intensity ratings (13: highest to 1: lowest)												
	PCZ50	PCZ10	PC50	PC10	PZC50	PZC10	PZ50	PZ10	PM50-T	PM10-T	RM15-T	RM10-T	MIX-T
8.41	3	1	8	5	2	6	4	7	13	9	12	11	10
4.87	2	1	7	10	3	4	5	6	13	8	11	12	9
4.07	3	1	7	5	2	8	6	4	11	10	12	13	9
3.37	3	1	7	8	2	5	4	6	13	10	12	11	9
3.13	6	1	10	13	2	5	4	3	12	9	11	8	7
3.02	3	1	9	8	2	6	5	4	13	10	12	11	7
2.63	2	1	7	5	3	6	11	9	13	8	12	10	4
1.69	2	1	10	6	3	5	7	4	13	11	12	9	8

As observed in Table 5-8, at one end is the sample PCZ10 (previously found to be the material with very low crystallinity) which is invariably ranked as the material containing the least amounts of crystalline indialite composition. This sample is followed by PZC50 and PCZ50 in the increasing order of the diffraction intensities. Samples RM10, RM15 and PM50 are located at the other end in increasing order (average ranking of 11 to 13), possessing the highest peak intensities. For the rest of the samples the variation of peak intensity values does not let a specified rank to be attributed to the sample. The reason why the ranking for a single sample is not consistent among different d-values could be a result of the diffraction peaks located and indexed by the proprietary software of the system. Due to predefined settings for certain peak shape parameters such as peak base or tip width, the software may not

characterise the exact point of the peak maximum. This is apart from other potential factors that generally affect the peak position and intensities in any XRD experiment. However, as a semi-quantitative measure for the cordierite content in different doped and undoped samples, it is possible to give a general ranking of all samples with respect to average diffraction peak intensities related to cordierite:

$$PM50\text{-}T > R15\text{-}T > R10\text{-}T > P10\text{-}T \geq MIX\text{-}T \geq$$

$$PC50 > PC10 > PZC10 \geq PZ50 > PZ10 > PCZ50 > PZC50 > PCZ10$$

5-4-2-3- SEM-EDX study

Scanning electron micrographs for the sintered samples containing functional oxide additives are presented in Figures 5-52 and 5-53 for the low and high activation conditions respectively. In each set of pictures, a comparison is made with the similar sample containing no additives. Moreover, in each set the picture on the left is giving a surface topography view under secondary electron scanning condition, while the one on the right (backscattered view) is used for phase characterisation and better evaluation of pore content. The latter images are presented in larger magnification for possibly a better study of the phase content.

A comparative look at the different sintered samples with low activation degree reveals the relative porosity distribution and size within the surface and bulk of the sample. The least porous structure is found in sample PZC10 which is in agreement with bulk density measurement data. In sample PCZ10, the pores show more regular and rounded shapes, and the surface appears to be smoother than other sampled materials. Pore size distribution, in general, ranges from an average 3-6 μm for small pores, 7-15 μm for intermediate and large pores, and in exceptional cases pores up to 30 μm can be found. Another distinguishing feature of sample PCZ10 is the relatively large-size phases with light grey colour and

irregular shapes. Distribution of zirconia and ceria through the matrix appears homogenous for all of the sintered bodies, which is a direct effect of the application of dry milling on precursor mixtures. The homogeneity of additives' distribution within the matrix increases with activation time.

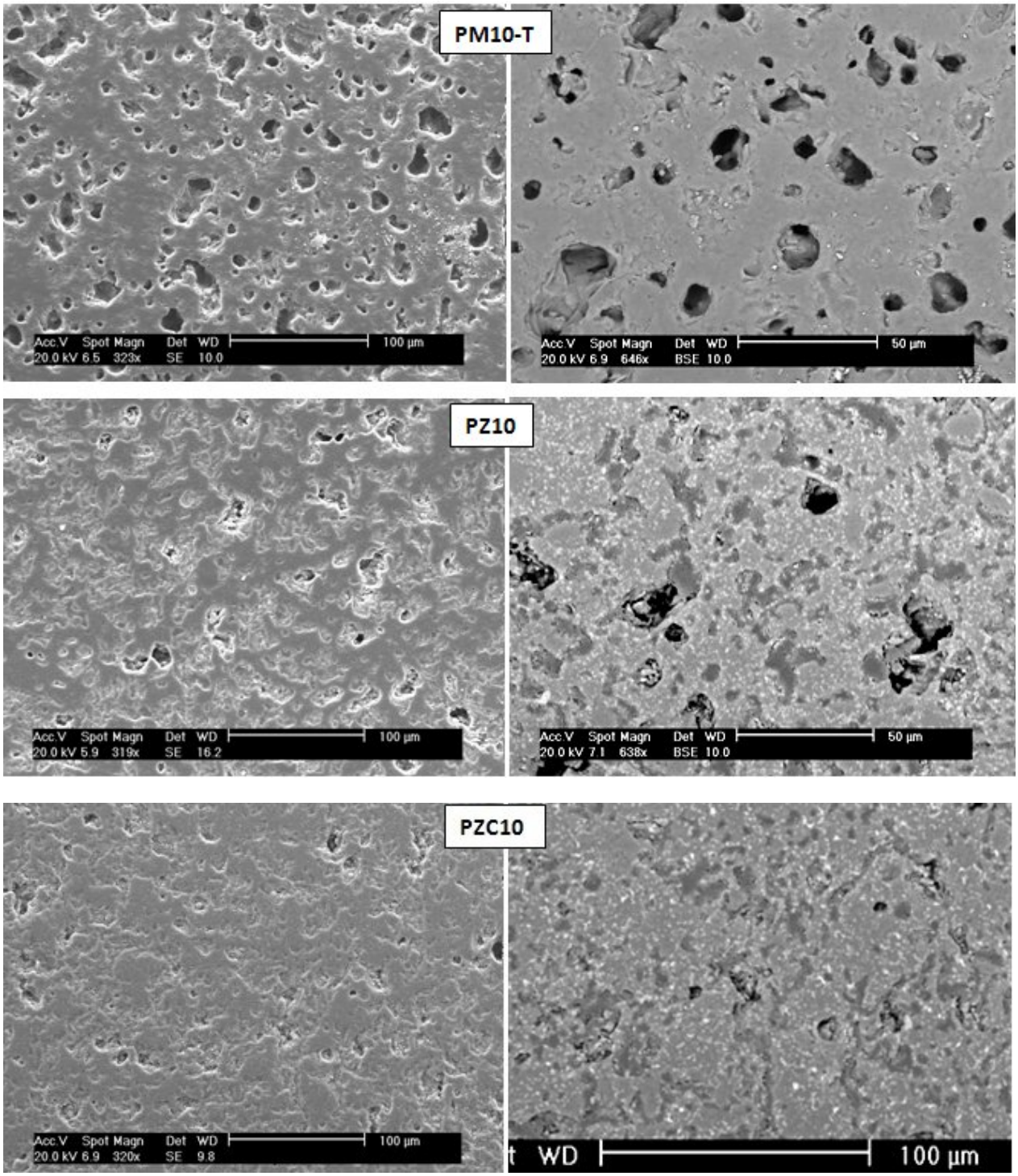

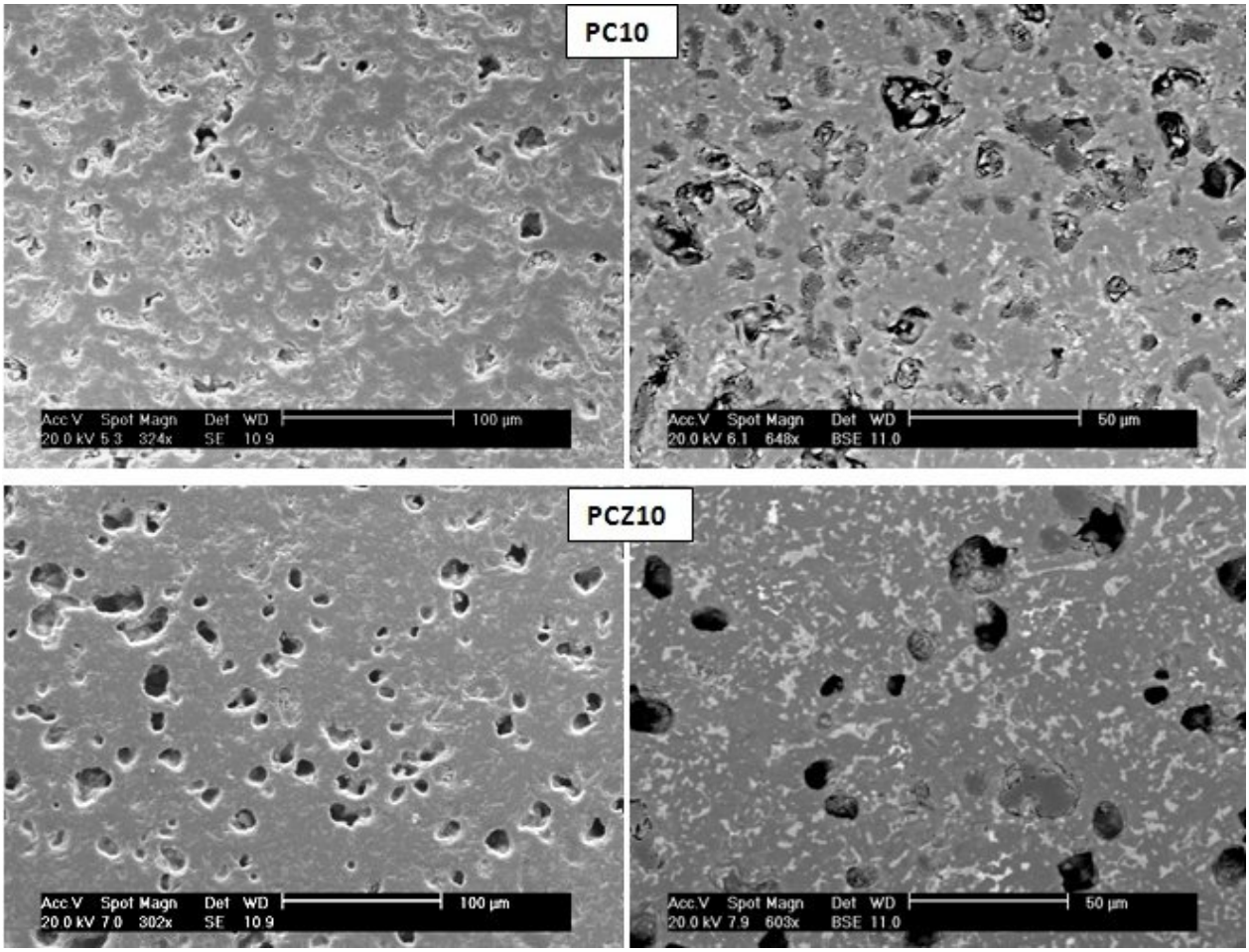

Figure 5-52: SEM micrographs of sintered samples of low activation degree with and without oxide additives; Left: secondary electron images, Right: Backscattered electron images at higher magnification

In general, samples after longer milling show a denser structure, as shown in Figure 5-53, confirming the previous density measurement data. The effect of additives on the densification is also observed in the SEM micrographs. The interpretation of porosity data from such SEM images is difficult due to the statistically unreliable nature of the images; however, it appears the sample possessing high ceria content (PCZ50) has the largest pore size distribution among others irrespective of the density.

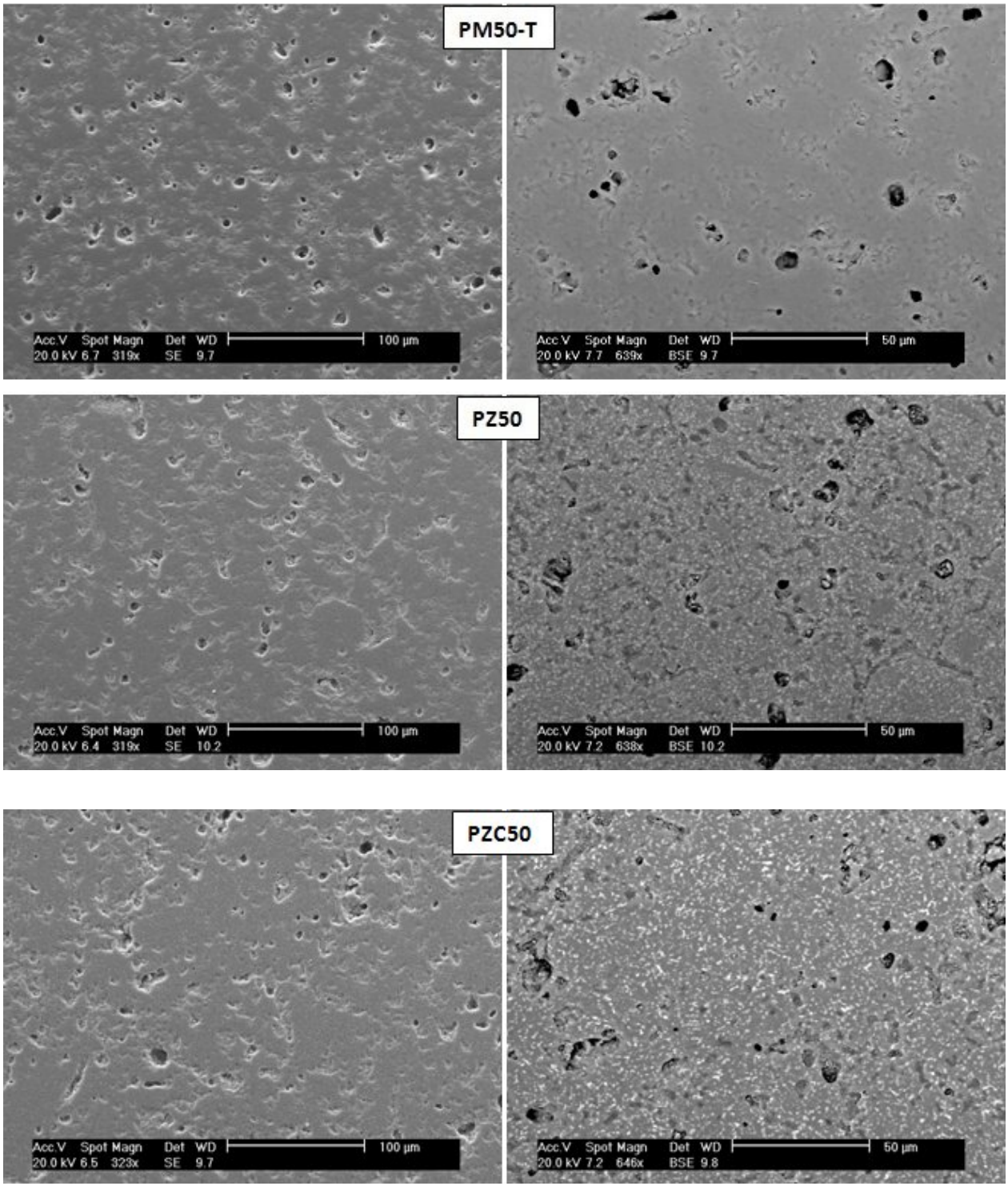
PM50-T
Acc.V Spot Magn Det WD 100 µm
20.0 kV 6.7 319x SE 9.7
Acc.V Spot Magn Det WD 50 µm
20.0 kV 7.7 639x BSE 9.7
PZ50
Acc.V Spot Magn Det WD 100 µm
20.0 kV 6.4 319x SE 10.2
Acc.V Spot Magn Det WD 50 µm
20.0 kV 7.2 638x BSE 10.2
PZC50
Acc.V Spot Magn Det WD 100 µm
20.0 kV 6.5 323x SE 9.7
Acc.V Spot Magn Det WD 50 µm
20.0 kV 7.2 646x BSE 9.8

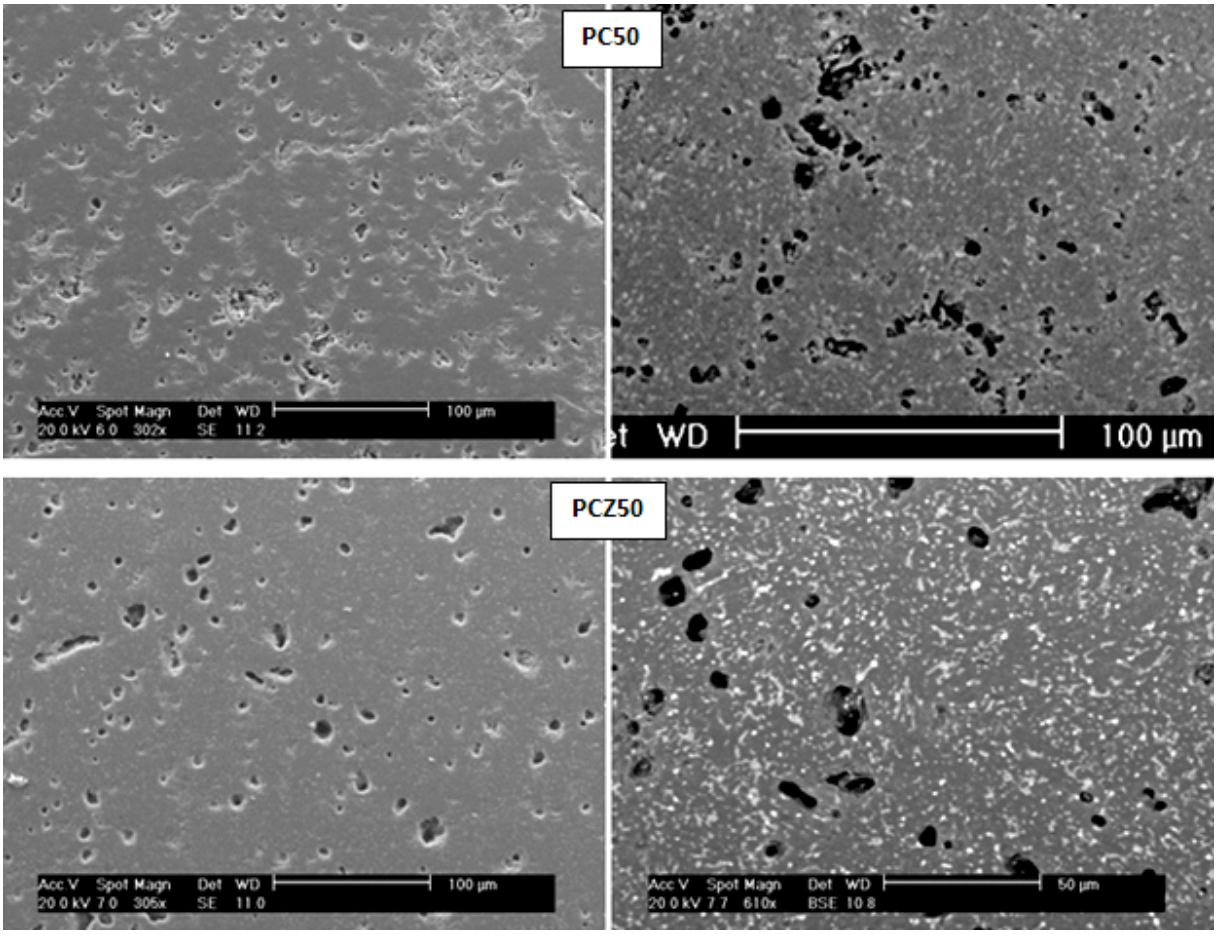

Figure 5-53: SEM micrographs of sintered samples of high activation degree with and without oxide additives; Left: secondary electron images, Right: Backscattered electron images at higher magnification

At higher magnification (Figures 5-54 and 5-55) and by doing EDX analysis, more information about phase constitution is obtainable. As seen in Figure 5-54, in samples PZ10 and PZ50 the white spots are predominantly zircon which is forming out of YSZ (still brighter spots). Small patches of lighter grey are spinel phases (indicated with "S"). It seems the formation of zirconium silicates (zircon) is increased at the edges of cavities possibly due to higher surface area and ionic potential available that promotes the reaction of Zr^{4+} with the silica tetrahedron. According to energy dispersive X-ray analysis, the weight percentages of yttrium in those white phases analysed in PZ samples varied from ~ 2.5 wt% to ~ 0.6 wt% which could support the hypothesis about loss of yttria during thermal processing of activated

YSZ composition and its destabilisation. It is also worth mentioning that unless manually set to detect yttria in the analysed phases the automatic EDX analysis did not include Y in less than 2 wt% contents.

The amounts of cerium in PZC samples were also variable from about 1-2 wt% in the matrix (cordierite phase), to about 5 wt% in white spots and up to 50 wt% in bright white spots. It was not possible to distinguish between zircon and cerium zirconium oxides within the white phases, however most of the analysed spots contained considerable amounts of silicon (therefore suspected to be zircon) and of course low cerium, and those spots that appeared brighter where in general high in cerium content and therefore suspected for either cerium oxide or combined cerium zirconium oxides with variable proportions of the elements.

The results of EDX analysis of different spots on SEM images of PC and PCZ samples are shown in Figure 5-55. The effect of the intensity/degree of mechanochemical processing on migration of Al^{3+} and Mg^{2+} back into the cordierite composition is reflected well in the EDX studies of PCZ10 and PCZ50. The former (less activated sample) possess compositions deprived of the above mentioned cations, possibly due to the diffusion of Ce^{4+} with a higher ionic potential – Z/r^2 – into the cordierite structure. It is also worth mentioning that the automatic X-ray analysis with EDX did not characterise zirconium in the composition of PCZ samples (possibly due to its low concentration), and in some cases a manual search for the relevant peaks was applied.

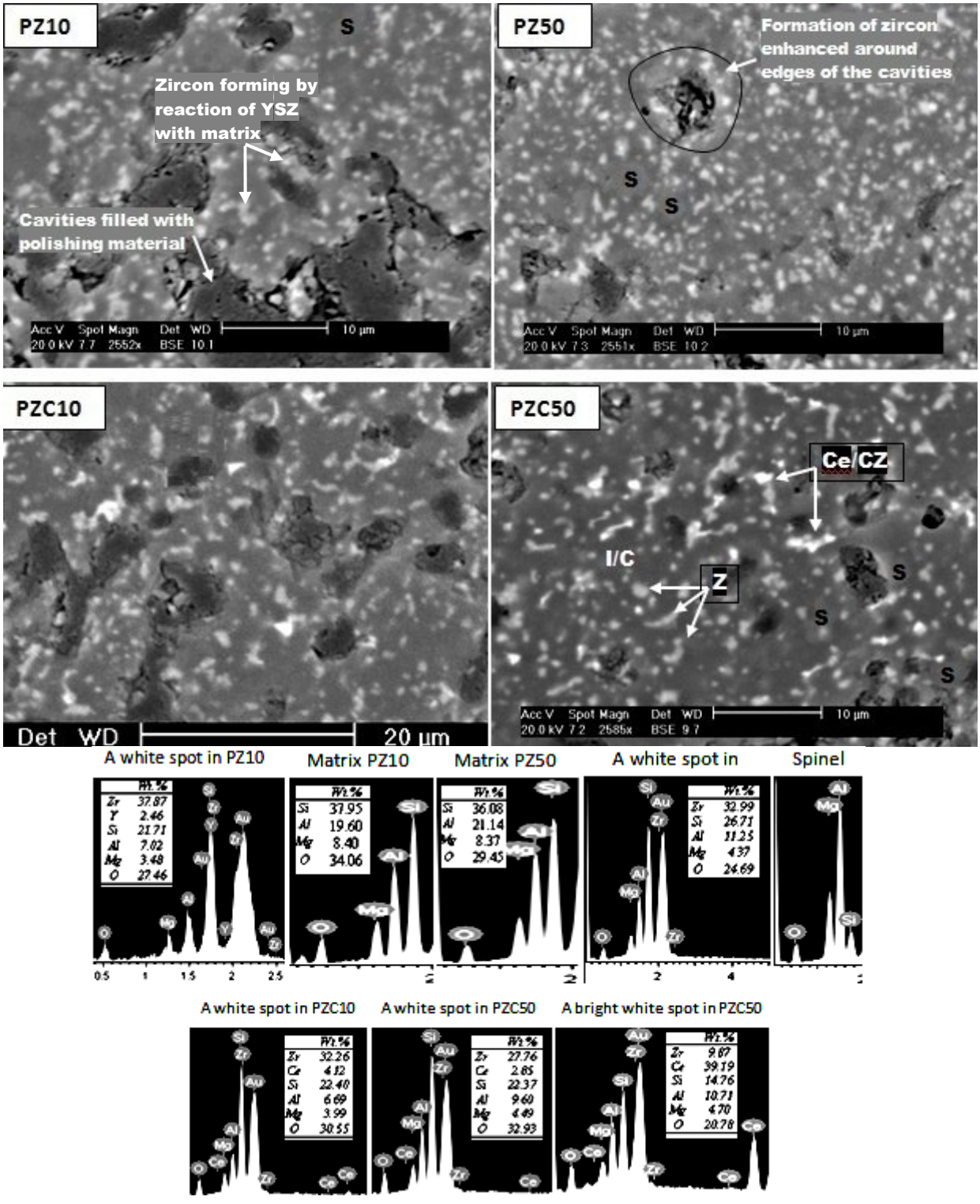

Figure 5-54: Phase characterisation in the SEM-EDX analysis of sintered samples with zirconia as the major additive; I/C: Indialite/Cordierite, Z: Zircon, Ce: Cerium oxide, CZ: cerium zirconium oxide, S: Spinel; Gold (Au) in EDX is due to applied coating for the analysis

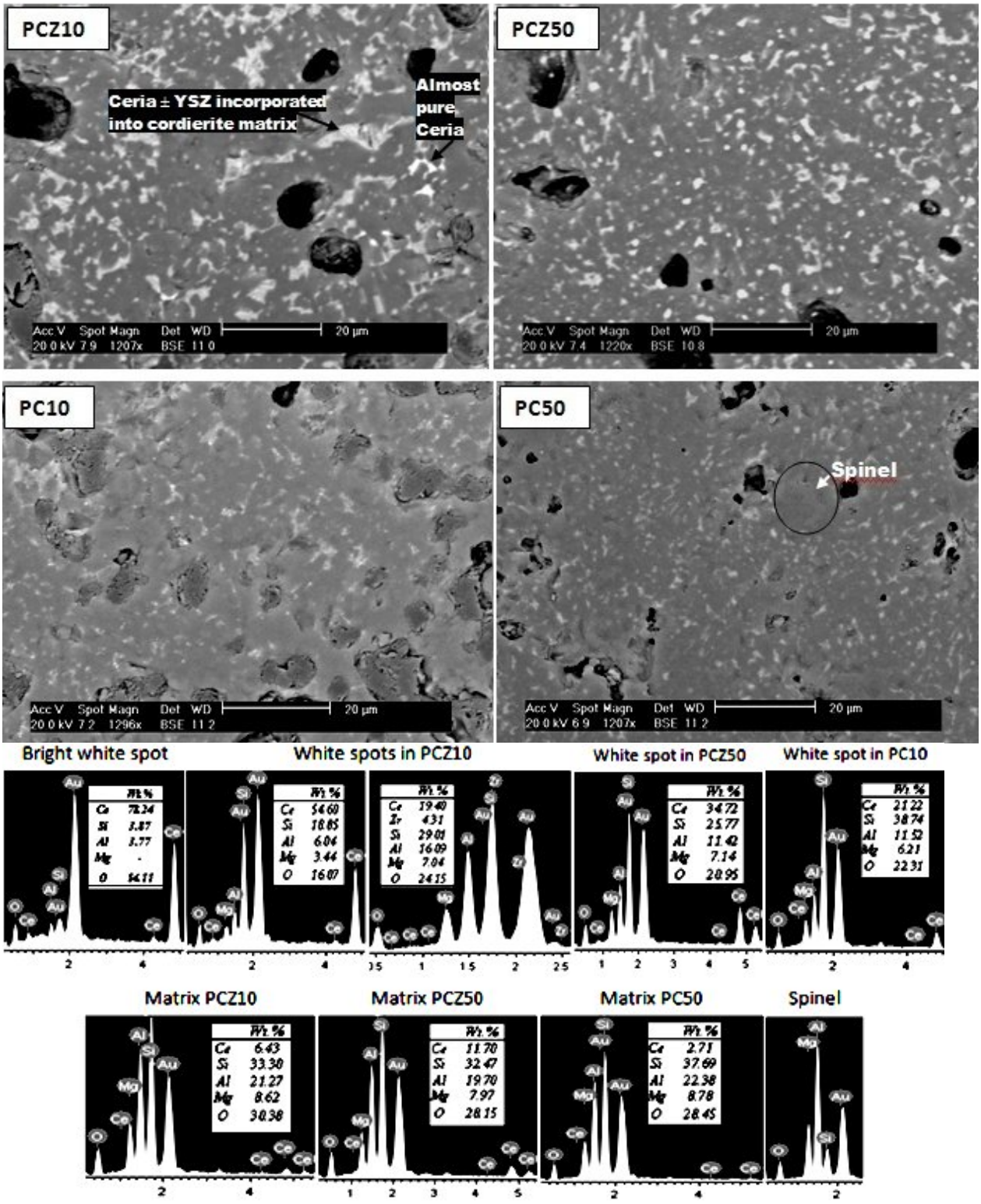

Figure 5-55: Phase characterisation and EDX analysis of selected points on the SEM micrographs of PC and PCZ samples; Gold (Au) in EDX is due to applied coating for the analysis

Sample PCZ10 which showed a reduction of crystallinity according to the results of XRD experiments, is distinguishable by its larger oxide additive phases. The white phases in these samples (Figure 5-55) were shown to be predominantly ceria-bearing compositions, though some minor proportion were zircon. They were divided in two groups after analysis with EDX; those larger spots with cerium content of ≤ 50 wt%, and the smaller and obviously brighter spots with high cerium content (>75 wt% Ce). The latter are considered to be ceria particles which have not been involved in any reaction or ion diffusion within the matrix or have just started to react. However, low ceria phases are considered to be those cerium oxide compounds which in many cases include zirconia (probably as solid solution) and their elemental analysis by EDX analysis show considerable amounts of silicon as well as minor aluminium and magnesium.

The ceria (CeO_2) addition in samples PC10 and PC50 were 4 wt% on the basis of the weight of dry powder mixture. However, in the EDX analysis of the samples (Figure 5-55), the weight percentages of cerium element/ion varied from as low as ~3 wt% in the cordierite matrix to no more than ~25 wt% in the white spots. High cerium containing phases (bright white spots) are not observed in the PC samples; this possibly indicates that such phases are combined cerium zirconium oxides tend to form in PCZ and PZC samples. Mechanochemical processing has caused better distribution of additives in the matrix (PC10 vs. PC50 in Figure 5-55) and consequently, as previously observed in the XRD results, more cordierite is formed with higher activation degree of precursor powders.

5-4-3- Dilatometry analysis – thermal expansion coefficient

Thermal expansion is the general term used to describe the change in dimensions that occurs with most materials as the temperature is increased or decreased. A thermal expansion

coefficient (TEC or CTE) is a characteristic of materials which is sensitive to processes such as: glass transition, phase transition, densification, sintering and also thermally induced stress. The variable of state for linear dilatometry is length, and linear expansion of a material is characterized by measuring how the length of material varies with temperature at constant stress [125, 126]:

$$\alpha = \frac{1}{L_0}\left(\frac{\partial L}{\partial T}\right)_{\sigma} \qquad (5\text{-}1)$$

where α is the coefficient of thermal expansion (CTE) [K^{-1}]. By simply measuring the change in length: ΔL, as a function of sample temperature: $T_S(t) = q \cdot t$, usually with a linear heating rate: q [Ks^{-1}], one can obtain CTE in a certain temperature range:

$$\alpha_L = \Delta L / L_0 \cdot (T_S - T_0) \qquad (5\text{-}2)$$

where L_0 and T_0 are the initial length and temperature, respectively.

Dilatometry is a technique for measurement of expansion or shrinking of materials when subjected to a controlled temperature program. For laboratory-scale experiments, the technique can also provide continuous monitoring of the linear shrinkage of the powder compact over the complete sintering schedule [95]. The results of such analysis for two compact samples (the non-activated, MIX) and the highly-activated ring-milled sample (RM15) are presented as diagrams in Figure 5-56. These experiments were done under 10ºC/min heating/cooling and 2 hours retention time program in order to conform to the conditions in the previous isothermal sintering tests. However a higher dwell temperature (1400ºC) was considered in the dilatometry tests to investigate further possible phase transformations.

According to Figure 5-56, the dehydrated intensely activated sample (RM15) starts to shrink earlier than the non-activated sample. Further, the amount of shrinkage (dL/L_0 %) is much greater for the latter. The point where the shrinkage almost ends followed by a slight expansion, is where the cordierite forms. From this point forward, the formation of cordierite gets completed, in other words, there would be no significant phase reaction other than possible polymorphic transformations to occur beyond that sintering limit. Position "A" on the graph related to sample RM15 represents the above mentioned point, indicating the formation of cordierite being almost complete after about 130 minutes from the begining of sintering test that have been reached 1300 ºC. This is where the previous sintering experiment in the furnace was performed. However, in case of the non-activated sample, this point is not reached only after sintering continued to 1400 ºC and even at such conditions, retention time must be given for the cordierite transformation to occur. As was previously seen, the sample MIX sintered at 1300 °C (2 h) still contained considerable corundum in the final structure.

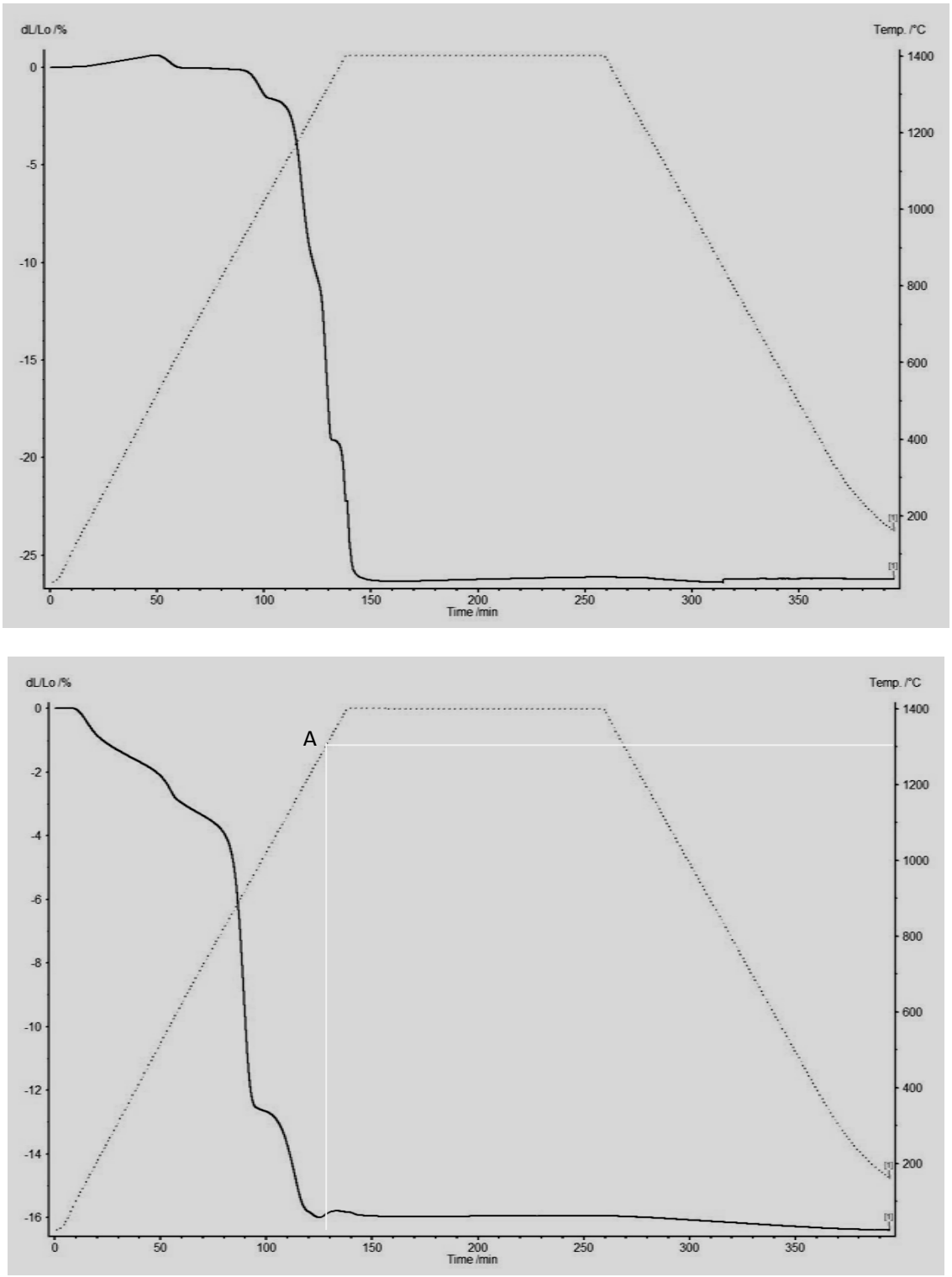

Figure 5-56: Dilatometric shrinkage tests applied for samples MIX (top) and RM15 (bottom); the temperature schedule is also shown as the dotted trend

Several steps in the diagrams reflect different exothermic/endothermic reactions within the compact sample during heat treatment. Considering the shrinkage-temperature relationship

diagram (Figure 5-57), it is possible to differentiate several steps related to phase transformation/reactions during thermal processing. It is observed that after reaching 1300 ºC, sample MIX continues to shrink, while sample RM15 has reached an almost steady state after formation of cordierite. The main reactions occurring at different steps of heat treatment (indicated with letters on the RM15 curve) are as the following [9, 13, 66, 72, 127]:

1) < 200 ºC, dehydration: desorption of adsorbed water (mostly in non-activated sample)
2) "A", ~500-570ºC formation of γ-alumina, kaolinite dehyroxylation, formation of metakaolin
3) "B", ~870-960ºC, talc dehyroxylation and formation of enstatite and μ-cordierite
4) "C", ~970-1100ºC, formation of intermediate phases: mullite, cristobalite, spinel, (corundum in activated sample)
5) "D", ~1100-1200ºC, reaction of intermediate phases
6) "E", >1300 ºC, formation of indialite/cordierite (at 1200ºC in activated sample)

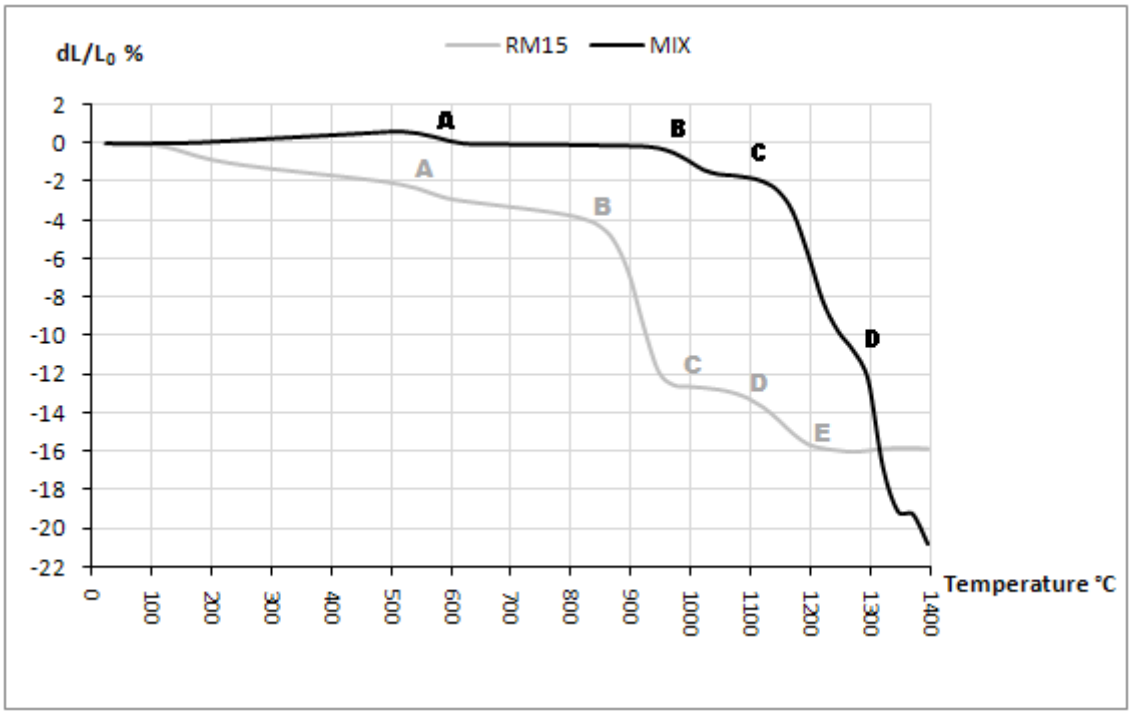

Figure 5-57: Shrinkage vs. temperature tests in the dilatometry analysis of samples MIX and RM15

Among the most important industrial applications for cordierite ceramics are uses wherein low thermal expansion as well as shock resistance of cordierite ($\Delta T>350^{o}C$) are sought, such as in refractory applications like kiln furniture or as catalyst substrates in automobile catalytic converters for pollution control. Therefore, measurement of the thermal expansion coefficient of some of the sintered samples in this research was evaluated. Using a push rod dilatometer (Netzsch 402E), measurements were conducted after calibration and at 5 ºC/min heating/cooling rates, and the results are presented in Figures 5-58 to 5-60 for samples PM50-T and RM15. Measurements were carried out (by the integrated software) at several temperature intervals starting from 200 °C and ending at 500 °C, 600 °C, 800 °C and 850 °C on both expansion and contraction curves. It is worth noticing that samples selected in these experiments both possessed higher cordierite XRD intensities compared to the rest of doped material, however, the major reason for not analysing other samples was the time constraints of the project.

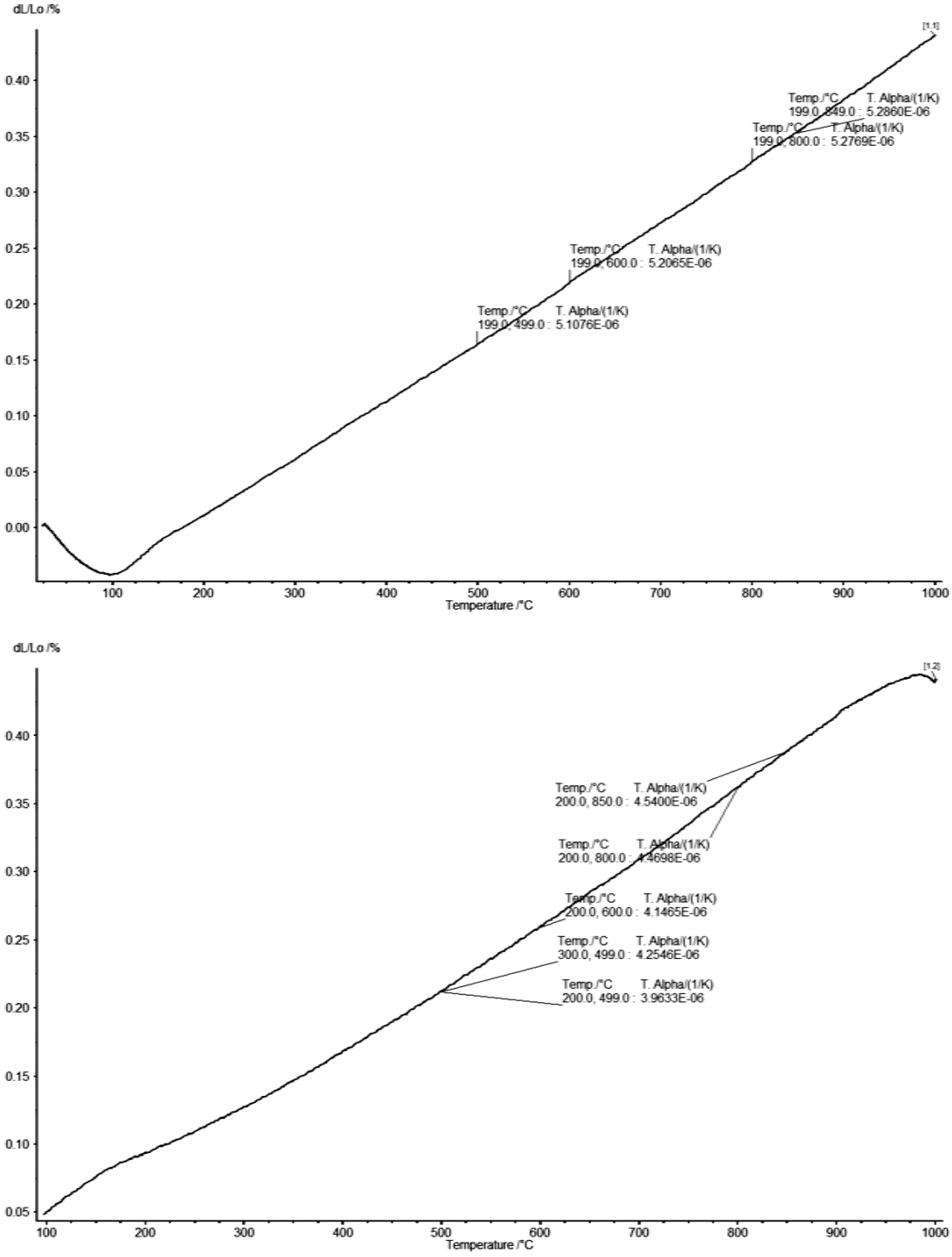

Figure 5-58: Measurement of thermal expansion coefficient for sample PM50-T; top: heating cycle, bottom: cooling cycle; there are four measurements comprising four ΔT values in each cycle

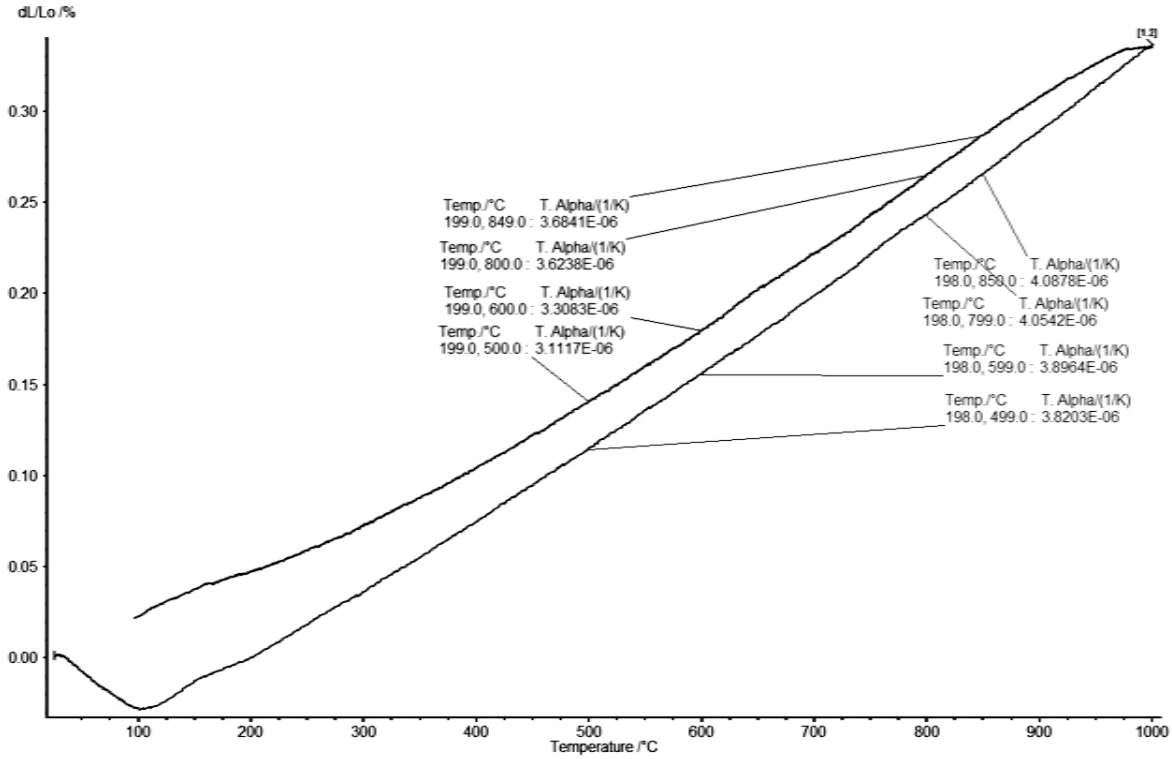

Figure 5-59: Measurement of thermal expansion coefficient for sample RM15 on both heating (top) and cooling (bottom) curves; there are four measurements comprising four ΔT values in each cycle

The measured values of the thermal expansion coefficient on the expansion cycle for sample PM50-T, are shown in Figures 5-58, change from $5.11 \times 10^{-6}\ ^{1}/_{K}$ at 500 °C to $5.29 \times 10^{-6}\ ^{1}/_{K}$ at 850 °C. For sample RM15-T over the same interval it changes from $3.82 \times 10^{-6}\ ^{1}/_{K}$ to $4.09 \times 10^{-6}\ ^{1}/_{K}$. Therefore lower values are obtained for the ring-milled sample. There are several factors considered influential in determining the thermal expansion coefficient in dilatometry tests; one of the factors, already observed in the graphs, is the effect of ΔT over which the measurement is performed. Apart from instrument settings and possible measurement errors, material factors are quite important with regard to determination of final thermal expansion of the material. Selection of starting materials is critical both as to mineral content and purity level, and they were well controlled in this research. Microstructural characteristics of the sintered body would also influence the measured value for the coefficient of thermal

expansion. For example it has been shown [128] that more homogeneous pore distribution in a sintered cordierite body could reduce its thermal expansion coefficient. Moreover, by appropriate controlling of the heat treatment process to produce microcracks (of up to 3 μm in size) with a certain distribution in the sintered body, the CTE of the material could be further decreased.

Degree of crystallisation, of the material, as indicated by Rohan *et al.* [129], has also significant effect on the linear thermal expansion coefficient. It has been seen that by variation of the glass content of the body through conventional processing, thermal expansion can be varied linearly between the calculated value of a 100% polycrystalline cordierite body and the measured value of a 100% glass body having the composition of cordierite, within the range 25 °C to 800 °C. Finally, sintering operating parameters such as temperature and retention time would also influence the final measured CTE of the sample [127, 130].

Result of similar measurements for sample PC50 is shown in Figure 5-60. This last experiment was performed in order to investigate how the small addition of cerium oxide might influence the thermal properties of sintered cordierite bodies. Although smaller expansion coefficients are measured for the ceria-doped sample ($4.47 \times 10^{-6}\ ^{1}/_{K}$ at 500 °C), compared to equivalent undoped PM50-T, once again it must be emphasised that other factors such as porosity volume and distribution in the sintered body as well as the degrees of crystallinity of the material are involved.

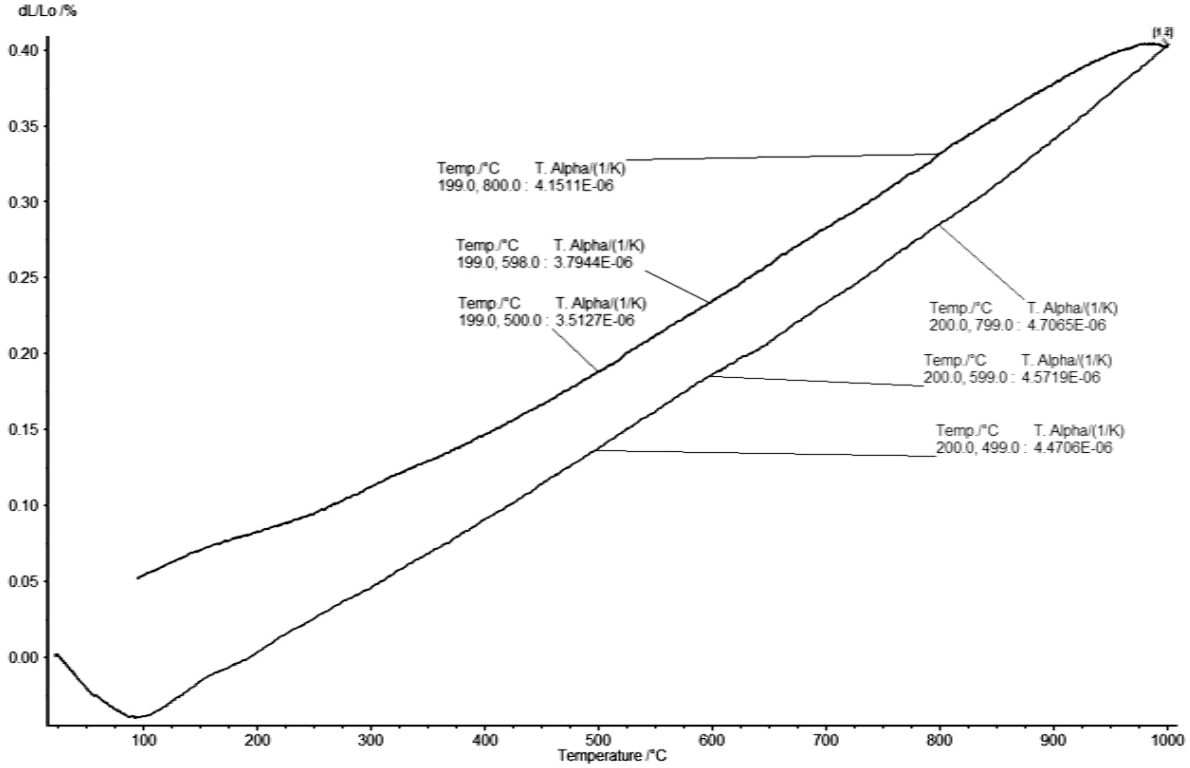

Figure 5-60: Measurement of thermal expansion coefficient for sample PC50 on both heating cycle and cooling curves

6. FINAL DISCUSSION AND CONCLUSION

6-1- Mechanochemical processing and formation of cordierite

- **The importance of homogeneity in properties of the precursor powders**

Although a nanocomposite or any nano-structured material does not have to consist of only nano-sized ingredients, the size homogeneity of the constituent precursor powders is important in the manufacturing process to achieve the desired properties. In this respect, initial size differences between at least one of the precursor materials (talc, Figure 5-2) in this study was found to be influential in both intensive milling and subsequent sintering tests. While surface chemical properties (such as hydrophobicity) are effective on mixing and size reduction process particularly during initial milling, the particle shape is considered as an important factor when a mixture of different powders are prepared for solid-state process both at grinding and sintering stages.

- **Mechanochemically intensified phase transformation**

What is probably more assured about the effects of the milling processes applied in this research, is the development and transformation of phases (appearance of new and consumption/reaction of previous phases) with respect to the milling time/intensity at a specified sintering temperatures. Formation of significant amounts of mullite from kaolin and alumina and its consequent incorporation in development of other emerging compositions was one the most distinguishable mechanically induced solid-state reactions during sintering. Transformation reaction to form mullite seems to be started (or accelerated) at the grain boundaries of the presumably amorphous alumina phases as characterised in the SEM-EDX

studies. It has also been proposed when mullite rather than corundum is the prevailing precursor in preparation of cordierite ceramics, the transformation temperature would be decreased [116, 131].

- **Mechanochemically induced grain growth**

Of the effects of mechanochemical activation on sintered material structure, which were well established in this study, was formation of complex large (up to tens of micrometers) intermediate compounds which tend to become more homogeneous with respect to chemical composition (according to EDX analysis) as milling time increased. These structures, usually possessing elongated rectangular shapes, were quite obvious while studying the SEM micrographs of the sintered bodies which were ring-milled and sintered at about 1000 °C. At higher temperatures, the emerging large grains of new phases were commonly found to be hegxagonal in cross-sections and of cordierite chemical composition.

- **Effect of grinding mechanism on the degree and the pathway of phase transformation**

The sintered material structure and phase constitution, determined by XRD and SEM analyses, were very dependent on the milling method applied. For example in the *low* temperature programme (950 °C), long planetary milling resulted in a material which showed the least crystallinity after sintering compared to the products of the other milling methods. On the other hand, when considering the same sintering condition, ring milling at the maximum applied intensity caused the formation of magnesium aluminium silicate phase (MAS), which was not observed in any other samples milled in different ways. There were also similar distinguishing features when the sintered materials from different milling machines were compared for the *high* temperature sintering programme (1050 °C). At this

temperature, the phase composition of the ring milled sintered samples was more diverse and included cristobalite among the characterised crystalline phases. Although the material of which the milling media is composed (e.g. WC in case of the ring mill) might have had an effect on such phase formations, these variations in chemistry and crystallinity could be somewhat attributed to the intensity and/or duration of the activation process, which were by no means the same in different milling methods. For example it might be expected that the phase transformation during sintering of the planetary/ball-milled material could result in similar composition/crystallinity if these latter millings were continued for longer times. To investigate this assumption, more systematic milling experiments with different machines would need to be performed, so that the effect of different parameters such as milling time, speed and grinding method are all investigated on a statistical basis and then evaluated at certain sintering conditions each time.

- **Effect of grinding mechanism on densification and microstructure**

Although ring milling proved to be more intense in terms of the rate and diversity of observed phase development, planetary milling resulted in higher density, lower porosity content and smaller pore size in the sintered bodies. From the results of density/porosity measurements (section 5-3-3), as well as microstructure study of the sintered material, it is proposed that planetary mill would be the most efficient activation process to apply for materials development studies. Ring mill, though according to XRD analysis, proved to result in large degree of structural deformation of the ground material in a short time, could not be a final selection for the purpose of mechanochemical activation due to its low capacity, less efficiency to grind the sheet crystalline structures such as kaolinite and talc, and finally the limitations in scale-up procedure compared to other milling machines. The reason why

mechanochemical milling of the precursor powders by planetary mill resulted in relatively higher densifications after sintering tests could be attributed to the grinding mechanism of such apparatus. As shown in Figure 6-1, planetary mills exploit the principle of centrifugal acceleration instead of gravitational acceleration. The enhancement of the forces acting on the balls in relation to the conventional ball mill is achieved by combined action of two centrifugal fields.

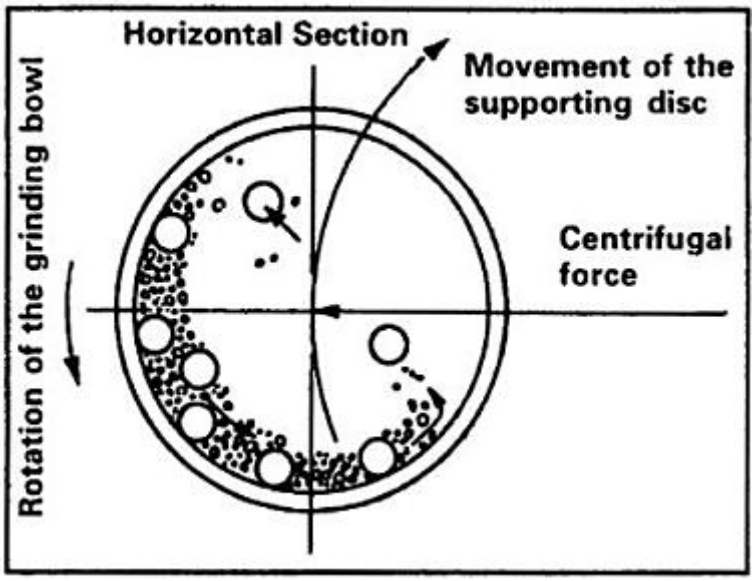

Figure 6-1: Schematic of the relative movements of the mill, media and material in a planetary milling process [32]

In reaction sintering, the reaction and densification processes occur in the same heating cycle. Taking into consideration the controlling factors that affect the densification process, it is important to remember that during reaction sintering, large energy changes associated with the reactions can lead to the microstructures that inhibit densification [95]. This was quite well observed in the SEM micrographs at section 5-3-2 in which large crystals of single phases were forming in the matrix.

- **Formation of cordierite (effect of milling on making transformation complete)**

Another important characteristic of the mechanically activated samples was the production of almost single-phase indialite/cordierite ceramics at 1300 °C; considering the fact that no sintering aids (that negatively affect the engineering properties of cordierite) were employed in the current experiments. As indicated in the XRD results, the unactivated sample contained free alumina (corundum), while the mechanically processed samples were found to contain only minor amounts of spinel as the only phase impurity in the cordierite body.

- **Green body preparation procedure**

Although die wall lubrication was performed regularly during compression tests, consideration must be given to a common problem in the uniaxial die compaction process which is due to the applied pressure not being transmitted uniformly to the powder as a result of friction between the powder and the die wall. Springback or expansion of compact when the pressure is released can be expected. Application of a uniaxial pressure to the powder leads to the generation of a radial stress and a shear (or tangential) stress at the die wall. The density variations caused by the pressure gradients generated during compaction, become magnified during sintering, often resulting in a limited final density and cracking [6]. In the time frame of this project it was not possible to investigate such effects and the density gradients in the samples, however, all of these factors must be taken into account in order to eliminate the possible flaws in the final microstructure of the sintered samples prepared for a target engineering application.

6-2- Effects of additives on sintering behaviour and microstructure

6-2-1- Samples containing yttria-stabilised zirconia as a major additive

Additives (stabilised zirconia and ceria) have been shown in this study to influence the microstructural development during thermal treatment following mechanochemical processing. When yttria-stabilised zirconia was the dopant (in PZ samples), longer mechanical activation resulted in increased XRD peak intensities for zircon, which is possibly due to an increase in the reaction rate of silica/cordierite and zirconia in the matrix. On the contrary, the activation process was apparently one of the factors responsible in the reduction of zircon XRD peak intensities where yttria-stabilised zirconia and ceria were used together as dopants (PZC samples). The latter is presumably the result of stabilisation of zirconia by ceria (formation of combined oxides), promoted by intensive milling action.

According to Sun *et al.* [83], homogeneous dispersion of nano-sized ZrO_2 on the surfaces of cordierite particles, due to achievement of a high degree of mixing could facilitate the nucleation process in the formation of zircon. Although mechanical activation might have had influenced the destabilisation of YSZ followed by formation of zircon in the current research, there are discussions on the reaction of YSZ with cordierite in the literature, where no mechanochemical activation of powders was applied. According to Wadsworth *et al.* [77], hot pressing of samples containing 20 vol% [ZrO_2-3mol% Y_2O_3] at 1350 °C for 1h resulted in appearance of a small diffraction peak due to zircon formation at $2\theta = 27°$ (Cu K_α), however, further ageing resulted in only a marginal increase in the zircon peak height. They concluded that the reaction between cordierite and zirconia is thermodynamically possible (>1280 °C) but might be kinetically slow under the conditions applied in the process. In this regard the

following well-stablished parameters are found determinative in transformability of zirconia inclusions:

- Zirconia particle size
- Zirconia grain morphology
- Stabilizer content
- Matrix constraint (difference in thermal expansion coefficients)

In the current study, zircon could not be easily distinguished in the SEM-EDX experiments, therefore some higher resolution techniques such as TEM might be useful to characterise the phase boundaries and locations of zircon in the matrix.

The effect of ceria addition (3 wt%) to cordierite precursor and zirconia powder mixture (PZC samples) is shown in the microstructure studies by the intensification of cordierite formation at low activation (PZC10 compared to. PZ10). When the same mixture was milled for longer time, cerium oxide was more able to act as a fluxing agent that caused the reduction of crystallinity of the pre-sintered material (PZC50 compared to PZ50 and PZC10). In conclusion, the addition of small amounts of ceria to the YSZ-cordierite precursor mixtures can result in more stability of t-zirconia in the matrix (by forming CeO_2-ZrO_2 double oxide) during heat treatment provided the mechanochemical milling is controlled up to an optimum level (less than 50 minutes planetary milling in these tests). In this case, addition of ceria would be of benefit in phase transformation and densification of composite cordierite-zirconia ceramics.

6-2-2- Samples containing ceria as a major additive

When ceria is the only additive (4 wt%) and the mixture mechanochemically activated, densification was enhanced. More cordierite is formed in the composite when longer milling

times are employed. However, the general effect of addition of ceria to the cordierite precursor, according to the XRD analysis results, was the reduction of intensity of the peaks observed in the activated sintered samples. On the other hand, when cerium was used in relatively large amounts (12 wt%) together with yttria-stabilised zirconia (3 wt%) there were two distinct effects on the sintered material microstructure at low and high activation degrees. At low mechanical activation, sample PCZ10 exhibited a very low degree of crystallinity after sintering, which in this respect it was comparable to sample PZC50, however PCZ10 had lower diffraction intensities. Almost no trace of tetragonal zirconia (YSZ) and very limited levels of zircon formation were found for the high ceria/low ziconia cordierite composites. On the contrary, the combined ceria-zirconia cubic structure was the predominant phase formed from the dopant in the sintered cordierite matrix. Longer milling times of 50 minutes (sample PCZ50), which reduced the crystallisation of sample PZC50, in this case promoted the formation of cordierite-ceria-zirconia-zircon composite. This latter process of course is accompanied by a relatively large shrinkage and densification rate.

Pure cordierite has a softening point in the range of 1450-1460 °C and a melting point of 1472 °C, while commercial extruded cordierite, containing variable amounts of alkaline or alkaline earth metal oxides (as common flux-making additives), shows a lower melting point (about 1450 °C). On the other hand, ceria is known to act as a fluxing agent in cordierite synthesis. Samples doped with cerium oxide show a further decrease of these temperatures; the lowest melting temperature reported in the literature is 1376 °C for 9.5% w/w CeO_2 cordierite [122]. This fact explains the formation of the glassy phase in the sample PCZ10 and reduction in crystallinity reported in X-ray diffraction test results. Intensive mechanochemical processing gives a better distribution of the ingredients, and further assists the ceria-zirconia combination process, pushing the system into a more glassy state.

Another fact concerning the effects of ceria when doped with cordierite precursor mixtures during solid-state synthesis is that it has been shown in the MgO-Al_2O_3-SiO_2-CeO_2 quaternary system, when all ions are in octahedral coordination, the combination of Mg-O and Al-O is weakened by the interaction of cerium ion with oxygen in MgO and Al_2O_3. On the other hand, Ce less affects the Si-O bond in the silica tetrahedron therefore cannot modify the diffusion of Si^{4+} ions [26]. This might be responsible for cordierite-ceria phase compositions with low Mg and Al contents (analysed by EDX) existing in sample PCZ10.

7. FURTHER WORK

At present, mechanochemistry appears to be a science with a sound theoretical foundation which exhibits a wide range of potential applications. Among its key benefits in advanced materials processing are lower reaction temperatures, increased reaction rate, increased dissolution and the formation of water soluble compounds. The research on high-energy mechanical milling has highlighted a major potential process for processing advanced materials. Materials scientists and engineers, who are interested in employing high-energy mechanical milling into an industrial process, take advantage of the results of experiments from mineral processing and powder consolidation technologies that helps improve the modeling and design of mills as well as the milling process for scaling up studies [132, 133].

Outside the development scope of the research in mechnochemistry and its application in producing advanced materials and composites, there are few points specific to the current study, which worth considering in further investigations:

1. Size reduction of talc (d50 ≈10μm) using some effective methods such as wet attrition milling or as successfully done by Pérez-Maqueda *et al.* [134], by application of sonication to prepare submicron particles is suggested.
2. Study of the particle agglomeration and deformation due to intensive milling action with respect to its possible effects on later compaction and sintering behaviour should be undertaken. Its influence on particle size should be considered too. It is suggested that these investigations at nanometer scale are performed by application of high resolution microscopy and/or taking advantage of surface chemistry techniques.

3. Methods such DTA/DTG thermal analysis should be applied as *dynamic* sintering studies in order to better distinguish the transient steps during heat treatment, most specifically in understanding the stage where destabilisation of yttria stabilised zirconia to form zircon occurs in the matrix.
4. TEM microscopy or similar techniques should be applied to give detailed analysis of the phase development and interactions in the matrix.
5. Study of the solid-state reaction mechanisms focusing on the effect of mechanical activation on phase transformation paths and products is important.
6. Application of binders in powder compaction tests and evaluation of its effect on densification and properties of the final structure should be considered.
7. Possible effects of longer soaking/retention times on sintering behaviour and phase transformation at 1300 °C could be evaluated.
8. Conducting the sintering test at higher temperature (e.g. about 1400 °C) to investigate probable effects on cordierite formation and stability of zirconia is suggested. However such temperatures are not suitable for sintering the high ceria-doped samples due to formation of melt phase.
9. Measurement and evaluation of mechanical properties of both doped and undoped samples, such as compressive/flexural strength and fracture toughness are necessary for proposed target applications.
10. Finally, although the main purpose of adding cerium oxide in the this study was to examine the phase transformation effects on synthesis of cordierite, the engineering functionality of ceria, which is mechanically activated in the milling processes and well dispersed in the matrix, would be worth considering. Presently CeO_2 is added to γ-alumina in automobile catalyst applications for oxygen storage. In their study, Shi *et*

al. [90], confirmed comparable oxygen storage capacity of cordierite doped with 10 wt% ceria to that of ceria catalytic wash coating on a cordierite substrate at a slight compensation for the thermal expansion properties of cordierite. However, such possible improvement necessitates the relevant tests and evaluations (such as oxygen storage measurements) to be performed.

Appendix

I) Phase diagrams

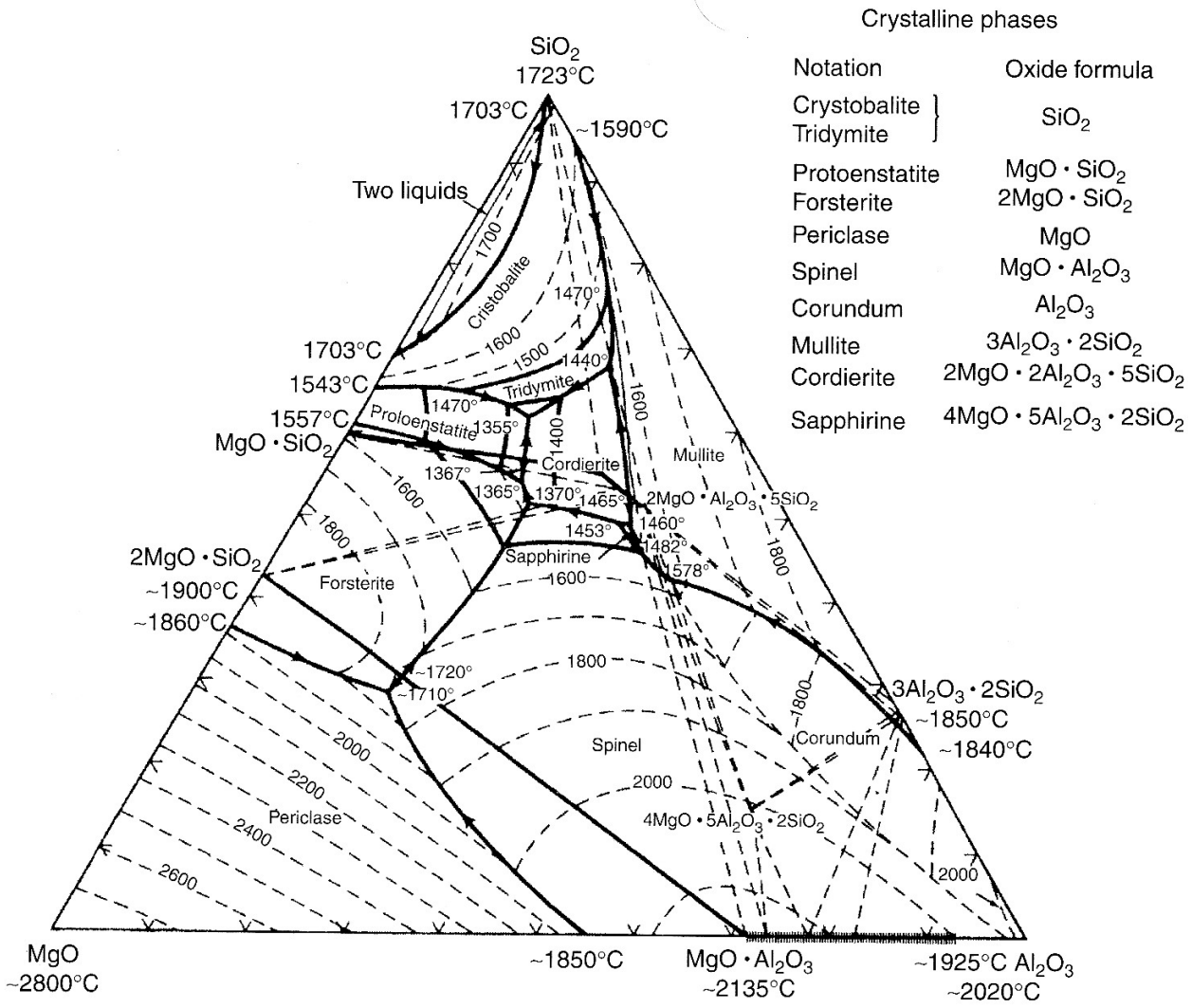

Ternary phase equilibrium diagram for the system MgO-Al_2O_3-SiO_2

Some important features of the above diagram [126]:

1. Congruently melting binary compounds ($2MgO \cdot SiO_2$ and $MgO \cdot Al_2O_3$)
2. Incongruently melting binary compound ($MgO \cdot SiO_2$)
3. Ternary eutectics and peritectics
4. Incongruently melting ternary compound ($2MgO \cdot 2Al_2O_3 \cdot 5SiO_2$)
5. Liquid immiscibility in the SiO_2-rich corner
6. Phase transformations in the SiO_2 primary-phase field
7. Solid solution of Al_2O_3 in $MgO \cdot Al_2O_3$ (spinel) and of $3Al_2O_3 \cdot 2SiO_2$ (mullite) in $2MgO \cdot 2Al_2O_3 \cdot 5SiO_2$ (cordierite).

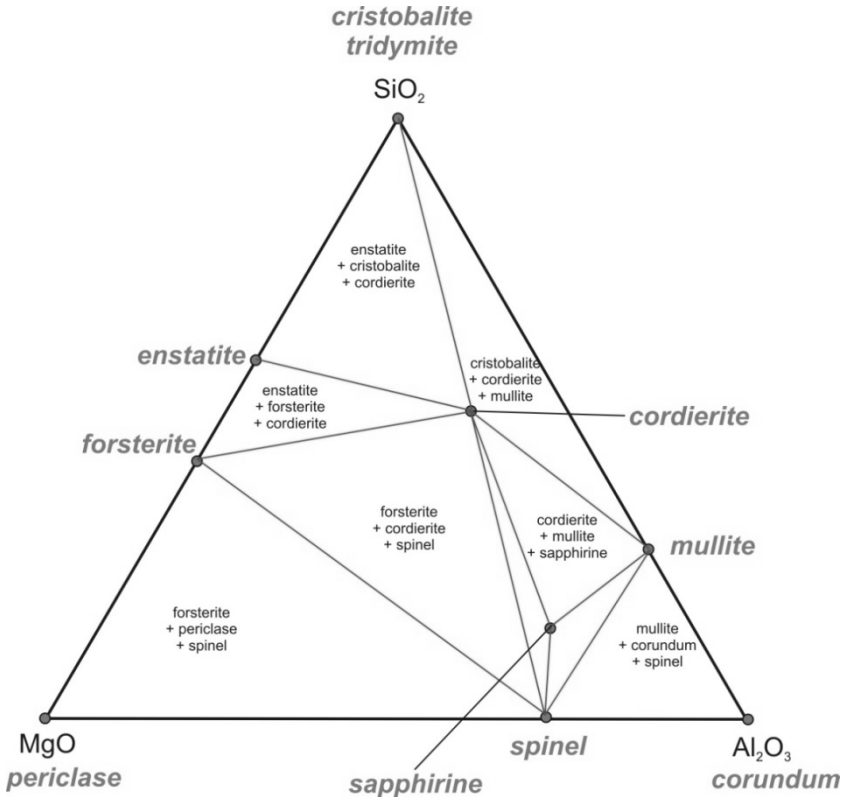

The system MgO-Al_2O_3-SiO_2 at 1 atm. pressure. Diagram shows final (subsolidus) stable mineral assemblages [135]

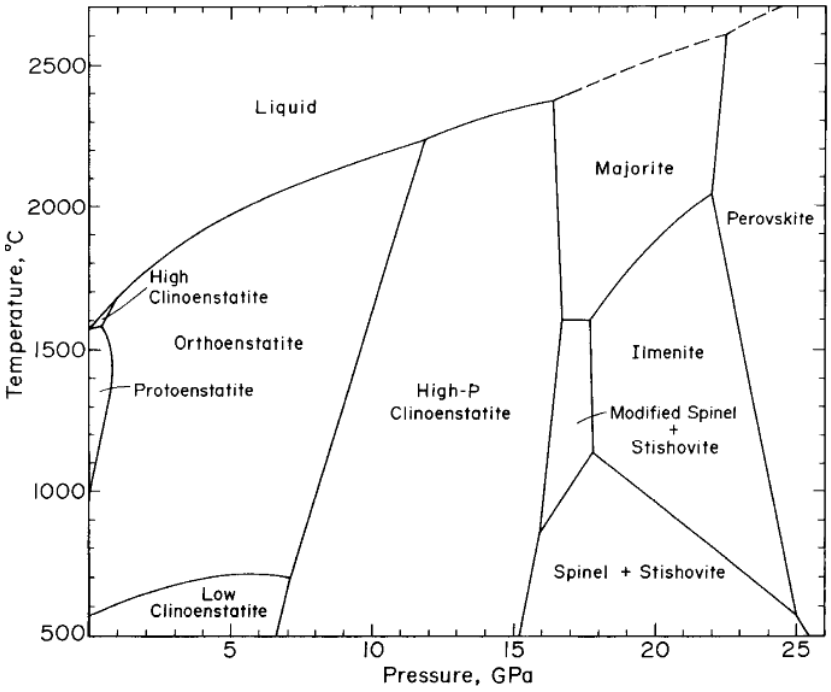

Isopleth for the composition $MgSiO_3$[136]

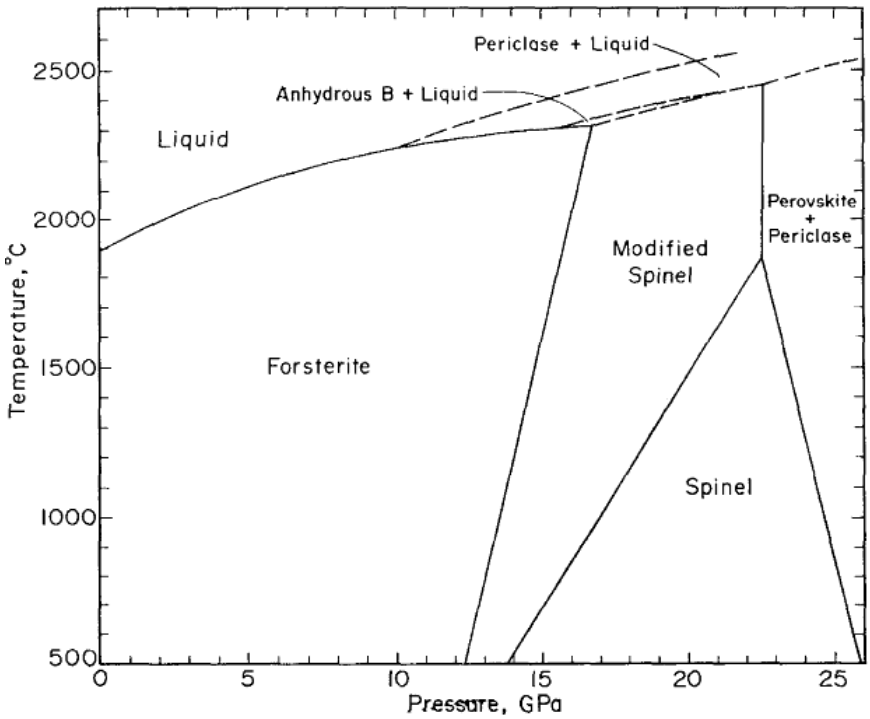

Isopleth for the composition Mg_2SiO_4 [136]

II) Crystal structures and thermal decomposition products

Boehmite:

Boehmite, AlO(OH), has an orthorhombic unit cell and consists of chains of AlO_6 octahedra giving double molecules:

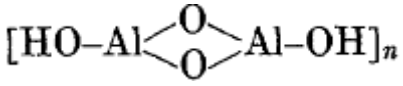

The chains are parallel, forming layers with the OH groups on the outside. The bonding between these layers is due to hydrogen bonds. The dehydration sequence follows the path (temperatures are approximate) [137]:

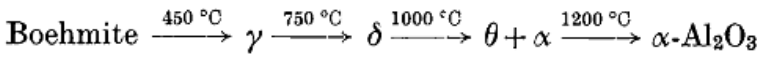

Diaspore and boehmite are polymorphs of the same mineral and differ in structural relationships by the packing of the oxygens [102].

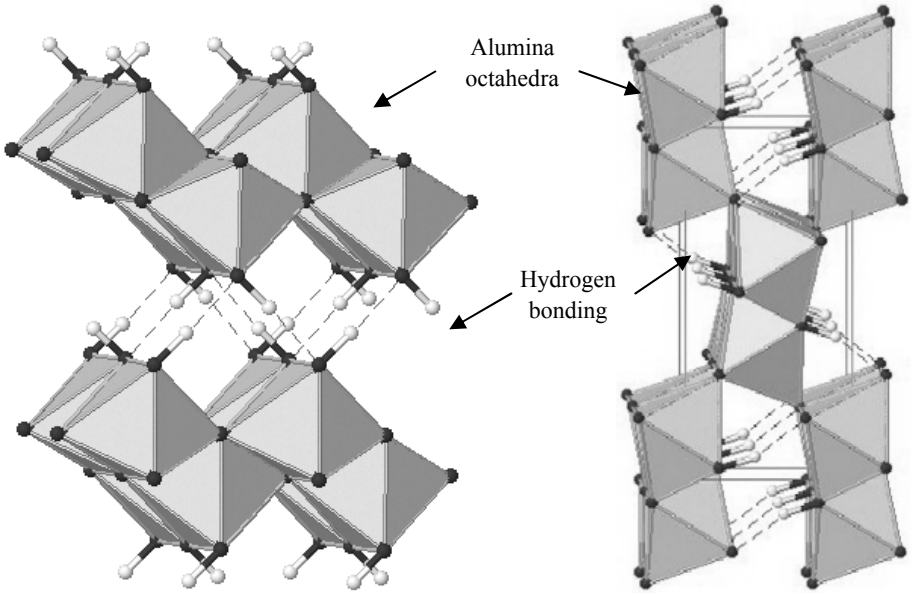

Crystal structures of left: boehmite, right: diaspore [138]

Kaolinite:

Kaolinite, $Al_2Si_2O_5(OH)_4$ is a dioctahedral layered hydrated aluminosilicate of the 1:1 type with two distinct interlayer surfaces. One side of the layer is gibbsite-like with aluminum atoms coordinated octahedrically to corner oxygen atoms and hydroxyl groups. The other side of the layer is constituted by a silica-like structure, where the silicon atoms are coordinated tetrahedrically to oxygen atoms. The adjacent layers are linked by hydrogen bonding involving aluminol (Al-OH) and siloxane (Si-O) groups.

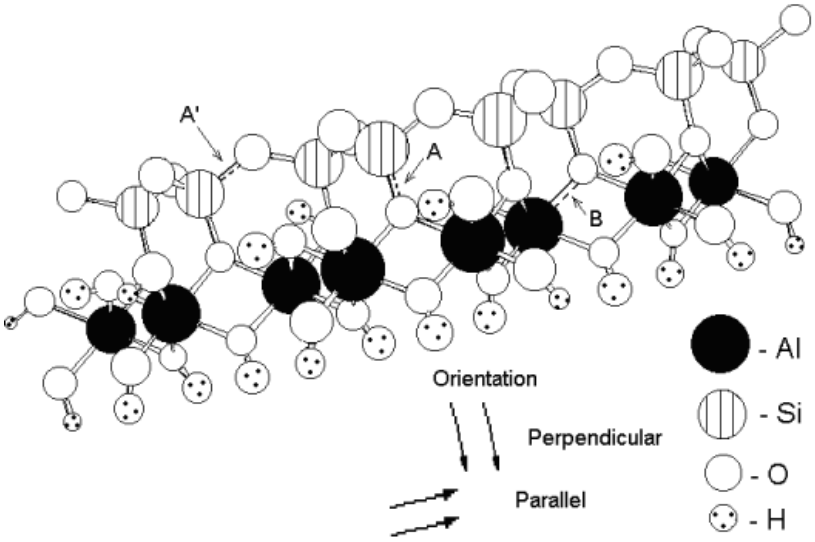

Detailed scheme of the kaolinite structure, with localised A, A' and B paramanetic centres [139]

The transformation of kaolinite to mullite and glassy phases occurs according to the following reactions [140]:

$$(1)\quad Al_2O_3 \cdot 2SiO_2 \cdot 2H_2O\ (\text{kaolinite}) \xrightarrow{673\text{–}773\ K} Al_2O_3 \cdot 2SiO_2\ (\text{metakaolinite}) + 2H_2O\ ,$$

$$(2)\quad 2(Al_2O_3 \cdot 2SiO_2)\ (\text{metakaolinite}) \xrightarrow{\sim 1253\ K} Si_3Al_4O_{12}\ (\text{spinel}) + SiO_2\ (\text{amorphous})\ ,$$

$$(3)\quad 3Si_3Al_4O_{12}\ (\text{spinel}) \xrightarrow{>1273\ K} 2(3Al_2O_3 \cdot 2SiO_2)\ (\text{mullite}) + 5SiO_2\ (\text{amorphous})\ ,$$

$$(4)\quad SiO_2\ (\text{amorphous}) \xrightarrow{>1473\ K} SiO_2\ (\text{cristobalite})\ .$$

Talc:

Talc, $Mg_3Si_4O_{10}(OH)_2$, is a hydrated magnesium sheet silicate. Its elementary sheet is composed of a layer of magnesium-oxygen/hydroxyl octahedra or brucite ($Mg(OH)_2$), sandwiched between two layers of silicon-oxygen tetrahedra or silica (SiO_2). The main or basal surfaces of this elementary sheet do not contain hydroxyl groups or active ions, which

explains talc's hydrophobicity and inertness. Weak Van der Waal's forces bond the crystal lattice of talc, thus, the mineral undergoes cleavage very readily and is very soft [141, 142].

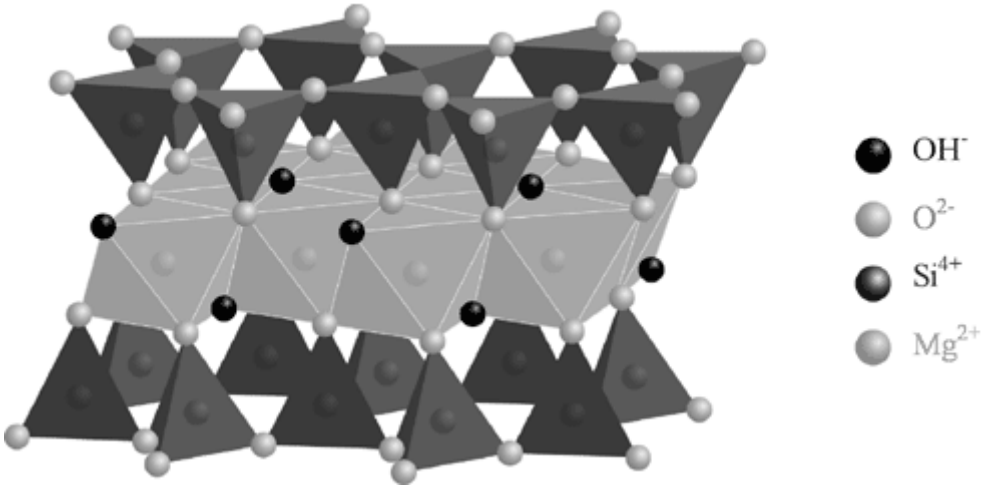

Talc crystal structure [141]

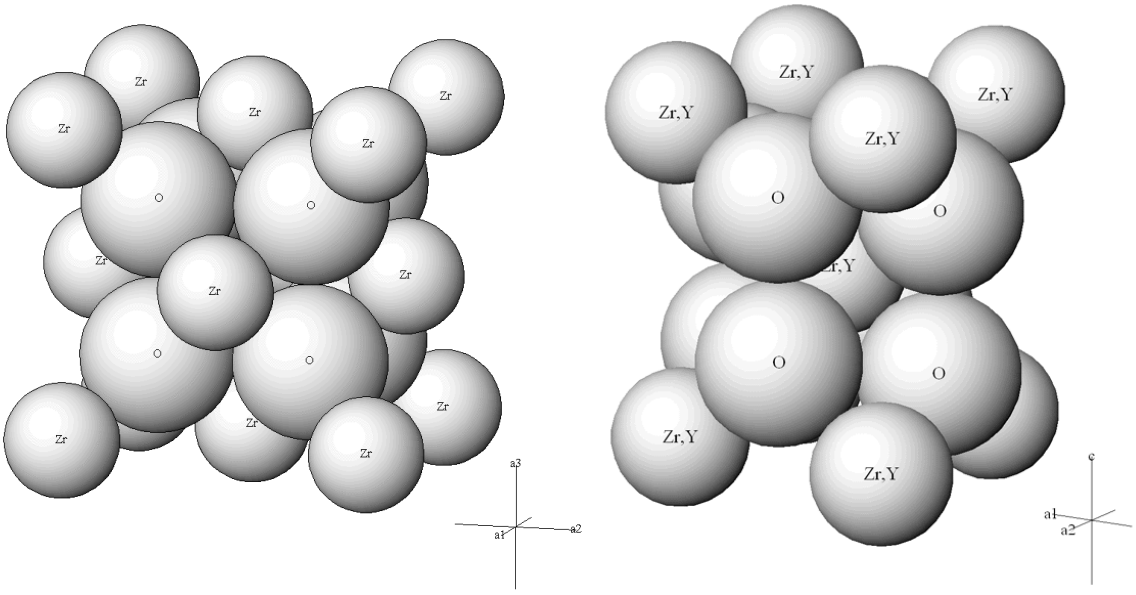

Left: Crystal structure of zirconia (monoclinic), Right: 3 mol% yttria stabilized zirconia (tetragonal) [143]

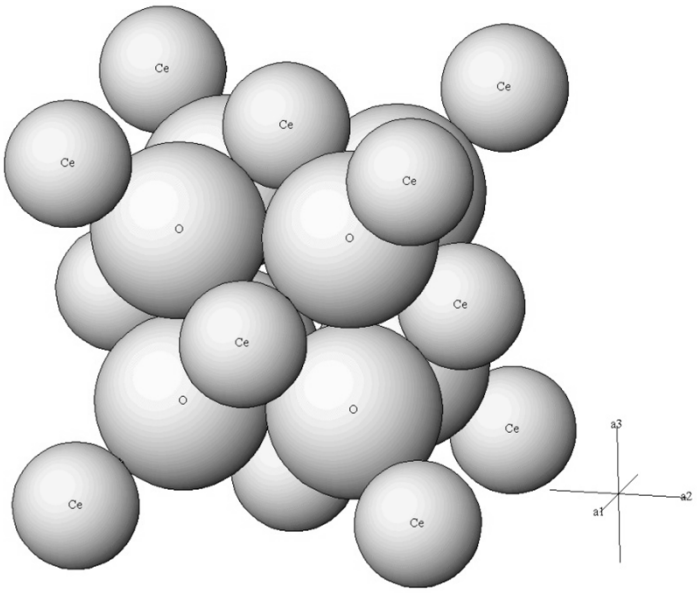

Crystal structure of ceria (cubic) [143]

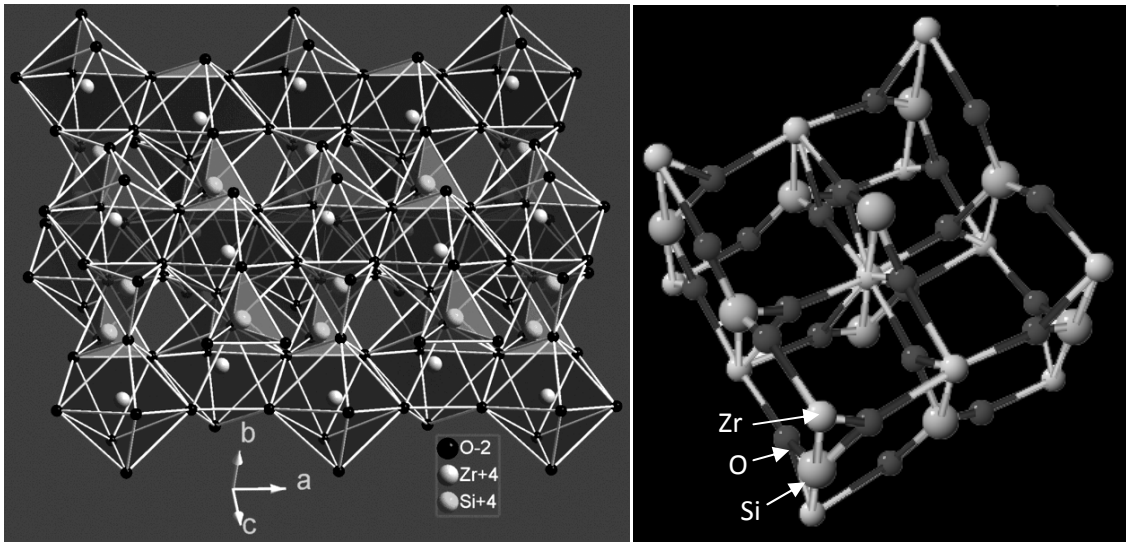

Zircon ($ZrSiO_4$) tetragonal crystal structure; left: repeated pattern, right: unit cell [144]

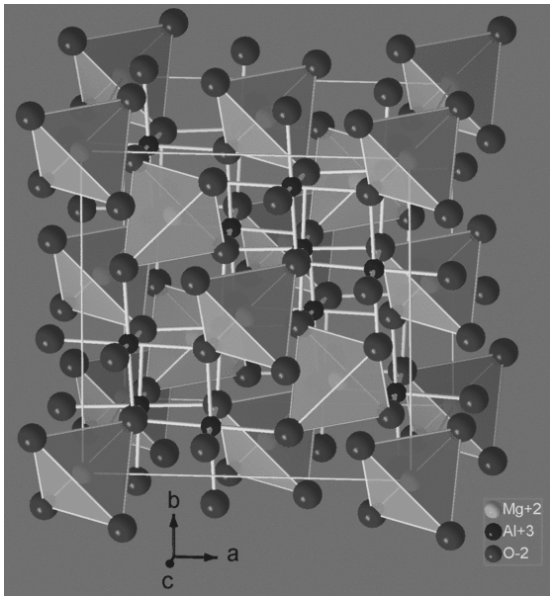

Crystal structure of spinel, $MgAl_2O_4$, (cubic)

III) Material properties data and table of elements

Cordierite properties [145]

Properties	Units	Test	Value
Physical			
Chemical Formula	-	-	$2MgO\text{-}2Al_2O_3\text{-}5SiO_2$
Density, ρ	g/cm^3	ASTM C20	2.60
Color	-	-	tan
Crystal Structure	-	-	orthorhombic
Water Absorption	% @R.T.	ASTM C373	0.02 - 3.2
Hardness	Moh's	-	7
Hardness	knoop (kg/mm^2)	Knoop 100g	--
Mechanical			
Compressive Strength	MPa @ R.T.	ASTM C773	350
Tensile Strength	MPa @ R.T.	ACMA Test #4	25.5
Modulus of Elasticity (Young's Mod.)	GPa	ASTM C848	70
Flexural Strength (MOR)	MPa @ R.T.	ASTM F417	117
Poisson's Ratio, υ	-	ASTM C818	0.21
Fracture Toughness, K_{Ic}	MPa x $m^{1/2}$	Notched Beam Test	--
Thermal			
Max. Use Temperature (* denotes inert atm.)	°C	No load cond.	1371
Thermal Shock Resistance	ΔT (°C)	Quenching	500
Thermal Conductivity	W/m-K @ R.T.	ASTM C408	3.0
Coefficient of Linear Thermal Expansion, α_l	µm/m-°C (~25°C through ±1000°C)	ASTM C372	1.7
Specific Heat, c_p	cal/g-°C @ R.T.	ASTM C351	0.35
Electrical			
Dielectric Constant	1MHz @ R.T.	ASTM D150	4.7
Dielectric Strength	kV/mm	ASTM D116	5.11
Electrical Resistivity	Ωcm @ R.T.	ASTM D1829	10^{14}

Mullite properties [145]

Properties	Units	Test	Value
Physical			
Chemical Formula	-	-	$3Al_2O_3$-SiO_2
Density, r	g/cm^3	ASTM C20	2.80
Color	-	-	tan
Crystal Structure	-	-	orthorhombic
Water Absorption	% @R.T.	ASTM C373	0.0
Hardness	Moh's	-	8
Hardness	Knoop (kg/mm^2)	Knoop 100g	1450
Mechanical			
Compressive Strength	MPa @ R.T.	ASTM C773	551
Tensile Strength	MPa @ R.T.	ACMA Test #4	103.5
Modulus of Elasticity (Young's Mod.)	GPa	ASTM C848	150
Flexural Strength (MOR)	MPa @ R.T.	ASTM F417	170
Poisson's Ratio, n	-	ASTM C818	0.25
Fracture Toughness, K_{Ic}	MPa x $m^{1/2}$	Notched Beam Test	2.0
Thermal			
Max. Use Temperature (* denotes inert atm.)	°C	No load cond	1700
Thermal Shock Resistance	DT (°C)	Quenching	300
Thermal Conductivity	W/m-K @ R.T.	ASTM C408	3.5
Coefficient of Linear Thermal Expansion, a	mm/m-°C (~25°C through ±1000°C)	ASTM C372	5.3
Specific Heat, c_p	cal/g-°C @ R.T.	ASTM C351	0.23
Electrical			
Dielectric Constant	1MHz @ R.T.	ASTM D150	6.0
Dielectric Strength	kV/mm	ASTM D116	9.8
Electrical Resistivity	Wcm @ R.T.	ASTM D1829	10^{13}

List of references

1. Chiang Y-M, Jakus K. Fundamental Research Needs in Ceramics NSF Workshop Report;University of Massachusetts; 1999 [accessed November 2008]; Available from: www-unix.ecs.umass.edu

2. Lee B, Komarneni S. Chemical Processing of Ceramics. Second ed. Florida: CRC Press, Taylor and Francis Group, LLC; 2005.

3. Masuda H, Higashitani K, Yoshida H. Powder Technology Handbook. Third ed. New York: CRC Press, Taylor & Francis Group; 2006.

4. McCormick P, Froes F. The Fundamentals of Mechanochemical Processing. JOM Journal of the Minerals, Metals and Materials Society. 1998;50(11):61-5.

5. Boldyrev VV, Pavlov SV, Goldberg EL. Interrelation between Fine Grinding and Mechanical Activation. International Journal of Mineral Processing. 1996;44-45:181-5.

6. Rahaman MN. Ceramic Processing. U.S.A.: CRC Press, Taylor & Francis Group; 2007.

7. Chowdhry U, Sleight AW. Ceramic Substrates for Microelectronic Packaging. Annual Review of Materials Science. 1987;17:323-40.

8. Costa Oliveira FA, Cruz Fernandes J. Mechanical and Thermal Behaviour of Cordierite-Zirconia Composites. Ceramics International. 2002;28(1):79-91.

9. Yalamaç E, Akkurt S. Additive and Intensive Grinding Effects on the Synthesis of Cordierite. Ceramics International. 2006;32(7):825-32.

10. Djordjevic N, Pavlovic L. The Influence of Activation and Relaxation Time on the Synthesis of Cordierite Ceramics. Journal of the Serbian Chemical Society. 2006;71(3):293-301.

11. Đorđević NG, Jovanić PB. Influence of Mechanical Activation on Elelctrical Properties of Cordierite Ceramics. Science of Sintering. 2008;40:47-53.

12. Rodrigues Neto JB, Moreno R. Effect of Mechanical Activation on the Rheology and Casting Performance of Kaolin/Talc/Alumina Suspensions for Manufacturing Dense Cordierite Bodies. Applied Clay Science. 2008;38(3-4):209-18.

13. Tamborenea S, Mazzoni AD, Aglietti EF. Mechanochemical Activation of Minerals on the Cordierite Synthesis. Thermochimica Acta. 2004;411(2):219-24.

14. Antsiferov VN, Porozova SE, Karmanov VI. Mechanochemical Activation of Batch During Fabrication of Highly-Porous Cordierite Materials Based on Natural Oxide Compounds. Science of Sintering. 2006;38(3):203-10.

15. d'Azevedo CA, Garrido FMS, Medeiros ME. The Effect of Mechanochemical Activation on the Reactivity in the Mgo-Al2o3-Sio2 System. Journal of Thermal Analysis and Calorimetry. 2006;83(3):649-55.

16. Catalytic Converter; BMW E34 website; 2008 [accessed Nov 2010]; Available from: http://www.bmwe34.net

17. Cordierite-Mullite Kiln Furniture;Import-Export Bulletin Board; 2010 [accessed Nov 2010]; Available from: http://www.imexbb.com/

18. Cordierite Refractory Tubes & Bobbin Set Sonya Ceramics; 2010 [accessed Nov 2010]; Available from: http://www.sonyaceramics.com

19. The Jet Turbines;The Rover Car Club of Auckland; 2010 [accessed Nov 2010]; Available from: http://www.rover.org.nz

20. Cordierite Electrical Insulators Associated Ceramics Technology, Inc.; 2009 [accessed Nov 2010]; Available from: http://www.associatedceramics.com

21. Ceramics in Telecommunications;Charles Sturt University; 1999 [accessed Nov 2010]; Available from: http://www.hsc.csu.edu.au

22. Die Bonder Suits Semiconductor/Electronic Packaging Markets;Thomas Publishing Company; 2003 [accessed Nov 2010]; Available from: http://news.thomasnet.com/news/materials-material-processing

23. Sun EH, Choa YH, Sekino T, Adachi T, Niihara K. Pressureless Sintering and Characterization of Cordierite/Zro2 Composites. Materials Research Innovations. 2002;6(3):105-11.

24. Hirvonen A, Nowak R, Yamamoto Y, Sekino T, Niihara K. Fabrication, Structure, Mechanical and Thermal Properties of Zirconia-Based Ceramic Nanocomposites. Journal of the European Ceramic Society. 2006;26(8):1497-505.

25. Gusev AA, Avvakumov EG, Vinokurova OB, Salostii VP. The Effect of Transition Metal Oxides on the Strength, Phase Composition, and Microstructure of Cordierite Ceramics. Glass and Ceramics. 2001;58(1-2):24-6.

26. Shi ZM, Liang KM, Gu SR. Effects of Ceo2 on Phase Transformation Towards Cordierite in Mgo-Al2o3-Sio2 System. Materials Letters. 2001;51(1):68-72.

27. Kim BH, Lee KH. Crystallization and Sinterability of Cordierite-Based Glass Powders Containing Ceo2. Journal of Materials Science. 1994;29(24):6592-8.

28. Venkataraman KS, Narayanan KS. Energetics of Collision between Grinding Media in Ball Mills and Mechanochemical Effects. Powder Technology. 1998;96(3):190-201.

29. Boldyrev VV, Tkacova K. Mechanochemistry of Solids: Past, Present, and Prospects. Journal of Materials Synthesis and Processing. 2000;8(3-4):121-32.

30. Gutman EM. Mechanochemistry of Materials. Cambridge: Cambridge International Science Publishing; 1998.

31. Gutman EM. Mechanochemistry of Solid Surfaces. Singapore: World Scientific Publishing Co. Ltd.; 1994.

32. Balaz P. Mechanochemistry in Nanoscience and Minerals Engineering. Berlin: Springer-Verlag; 2008.

33. Carniglia SC, Barna GL. Handbook of Industrial Refractories Technology, Principles, Types, Properties and Applications. New York: Noyes Publications; 1992.

34. Lin I. Implications of Fine Grinding in Mineral Processing Mechanochemical Approach. Journal of Thermal Analysis and Calorimetry. 1998;52(2):453-61.

35. Boldyrev VV. Mechanochemistry of Inorganic Solids. Thermochimica Acta. 1987;110:303-17.

36. Tkacova K, Heegn H, Stevulova N. Energy Transfer and Conversion During Comminution and Mechanical Activation. International Journal of Mineral Processing. 1993;40(1-2):17-31.

37. Avvakumov E, Senna M, Kosova N. Soft Mechanochemical Synthesis: A Basis for New Chemical Technologies. Dordrecht: Kluwer Academic Publishers; 2001.

38. Naito M, Kondo A, Yokoyama T. Applications of Comminution Techniques for the Surface Modification of Powder Materials. ISIJ International. 1993;33(9):915-24.

39. Inoue SI, Senna M. Differences between the Dissolution and the Decomposition Kinetics of Mechanically Activated Magnesium Hydroxide. Reactivity of Solids. 1988;5(2-3):155-66.

40. Senna M. Incipient Chemical Interaction between Fine Particles under Mechanical-Stress - a Feasibility of Producing Advanced Materials Via Mechanochemical Routes. Solid State Ionics. 1993;63-5:3-9.

41. Temuujin J. Mechanochemical Treatment of Solid Mixtures – a Promising Way of Synthesizing Ceramic Precursors. Chemistry for Sustainable Development. 2001;9:589-95.

42. Carmody O, Kristof J, Frost RL, Mako E, Kloprogge JT, Kokot S. A Spectroscopic Study of Mechanochemically Activated Kaolinite with the Aid of Chemometrics. Journal of Colloid and Interface Science. 2005;287(1):43-56.

43. Sanchez-Soto PJ, de Haro MDJ, Perez-Maqueda LA, Varona I, Perez-Rodriguez JL. Effects of Dry Grinding on the Structural Changes of Kaolinite Powders. Journal of the American Ceramic Society. 2000;83(7):1649-57.

44. Frost RL, Mako E, Kristof J, Horvath E, Kloprogge JT. Mechanochemical Treatment of Kaolinite. Journal of Colloid and Interface Science. 2001;239(2):458-66.

45. Vagvolgyi V, Kovacs J, Horvath E, Kristof J, Mako E. Investigation of Mechanochemically Modified Kaolinite Surfaces by Thermoanalytical and Spectroscopic Methods. Journal of Colloid and Interface Science. 2008;317(2):523-9.

46. Filio JM, Sugiyama K, Saito F, Waseda Y. A Study on Talc Ground by Tumbling and Planetary Ball Mills. Powder Technology. 1994;78(2):121-7.

47. Dellisanti F, Valdrè G, Mondonico M. Changes of the Main Physical and Technological Properties of Talc Due to Mechanical Strain. Applied Clay Science. 2009;42(3-4):398-404.

48. Aglietti EF. The Effect of Dry Grinding on the Structure of Talc. Applied Clay Science. 1994;9(2):139-47.

49. Liao JF, Senna M. Thermal-Behavior of Mechanically Amorphized Talc. Thermochimica Acta. 1992;197(2):295-306.

50. Wieczorek-Ciurowa K, Gamrat K. Mechanochemical Syntheses as an Example of Green Processes. Journal of Thermal Analysis and Calorimetry. 2007;88(1):213-7.

51. Lin IJ, Nadiv S. Review of the Phase-Transformation and Synthesis of Inorganic Solids Obtained by Mechanical Treatment (Mechanochemical Reactions). Materials Science and Engineering. 1979;39(2):193-209.

52. Pourghahramani P. Effects of Grinding Variables on Structural Changes and Energy Conversion During Mechanical Activation Using Line Profile Analysis (Lpa). Lulea: Lulea University of Technology; 2006.

53. Ajayan PM, Schandler LS, Braun PV. Nanocomposites Science and Technology. First ed. Weinheim: Wiley-VCH Verlag; 2003.

54. Dushkin AV. Potential of Mechanochemical Technology in Organic Synthesis and Synthesis of New Materials. Chemistry for Sustainable Development. 2004;12:251-73.

55. Wu W, Lu S, Wang J. Mechanochemical Surface Modification of Particles by Polymer Grafting. Chemistry for Sustainable Development. 2005;13:149-54.

56. Voronov A, Kohut A, Synytska A, Peukert W. Mechanochemical Modification of Silica with Poly(1-Vinyl-2-Pyrrolidone) by Grinding in a Stirred Media Mill. Journal of Applied Polymer Science. 2007;104(6):3708-14.

57. de Paiva LB, Morales AR, Valenzuela Díaz FR. Organoclays: Properties, Preparation and Applications. Applied Clay Science. 2008;42(1-2):8-24.

58. Patel HA, Somani RS, Bajaj HC, Jasra RV. Nanoclays for Polymer Nanocomposites, Paints, Inks, Greases and Cosmetics Formulations, Drug Delivery Vehicle and Waste Water Treatment. Bulletin of Materials Science. 2006;29(2):133-45.

59. Yoshimoto S, Ohashi F, Kameyama T. Insertion of Polypyrrole Chains into Montmorillonite Galleries by a Solvent-Free Mechanochemical Route. Macromolecular Rapid Communications. 2005;26(6):461-6.

60. Hasegawa M, Kimata M, Takahashi I. Mechanochemical Polymerization of Styrene Initiated by the Grinding of Layered Clay Minerals. Advanced Powder Technology. 2007;18(5):541-54.

61. Yoshimoto S, Ohashi F, Ohnishi Y, Nonami T. Synthesis of Polyaniline-Montmorillonite Nanocomposites by the Mechanochemical Intercalation Method. Synthetic Metals. 2004;145(2-3):265-70.

62. Ebrahimi-Basabi M, Javadpour J, Rezaie H, Goodarzi M. Mechanochemical Synthesis of Alumina-Zirconia Nanocomposite Powder. Advances in Applied Ceramics. 2008;107:318-21.

63. Gajovic A, Santic A, Djerdj I, Tomasic N, Mogus-Milankovic A, Su DS. Structure and Electrical Conductivity of Porous Zirconium Titanate Ceramics Produced by Mechanochemical Treatment and Sintering. Journal of Alloys and Compounds. 2009;479(1-2):525-31.

64. Hwang SJ, Lee Jh. Mechanochemical Synthesis of Cu-Al2o3 Nanocomposites. Materials Science and Engineering: A. 2005;405(1-2):140-6.

65. Zyryanov VV, Kostrovskii VG. Polymorphism of Zro2 Nanopowders and Mechanochemical Synthesis of Zr0.88sc0.1ce0.01y0.01o1.955. Inorganic Materials. 2008;44(12):1322-9.

66. Rodrigues Neto JB, Moreno R. Rheological Behaviour of Kaolin/Talc/Alumina Suspensions for Manufacturing Cordierite Foams. Applied Clay Science. 2007;37(1-2):157-66.

67. Kikuchi N, Sei T, Tsuchiya T, Hayashi S, Hayamizu K. Preparation of Cordierite Ceramics by the Sol-Gel Process and Their Properties. Nippon Seramikkusu Kyokai Gakujutsu Ronbunshi-Journal of the Ceramic Society of Japan. 1993;101(7):824-9.

68. Yamuna A, Johnson R, Mahajan YR, Lalithambika M. Kaolin-Based Cordierite for Pollution Control. Journal of the European Ceramic Society. 2004;24(1):65-73.

69. Zhang B, Cao CB, Zhu HS, Li GB. Preparation Low Dielectric Constant Material of Cordierite with Polyacrylamide Gel Method. Journal of Materials Science. 2005;40(7):1781-3.

70. Mu-Tsun T. Alkoxide Sol-Gel-Processed Cordierite Fiber. Journal of the American Ceramic Society. 2002;85(6):1637-9.

71. Stoyanova DD, Vladov DC, Kasabova NA, Mekhandzhiev DR. Cordierite-Like Catalyst Supports Based on Clay Materials. Kinetics and Catalysis. 2005;46(4):609-12.

72. Khabas TA, Vereshchagin VI, Vakalova TV, Kirchanov AA, Kulikovskaya NA, Kozhevnikova NG. Low-Temperature Synthesis of the Cordierite Phase in Ceramic Mixtures of Natural Raw Materials. Refractories and Industrial Ceramics. 2003;44(3):181-5.

73. Khabas TA, Vereshchagin VI, Vakalova TV, Kirchanov AA, Kulikovskaya NA, Kozhevnikova NG. Low-Temperature Synthesis of Cordierite Using Naturally Occurring Ceramic Materials. Refractories and Industrial Ceramics. 2002;43(9):314-8.

74. Kobayashi Y, Sumi K, Kato E. Preparation of Dense Cordierite Ceramics from Magnesium Compounds and Kaolinite without Additives. Ceramics International. 2000;26(7):739-43.

75. Trumbulovic L, Acimovic Z, Panic S, Andric L. Synthesis and Characterization of Cordierite from Kaolin and Talc for Casting Application. FME Transactions. 2003;31:43-7.

76. Logvinkov S, Semchenko G, Kobyzeva D. Thermodynamic Aspects of Synthesis of Refractories from Talc-Kaolin-Alumina Compositions. Refractories and Industrial Ceramics. 1998;39(3):135-8.

77. Wadsworth I, Wang J, Stevens R. Zirconia Toughened Cordierite. Journal of Materials Science. 1990;25(9):3982-9.

78. Adams RW, Clarke DR, Knickerbocker SH, Rapp LL, Schwartz B, inventors; International Buisiness Machines Corp., assignee. Zirconia Toughening of Glass-Ceramic Materials. Unites States. 1991.

79. Keefer KD, Michalske TA, inventors; Glass Ceramic Toughened with Tetragonal Zirconia. United States. 1986.

80. Ltd. SSEC. Zirconia Toughened Alumina;SAF Electronics; 2007 [accessed 01 June 2010]; Available from: www.saf-electronics.com

81. Biolox® Delta Ceramic Material;Zimmer Nederland; 2008 [accessed 01 June 2010]; Available from: www.zimmer.nl

82. Sun E, Choa Y-H, Seikino T, Niihara K. Fabrication and Mechanical Properties of Cordierite/Zro2 Composites by Pressureless Sintering. Journal of Ceramic Processing Research. 2000;1(1):9-11.

83. Sun EH, Kusunose T, Sekino T, Niihara K. Fabrication and Characterization of Cordierite/Zircon Composites by Reaction Sintering: Formation Mechanism of Zircon. Journal of the American Ceramic Society. 2002;85(6):1430-4.

84. Costa Oliveira FA, Franco JA, Cruz Fernandes J, Dias D. Newly Developed Cordierite-Zircon Composites. British Ceramic Transactions. 2002;101:14-21.

85. Travitzky NA, Claussen N. Chemical Stability of Cordierite-Zro2 Composites. Journal of the European Ceramic Society. 1989;5(5):327-31.

86. Liang C, Qiu J, Li Z, Li C. Synthesis of Nanostructured Ceria, Zirconia and Ceria-Zirconia Solid Solutions Using an Ultrahigh Surface Area Carbon Material as a Template. Nanotechnology. 2004;15(7):843-7.

87. Tsuzuki T, McCormick PG. Synthesis of Ultrafine Ceria Powders by Mechanochemical Processing. Journal of the American Ceramic Society. 2001;84(7):1453-8.

88. Shi ZM, Bai X, Wang XF. Ce4+-Modified Cordierite Ceramics. Ceramics International. 2006;32(6):723-6.

89. Shi ZM. Cordierite-Ceo2 Composite Ceramic: A Novel Catalytic Support Material for Purification of Vehicle Exhausts. Key Engineering Materials; 2005. p. 1075-8.

90. Shi ZM, Liu Y, Yang WY, Liang KM, Pan F, Gu SR. Evaluation of Cordierite-Ceria Composite Ceramics with Oxygen Storage Capacity. Journal of the European Ceramic Society. 2002;22(8):1251-6.

91. Shi ZM. Preparation of Cordierite Ceramic Using Mixtures of Ce4+-Modified Amorphous Powder and Oxide Powders. Journal of Rare Earths. 2006;24:263-5.

92. Senguttuvan G, Settu T, Kuppusamy P, Kamaraj V. Sol-Gel Synthesis and Thermal Evaluation of Cordierite–Zirconia Composites (Ce–Zro2, Y–Ce–Zro2). Journal of Materials Synthesis and Processing. 1999;7(3):175-85.

93. Djuricic B, Pickering S, McGarry D, Tambuyser P, Thomas P. Preparation and Properties of Alumina-Ceria Nano-Nano Composites. Journal of Materials Science. 1999;34(8):1911-9.

94. Wei ZL, Li HM, Zhang XY, Yan SH, Lv Z, Chen YQ, et al. Preparation and Property Investigation of Ceo2-Zro2-Al2o3 Oxygen-Storage Compounds. Journal of Alloys and Compounds. 2008;455(1-2):322-6.

95. Rahaman MN. Sintering of Ceramics. New York: CRC Press, Taylor & Francis Group; 2008.

96. Morgado E, Lam YL, Menezes SMC, Nazar LF. Characterization of Peptized Boehmite Systems: An Al-27 Nuclear Magnetic Resonance Study. Journal of Colloid and Interface Science. 1995;176(2):432-41.

97. SanchezSoto PJ, Wiewiora A, Aviles MA, Justo A, PerezMaqueda LA, PerezRodriguez JL, et al. Talc from Puebla De Lillo, Spain .2. Effect of Dry Grinding on Particle Size and Shape. Applied Clay Science. 1997;12(4):297-312.

98. Keck CM, Muller RH. Size Analysis of Submicron Particles by Laser Diffractometry-90% of the Published Measurements Are False. International Journal of Pharmaceutics. 2008;355(1-2):150-63.

99. Virden A. Laser Diffraction Masterclass 4: Validation of Laser Diffraction Methods (Recorded Webcast);Malvern Instruments Ltd.; 2009 [accessed 30 May 2010]; Available from: www.malvern.com

100. Lu J, Gao L, Guo J. Preparation and Phase Transition of Superfine Boehmite Powders with Different Crystallinity. Journal of Materials Science Letters. 2001;20(20):1873-5.

101. Ruan H. Spectroscopic Studies of Nano-Structures of Al and Fe Phases, Bauxite and Their Thermally Activated Products(Qut Thesis);Queensland University of Technology; 2005 [accessed November 2009]; Available from: http://eprints.qut.edu.au

102. Tettenhorst RT. Comparison of Experimental and Calculated X-Ray-Powder Diffraction Data for Boehmite. Clays and Clay Minerals. 1988;36(2):181-3.

103. Refractive Index Selection for Powder Mixtures AN157 Refractive Index Selection;HORIBA Instruments, Inc.; 2008 [accessed 23 March 2009]; Available from: www.horiba.com

104. Kano J, Miyazaki M, Saito F. Ball Mill Simulation and Powder Characteristics of Ground Talc in Various Types of Mill. Advanced Powder Technology. 2000;11(3):333-42.

105. Frost RL, Horvath E, Mako E, Kristof J. Modification of Low- and High-Defect Kaolinite Surfaces: Implications for Kaolinite Mineral Processing. Journal of Colloid and Interface Science. 2004;270(2):337-46.

106. Yang HM, Yang WG, Hu YH, Du CF, Tang AD. Effect of Mechanochemical Processing on Illite Particles. Particle & Particle Systems Characterization. 2005;22(3):207-11.

107. Mendelovici E. Selective Mechanochemical Reactions on Dry Grinding Structurally Different Silicates. Journal of Materials Science Letters. 2001;20(1):81-3.

108. Holt CB. The Shape of Particles Produced by Comminution - a Review. Powder Technology. 1981;28(1):59-63.

109. Gonzalez-Velasco JR, Gutierrez-Ortiz MA, Ferret R, Aranzabal A, Botas JA. Synthesis of Cordierite Monolithic Honeycomb by Solid State Reaction of Precursor Oxides. Journal of Materials Science. 1999;34(9):1999-2002.

110. Goel A, Shaaban ER, Melo FCL, Ribeiro MJ, Ferreira JMF. Non-Isothermal Crystallization Kinetic Studies on Mgo-Al2o3-Sio2-Tio2 Glass. Journal of Non-Crystalline Solids. 2007;353(24-25):2383-91.

111. Hwang SP, Wu JM. Effect of Composition on Microstructural Development in Mgo-Al2o3-Sio2 Glass-Ceramics. Journal of the American Ceramic Society. 2001;84(5):1108-12.

112. Miller DM, inventor Corning Glass Works (Corning, NY), assignee. Sintered Cordierite Glass-Ceramic Bodies. United States patent 3926648 1974 12/16/1975.

113. Miyashiro A, Iiyama T, Yamasaki M, Miyashiro T. The Polymorphism of Cordierite and Indialite. American Journal of Science. 1955;253(4):185-208.

114. Jang HM, Lim BC. Effects of the Scale of Precursor Mixing on Densification Behaviors and Phase-Transformation Kinetics of Cordierite Gels. Journal of Materials Research. 1994;9(10):2627-33.

115. Bogue RH, Newkirk TF. Heterogeneous Equilibria and Phase Diagrams. Annu Rev Phys Chem. 1953;4:23-48.

116. Graf RB, Wahl FM, Grim RE. Phase Transformations in Silica-Alumina-Magnesia Mixtures as Examined by Continuous X-Ray Diffraction .1. Talc-Kaolinite Compositions. American Mineralogist. 1962;47(11-1):1273-&.

117. Yamaguchi T. Pores in Ceramic Processing. In: Yanagida H, Fukunaga O, editors. Ceramics Databook. Montreux: Gordon and Breach Science Publishers; 1987. p. 739.

118. Mercury Prosimetry Brochure;Micromeritics; 2009 [accessed May 2009]; Available from: www.micromeritics.com

119. Othman AGM. Influence of Talc Grain Size on Formation and Physico-Mechanical Properties of Cordierite. Cfi-Ceramic Forum International. 2006;83(2):E39-E43.

120. Nakahara M, Kondo Y, Hamano K. Effect of Particle Size of Powders Ground by Ball Milling on Densification of Cordierite Ceramics. Journal of the Ceramic Society of Japan. 1999 Apr;107(4):308-12.

121. Nakahara M, Kondo Y, Hamano K. Effect of Talc Grain-Size on Microstructure of Cordierite Ceramics. Journal of the Ceramic Society of Japan. 1995;103(10):1051-6.

122. Montorsi MA, Delorenzo R, Verne E. Cordierite-Cerium(Iv) Oxide System - Microstructure and Properties. Ceramics International. 1994;20(6):353-8.

123. Trovarelli A, Zamar F, Llorca J, deLeitenburg C, Dolcetti G, Kiss JT. Nanophase Fluorite-Structured Ceo2-Zro2 Catalysts Prepared by High-Energy Mechanical Milling - Analysis of Low-Temperature Redox Activity and Oxygen Storage Capacity. Journal of Catalysis. 1997;169(2):490-502.

124. Tompsett GA, Sammes NM, Yamamoto O. Ceria–Yttria-Stabilized Zirconia Composite Ceramic Systems for Applications as Low-Temperature Electrolytes. Journal of the American Ceramic Society. 1997;80(12):3181-6.

125. Kamasa P, Myslinski P, Staskiewicz J. Instantaneous Coefficient of Thermal Expansion Determined by Temperature-Modulated Dilatometry. Czechoslovak Journal of Physics. 2004;54:D627-D30.

126. Richerson DW. Modern Ceramic Engineering (Properties, Processing, and Use in Design). Third ed. New York: CRC Press, Taylor & Francis Group; 2006.

127. Goren R, Gocmez H, Ozgur C. Synthesis of Cordierite Powder from Talc, Diatomite and Alumina. Ceramics International. 2006;32(4):407-9.

128. Manzhen D, Lirong Y, Jiageng C. Factors Affecting Thermal Expansion Coefficients of Synthesized Cordierite. NAIHUO CAILIAO. 2007;41(3):201-4.

129. Rohan P, Neufuss K, Matejícek J, Dubský J, Prchlík L, Holzgartner C. Thermal and Mechanical Properties of Cordierite, Mullite and Steatite Produced by Plasma Spraying. Ceramics International. 2004;30(4):597-603.

130. Fritsch CW, Buljan ST, inventors; GTE Sylvania Incorporated (Stamford, CT) assignee. Low Thermal Expansion Coefficient Synthetic Cordierite-Containing Ceramic Bodies and Method for Producing Same United States. 1976.

131. Graf RB, Grim RE, Wahl FM. Phase Transformations in Silica-Alumina-Magnesia Mixtures as Examined by Continuous X-Ray Diffraction .2. Spinel-Silica Compositions. American Mineralogist. 1963;48(1-2):150-&.

132. Zhang DL. Processing of Advanced Materials Using High-Energy Mechanical Milling. Progress in Materials Science. 2004;49(3-4):537-60.

133. Baláž P, Choi WS, Fabián M, Godočíková E. Mechanochemistry in the Preparation of Advanced Materials. Acta Montanistica Slovaca. 2006;11(2).

134. Perez-Maqueda LA, Duran A, Perez-Rodriguez JL. Preparation of Submicron Talc Particles by Sonication. Applied Clay Science. 2005;28(1-4):245-55.

135. Ternary Phase Diagrams Teaching Phase Equilibria;Montana State University, Science Education Resource Center; 2007 [accessed May 2009; Available from: http://serc.carleton.edu

136. Presnall DC. Phase Diagrams of Earth-Forming Minerals;The American Geophysics Union; 1995 [accessed May 2009]; Available from: www.agu.org

137. Lippens BC, Deboer JH. Study of Phase Transformations During Calcination of Aluminum Hydroxides by Selected Area Electron Diffraction. Acta Crystallographica. 1964;17(10):1312-&.

138. Animating the Crystal06 Vibrational Frequencies by Jmol Engine;UNIVERSITY OF TORINO; 2010 [accessed 01 June 2010]; Available from: www.crystal.unito.it

139. Lombardi KC, Guimaraes JL, Mangrich AS, Mattoso N, Abbate M, Schreiner WH, et al. Structural and Morphological Characterization of the Pp-0559 Kaolinite from the Brazilian Amazon Region. Journal of the Brazilian Chemical Society. 2002;13(2):270-5.

140. Chen YF, Wang MC, Hon MH. Transformation Kinetics for Mullite in Kaolin-Al2o3 Ceramics. Journal of Materials Research. 2003;18(6):1355-62.

141. Talc in Plastics Technical Bulletin 1301;MONDO MINERALS B.V.[accessed January 2010]; Available from: www.mondominerals.com

142. Talc Mineralogy About Talc;Luzenac[accessed January 2010]; Available from: www.luzenac.com

143. Materials for Solid Oxide Fuel Cells (Sofcs), Crystal Structure Gallery;Advanced Industrial Science and Technology (AIST); 2002 [accessed 01 June 2010]; Available from: http://staff.aist.go.jp

144. Zircon;Wikipedia, the free encyclopedia; 2010 [accessed 01 June 2010]; Available from: http://en.wikipedia.org

145. Ceramic Properties Tables;Ferro-Ceramic Grinding Inc.; 2005 [accessed August 2009]; Available from: http://www.ferroceramic.com